

# ALR induced disulfides impact CPOX biogenesis and affect porphyrin metabolism

Inaugural-Dissertation

zur

Erlangung des Doktorgrades

der Mathematisch-Naturwissenschaftlichen Fakultät

der Universität zu Köln



vorgelegt von

**Julia Racho**

Aus Leverkusen

angenommen im Jahr 2025



Tag der mündlichen Prüfung: 07.02.2025



*Für meine Familie*



## List of Contents

List of Contents.....	I
List of Figures.....	IV
List of Tables.....	V
Zusammenfassung.....	VII
Abstract.....	VIII
1. Introduction.....	1
1.2 Protein import into the IMS.....	2
1.2.1 MTS-driven import.....	2
1.2.2 Oxidation-dependent import.....	6
1.2.3 Affinity-driven import.....	10
1.3 Protein functions in the IMS.....	11
1.4 Heme biogenesis.....	15
1.4.1 The essentiality of heme.....	15
1.4.2 Heme biosynthesis.....	16
1.4.3 Trafficking of porphyrins across the cell.....	20
1.4.4 Heme biosynthesis defects.....	23
1.5 Aims of this work.....	25
2. Results.....	27
2.1 CPOX is a novel interactor of ALR.....	27
2.1.1 ALR has functions beyond the disulfide relay.....	27
2.1.2 ALR interacts with CPOX covalently.....	29
2.1.3 ALR interacts with CPOX via specific cysteines.....	30
2.1.4 CPOX contains oxidized cysteines.....	33
2.2 CPOX cysteines are critical for its stability during processing in the IMS.....	36
2.2.1 CPOX KO is characterized by a distinct phenotype.....	36
2.2.2 The two CPOX cysteine pairs are not equally relevant for its function.....	38
2.2.3 Lack of a certain CPOX cysteine pair impacts CPOX processing and stability.....	40
2.2.4 Cytosolic CPOX is not dependent on cysteines.....	46
3. Discussion.....	49
3.1 ALR could impact several mitochondrial processes.....	49
3.2 ALR induced disulfides are important for CPOX stabilization in the IMS.....	53
3.3 The complex CPOX maturation and its role for regulation and quality control.....	54
3.4 Mitochondrial CPOX localization avoids protoporphyrinogen IX accumulation.....	60
4. Outlook.....	65
5. Methods.....	67

## List of Contents

5.1	Molecular Biology .....	67
5.1.1	Polymerase chain reaction (PCR) .....	67
5.1.2	Site-directed mutagenesis .....	67
5.1.3	Agarose gel electrophoresis.....	68
5.1.4	Restriction digest and ligation of DNA .....	68
5.1.5	Transformation of plasmid DNA into chemically competent <i>E. coli</i> DH5 $\alpha$ .....	69
5.1.6	Plasmid isolation from <i>E.coli</i> .....	69
5.2	Mammalian Tissue Culture .....	70
5.2.1	Culturing human cells .....	70
5.2.2	Seeding human cells .....	70
5.2.3	Freezing and thawing of human cells .....	70
5.2.4	SiRNA-mediated knockdown in human cells .....	71
5.2.5	Generation of CRISPR/Cas9-mediated knockout cell lines .....	71
5.2.6	Generation of stable inducible cell lines with the Flp-In <sup>TM</sup> T-Rex <sup>TM</sup> system.....	72
5.2.7	Generation of stable inducible cell lines with the PiggyBac system .....	72
5.2.8	Galactose shift .....	73
5.2.9	Proliferation assay.....	73
5.2.10	Immunofluorescence.....	73
5.3	Protein Biochemistry.....	74
5.3.1	SDS-PAGE .....	74
5.3.2	Western Blot .....	75
5.3.3	Immunological detection of proteins.....	75
5.3.4	Autoradiography .....	75
5.3.5	Native and denaturing immunoprecipitation .....	76
5.3.6	Alkaline extraction .....	77
5.3.7	Inverse redox shift assay .....	77
5.3.8	Radioactive pulse chase.....	78
5.3.9	Oxidation kinetic .....	78
5.3.10	Whole cell proteomics.....	79
5.3.11	Generation of an interactome .....	80
5.3.12	HPLC-based measurement of heme biosynthesis intermediates.....	80
5.4	Bioinformatics .....	81
5.4.1	Protein sequence conservation analysis.....	81
5.4.2	Protein structure visualization .....	81
5.4.3	Analysis of proteomics data.....	81
5.4.4	Quantification and statistical analysis.....	81

5.4.5	Data availability .....	82
6.	Materials .....	83
6.1	Plasmids and cell lines .....	83
6.2	Oligonucleotides .....	85
6.3	Antibodies .....	86
6.4	siRNA.....	87
7.	Abbreviations .....	88
	Amino Acids.....	94
8.	Appendix .....	95
9.	References.....	100

## List of Figures

Figure 1: Mitochondrial ultrastructure.....	2
Figure 2: Bipartite MTS-driven import into the IMS.....	6
Figure 3: Many disulfide containing proteins in the IMS undergo oxidation-dependent import.....	7
Figure 4: The disulfide relay.....	9
Figure 5: Receptor-driven import.....	11
Figure 6: Functions of IMS proteins.....	14
Figure 7: Heme biosynthesis and function of CPOX.....	22
Figure 8: ALR might have functions beyond the disulfide relay.....	26
Figure 9: ALR has functions beyond the disulfide relay.....	28
Figure 10: ALR covalently interacts with CPOX.....	29
Figure 11: ALR interacts with CPOX via specific cysteine pairs.....	31
Figure 12: Single cysteines variants of CPOX interact with ALR.....	33
Figure 13: CPOX contains oxidized cysteines.....	34
Figure 14: CPOX contains one or two disulfide bonds.....	35
Figure 15: CRISPR/Cas9 mediated CPOX KO shows elevated ALAS1 levels.....	37
Figure 16: CPOX KO cells accumulate CPPgenIII and show growth defect after galactose shift.....	38
Figure 17: The cysteine pair C304-C357 is required for optimal CPOX functionality.....	39
Figure 18: CPOX processing is complex and affected by cysteines.....	41
Figure 19: CPOX enters mitochondria via a bipartite presequence and is processed by the IMMP1/2.....	43
Figure 20: Lack of the disulfide between C304 and C357 impairs CPOX stability.....	45
Figure 21: Activity of cytosolic CPOX is not dependent on cysteines.....	47
Figure 22: Possible ways of ALR interaction with novel substrates.....	52
Figure 23: An ALR induced structural disulfide stabilizes CPOX in the IMS.....	53
Figure 24: CPOX' second cysteine pair increases its temperature stability.....	54
Figure 25: CPOX processing might involve MIP cleavage.....	55
Figure 26: Some mitochondrial proteases can sense their substrates folding state.....	57
Figure 27: CPOX' conserved negative stretch might influence its last processing step.....	59
Figure 28: CPOX is localized to the intermembrane space of mitochondria in higher eukaryotes.....	61
Figure 29: Mitochondrial localization of CPOX prevents PPgenIX accumulation and its toxic effects ..	63

## List of Tables

Table 1: Overview over the eight different porphyrias .....	23
Table 2: PCR reaction mixture pipetting scheme .....	67
Table 3: PCR program .....	67
Table 4: PCR reaction mixture pipetting scheme for site-directed mutagenesis .....	68
Table 5: PCR program for site-directed mutagenesis .....	68
Table 6: Restriction digest reaction mixture.....	69
Table 7: Ligation reaction mixture.....	69
Table 8: Required amounts for siRNA-mediated reverse transfection of cells with Lipofectamine™ RNAiMAX.....	71
Table 9: Pipetting scheme for Tris-Glycine acrylamide gels .....	74
Table 10: Pipetting scheme for Tris-Tricine acrylamide gels.....	75
Table 11: Cell lines and plasmids used in this work .....	83
Table 12: Oligonucleotide primers used in this work .....	85
Table 13: Antibodies used in this work.....	86
Table 14: SiRNAs used in this work.....	87



## Zusammenfassung

Die Sulfhydryl-Oxidase „Augmenter of liver regeneration“ (ALR, z. dt. Erhöher der Leberregeneration) ist bekannt für ihre Funktion im sogenannten „Disulfide Relay“, einem Importweg für mitochondriale Proteine mit konservierten Cysteinen, die den Intermembranraum erreichen sollen. Dabei reoxidiert ALR die Oxidoreduktase MIA40 durch einen Thiol-Disulfid Übertragungsmechanismus und schleust die bei dieser Reaktion frei gewordenen Elektronen in die Atmungskette ein. Eine andere Funktion ALRs war bisher nicht bekannt. In dieser Arbeit konnte jedoch gezeigt werden, dass ALR Funktionen besitzt, die über die Rolle für den „Disulfide Relay“ hinausgehen, indem mindestens sechs neue Interaktionspartner von ALR identifiziert wurden. Die Interaktion mit einem dieser neu identifizierten Interaktoren, Coproporphyrinogen Oxidase CPOX, wurde detaillierter charakterisiert. CPOX enthält konservierte Cysteine und ist wie ALR im Intermembranraum der Mitochondrien lokalisiert. Dort katalysiert es den drittletzten Schritt der Häm Biosynthese. Es konnte festgestellt werden, dass CPOX mit ALR über ausgewählte Cysteine interagiert und dabei mindestens eine Disulfidbrücke erlangt.

Auf der Suche nach dem Zweck dieser ALR-CPOX Interaktion und nach der Relevanz der Disulfidbrücke für CPOX wurde entdeckt, dass CPOX während seiner Maturierung einer mehrstufigen Prozessierung unterzogen und dabei viermal geschnitten wird. Es kann angenommen werden, dass der erste Schnitt durch die Matrixmetalloprotease MPP vollzogen wird, während experimentell bewiesen werden konnte, dass der Innenmembran-Protease-Komplex IMMP1/2 für den dritten Schnitt verantwortlich ist, nach welchem CPOX in den Intermembranraum entlassen wird. Es konnte außerdem festgestellt werden, dass die Schnitteffizienz des IMMP1/2 Komplexes abhängig von der Präsenz der Disulfidbrücke zwischen den CPOX Cysteinen C304 und C357 ist. Zusätzlich benötigt CPOX diese Disulfidbrücke auch zur Stabilisierung im mitochondrialen Intermembranraum und um Aggregation zu verhindern. Zuletzt zeigen die Daten, welche im Laufe der hier präsentierten Arbeit generiert wurden, dass die Funktion cytosolischer Varianten von CPOX, inklusive des aus der Hefe stammenden CPOX Homologes Hem13, komplett unabhängig von Cysteinen ist, da diese Varianten nicht prozessiert werden müssen. Allerdings führt die cytosolische Lokalisation dieser Proteine zur Akkumulation des potenziell toxischen CPOX Produktes Protoporphyrinogen IX.

## Abstract

The sulfhydryl oxidase augments liver regeneration (ALR) is well known for its function in the disulfide relay, an important machinery for mitochondrial IMS proteins with conserved cysteines. Here, it reoxidizes oxidoreductase MIA40 in a thiol-disulfide exchange mechanism and feeds electrons from this reaction into the respiratory chain. No other role has been known for ALR yet. In this work, it was shown that ALR has functions beyond the disulfide relay by identification of at least six novel ALR interaction partners. The interaction of ALR with one of these newly defined interactors, coproporphyrinogen oxidase (CPOX), has been further characterized. CPOX contains conserved cysteines and is localized in the IMS like ALR. There, it catalyzes the third last step of the heme biosynthesis pathway. It was found that CPOX interacts with ALR over selected cysteines, thereby gaining at least one disulfide.

Investigating the purpose of the ALR-CPOX interaction and the relevance of CPOX' disulfides, it was discovered that CPOX undergoes complex multi-step processing. During its maturation, CPOX is cleaved four times. The first step is assumed to be mediated by matrix metalloprotease MPP. The third cleavage step releasing CPOX into the IMS is discovered to be carried out by the IMMP1/2 complex. It could be shown that cleavage efficiency of CPOX by IMMP1/2 is dependent on the presence of a disulfide between CPOX cysteines C304 and C357. Additionally, CPOX needs this disulfide in the IMS to stabilize it and prevent aggregation. Lastly, data generated in the course of this thesis revealed that cytosolic versions of CPOX including its yeast homologue Hem13 are not dependent on cysteines at all for proper functionality as they do not undergo processing. However, the cytosolic localization of CPOX resulted in potentially toxic accumulation of the CPOX product protoporphyrinogen IX.

# 1. Introduction

## 1.1 The IMS is a versatile subcompartment

Mitochondria are essential organelles most widely known for their function in energy metabolism, being the major supplier of adenosine triphosphate (ATP) in the cell [1, 2]. However, mitochondria also fulfil a wide range of other crucial functions. They are involved in synthesis of cofactors, for example iron-sulfur clusters or porphyrins [3-5], take part in cellular ion homeostasis regulating the pools of calcium, iron and copper [6-9] and mediate turnover of fatty acids and amino acids. Further, mitochondria are embedded into the cellular signaling network, thereby influencing the whole cell [10-14].

These diverse functions are enabled by the unique mitochondrial ultrastructure (Figure 1). Mitochondria consist of four different subcompartments, two lipid bilayers, the outer mitochondrial and the inner mitochondrial membrane (OMM & IMM), and two aqueous compartments, the intermembrane space (IMS) and the matrix. The matrix is the largest mitochondrial compartment. It harbors the mitochondrial DNA and its translation machinery and is also a platform for metabolic processes, where  $\beta$ -oxidation, the TCA cycle and steps of different biosynthetic pathways take place [3, 15-18]. In contrast, the IMS is a very small compartment, yet it is highly versatile and contributes to most mitochondrial functions. Located between the outer and the inner membrane, it is the interface between cytosol and matrix. The so-called peripheral IMS mediates mitochondrial logistics like transport of metabolites or export of iron-sulfur clusters, and is interconnected with the cytosol due to OMM permeability. This enables communication with the outside of mitochondria, for example by integration of calcium signaling [19, 20]. The IMM on the other hand is nearly impermeable and contains highly selective carriers and transporters for all metabolites that need to be exchanged [21, 22]. It is also structurally much more complex than the OMM and forms membrane invaginations called cristae. The cristae lumen belongs to the IMS; however, cristae are constricted areas, separated from the peripheral IMS by cristae junctions (CJs) CJs are formed with the help of the mitochondrial contact site and cristae organizing system (MICOS) complex and optic atrophy 1 (OPA1). They are often close to contact sites between OMM and IMM, established by MICOS and sorting and assembly machinery (SAM) [23-25]. Presence of cristae increases the surface of the IMM and provides the structural framework for respiration [26]. Hence, the IMS can be seen as a subcompartment divided into subcompartments. Besides that, IMS proteins take part in biosynthetic pathways like porphyrin biosynthesis [4, 27, 28] and the IMS is the major source of reactive oxygen species (ROS) in the cell, which can be toxic at high concentrations but is also an important signaling molecule [14, 29].

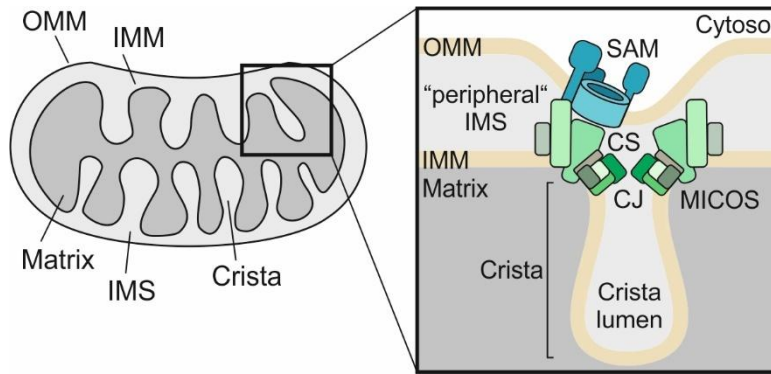


*Figure 1: Mitochondrial ultrastructure*

The ultrastructure of mitochondria is unique. They consist of the outer mitochondrial membrane that engulfs the whole organelle and the inner mitochondrial membrane. The narrow space between the two membranes is called intermembrane space. The IMM forms invaginations called cristae, which are constricted areas separated from the peripheral IMS by crista junctions. CJs are established by the MICOS complex. MICOS also often interacts with SAM to form contact sites (CSs) between outer and inner membrane at CJs.

## 1.2 Protein import into the IMS

Like the most mitochondrial proteins, all IMS proteins are encoded by nuclear DNA and translated in the cytosol. To reach the IMS, they need to be imported using either mitochondrial targeting signal (MTS)-driven, oxidation-driven, or affinity-driven import pathways [30].

### 1.2.1 MTS-driven import

Most mitochondrial proteins use a mitochondrial targeting signal to reach their destined location within mitochondria. Consequently, there are also IMS proteins using an MTS-driven pathway for import. A classical MTS consist of an N-terminal amphipathic  $\alpha$ -helix with positive charges on one site and hydrophobic residues on the other [31, 32]. However, the presequence of IMS proteins is more complex. In the so-called bipartite presequence, the MTS is followed by a cleavable hydrophobic transmembrane domain that acts as a second sorting signal [33].

### *Entering mitochondria via TOM*

Proteins with a bipartite sequence first need to pass the translocase of the outer membrane (TOM) complex to enter mitochondria (Figure 2, top). TOM consists of the channel forming TOM40 that associates with small TOMs (TOM5, 6 and 7) and is linked to another TOM40-small TOMs subunit via the central receptor TOM22. TOM22 is also needed for docking of the initial receptors TOM20 and TOM70, which mediate the first interaction with a nascent protein chain to initiate import [34]. It was shown that cytosolic ribosomes can associate to the mitochondrial surface to facilitate interaction with translocases [35, 36]. Another way to target protein precursors to TOM is via the chaperones heat shock protein 70 and 90 (HSP70 and HSP90), which can bind to TOM70 [37, 38].

### *Membrane insertion by TIM23*

Once inside the mitochondria, proteins with bipartite MTS use the translocase of the inner membrane 23 (TIM23) complex for further transport (Figure 2, top). Translocation over the IMM is driven by the membrane potential ( $\Delta\Psi$ ) that activates TIM23. Nonetheless, little is known about the exact mechanism of TIM23 translocation. The TIM23 complex consists of several subunits with TIM23, TIM17 and TIM50 forming its core. TIM50 is a single-span IMM protein that acts as receptor for MTS-containing proteins and is responsible for gating of the channel in a  $\Delta\Psi$ - and presequence-dependent manner [39, 40]. Protein precursors are recognized and taken over from TOM by the IMS exposed part of TIM50 via their MTS. Recent studies propose that the multi-span IMM proteins TIM23 and TIM17 both participate in formation of the actual channel and help the protein precursors translocate further, once transfer was initiated by TIM50 [41-43].  $\Delta\Psi$ -dependent translocation of precursors with bipartite presequence is arrested as soon as the hydrophobic second part of the presequence is reached. Because of its hydrophobicity, it acts as a stop-transfer signal and can be laterally released into the inner membrane. Structural analyses revealed that TIM17 forms a lateral cavity reaching into the IMM, that is sealed in yeast by Mrg2 and in humans by reactive oxygen species modulator 1 (ROMO1), a recently discovered subunit of the TIM23 complex [41, 42, 44, 45]. It has been shown in yeast that Mrg2 interacts differently with precursors targeted to the matrix and proteins with stop-transfer signal, stabilizing interaction of the latter group of proteins with the TIM23 complex. It thereby determines the mode of action of the TIM23 complex (matrix translocation versus lateral release) and adds a quality control step for IMM proteins. Mutations in Mrg2 and ROMO1 impair sorting of proteins into the IMM [44, 46, 47].

### *IMMP1/2 cleavage*

After the protein precursor has been inserted into the IMM, the MTS is cleaved off from the matrix site by matrix processing peptidase (MPP) [48, 49]. To release the soluble protein from the IMM into the IMS, the transmembrane domain that has acted as a stop-transfer signal before needs to be cleaved off either within or at the or at the IMS site of the IMM. For most proteins with a bipartite MTS, this cleavage is mediated either by the inner mitochondrial membrane protease 1/2 (IMMP1/2) complex (Imp1/2 in yeast) (Figure 2, bottom left) or by the rhomboid protease presenilin-associated rhomboid like (PARL; Pcp1 in yeast) (Figure 2, bottom middle) [50]. In mammals, the IMMP complex consists of two subunits, IMMP1L and IMMP2L. In yeast, the complex is formed by Imp1, Imp2 and an additional subunit for substrate recognition, sorting mitochondrial 1 (Som1). The four inner membrane proteases from yeast and the mammalian system do not share much sequence identity, but common features in their tertiary structure are conserved. They all have an N-terminal transmembrane and a C-terminal catalytic domain with a serine/lysine dyad. Two conserved glycines in each of the two Imp/IMMP subunits of the complex stabilize each other and are necessary for proteolytic activity [51-54]. Despite

## Introduction

these common features, both subunits are catalytically active independent of each other and show different substrate specificity [54]. They also have a different topology, as Imp2/IMMP2L has a second transmembrane domain. A consensus motif of the subunits has not been identified yet. Imp1 seems to preferably cleave when asparagine is at position -1, but it also tolerates serine, methionine, alanine, leucine, or cysteine. A hydrophobic, non-aromatic residue is favored at position -3 and an acidic residue at position +1. Known substrates of Imp1 with bipartite MTS are cytochrome  $b_2$ , NADH-cytochrome  $b_5$  reductase Mcr1 and the mitochondrial FAD-dependent glycerol-3-phosphate dehydrogenase Gut2 [51, 54]. For Imp2 on the opposite, the +1 position does not seem to play a role for cleavage. Imp2 shows a strong requirement for alanine at position -1 and a preference for small hydrophobic residues, and one small polar residue (serine) at the position -3 (Figure 2 B, right) [53-57]. It has been shown to cleave Prx1 and cytochrome  $c_1$ , which are both proposed to undergo multi-step processing during import [51, 53, 58, 59]. For the mammalian IMMPS, a common feature for cleavage is not known yet due to less known substrates. In mice, cytochrome  $c_1$  (CYC1) and mitochondrial glycerol 3-phosphate dehydrogenase GPD2, the homologue of Gut2, are also IMMPS substrates. CYC1 is an IMMPS2L substrate like in yeast, but interestingly, GPD2 seems to be an IMMPS2L substrate in mice whereas Gut2 is cleaved by Imp1 in yeast [60, 61]. It is not clear, how the lack of a third subunit influences substrate specificity and distribution of the IMMPS1/2 subunits in the mammalian system, so it can just be estimated, that most mammalian substrates behave similar to their yeast counterpart.

### *PARL cleavage*

The other protease known to cleave several substrates with bipartite sequence for their release into the IMS is PARL in humans or Pcp1 in yeast, respectively (Figure 2 C). PARL and Pcp1 belong to the rhomboid protease family, which means that they share a catalytic domain composed of six transmembrane helices, the rhomboid domain. Human PARL has an additional 7<sup>th</sup> transmembrane helix at the N-terminal site of the catalytic domain. Rhomboid proteases are structurally highly conserved and it was shown that PARL and Pcp1 are interchangeable [62]. They both have catalytic serine and histidine residues that mediate the cleavage (S277/H335 in PARL, S256/H313 in Pcp1) and are highly conserved in their position within the protein structure [63]. Established PARL substrates with bipartite MTS are PTEN induced kinase 1 (PINK1), SMAC/DIABLO, HtrA serine peptidase 2 (HTRA2) and StAR-related lipid transfer domain protein 7 (STARD7) [64-67]. A certain PARL cleavage site has not been identified yet, but comparison of the known PARL substrates shows a preference for small aliphatic amino acids at the positions +1, -1, and -4 (Figure 2 C, right) [65]. *In vitro* studies on purified PARL in liposomes with peptide substrates proposed that PARL preferentially cleaves substrates with certain residues at position 1, 4, -1, -2 and -4 [68]. However, suggested characteristics of amino acids at these positions are not fitting with known substrates and raise the question whether a defined consensus motif for PARL exists. In the IMM, PARL is found in a complex with the i-AAA protease yeast

mitochondrial escape-like 1 (YME1L1), which mediates degradation of IMS proteins, and the stress-induced peptidase “overlapping activity with *m*-AAA protease 1” (OMA1), hold by stomatin-like protein 2 (SLP2) acting as scaffold protein [69]. Participation of PARL in this complex allows for its regulation and has been shown to facilitate cleavage of its substrate PINK1. Interestingly, a special protein sorting mechanism associated with PARL has been discovered for PARL substrate STARD7. STARD7 is dually localized in the cytosol and the IMS. For both locations, STARD7 first needs to enter mitochondria and encounter PARL-cleavage during its maturation process. It was discovered that PARL seems to recognize a negatively charged amino acid patch only a few residues downstream of the PARL cleavage site of STARD7 and uses this negative stretch as sorting signal, since its mutation led to exclusive IMS localization. The same study showed that in case of PARL deletion, other proteases can take over to produce mature STARD7, however less efficiently [66]. The mechanism of STARD7 relocalization describes a novel kind of protein sorting during maturation mediated by PARL.

#### *Cleavage by AAA-proteases*

Although the IMMP1/2 complex and PARL are the most prominent proteases acting during protein import into the IMS, there are a few cases in which AAA-proteases (ATPases associated with diverse cellular activities) take over the second or even both cleavage steps during bipartite sequence dependent import. AAA-proteases are hexamers. In each subunit, the membrane-inserted domain is followed by a conserved ATPase domain, the AAA-domain and then by a conserved HExxH motif that serves as metal binding site and proteolytic center [70]. Besides those common features, there are two different types of AAA-proteases. The active center of *m*-AAA-proteases is facing the matrix, while the active center of *i*-AAA proteases is oriented towards the IMS (Figure 2, bottom right). In yeast, the *m*-AAA-protease is a complex that can be built up by Yta10 and Yta12 (belonging to the Yta family of ATPases), the human homologue can consist of ATPase family gene 3-like 2 (AFG3L2) and paraplegin [71]. Depending on the oligomeric composition, processing products can differ [72]. Yeast *m*-AAA-protease mediates Mgm1 (OPA1 homologue) cleavage after its MTS was removed by MPP and is involved in both cleavage steps during import of cytochrome *c* peroxidase (Ccp1) [72-74]. Interestingly, in addition to the *m*-AAA protease cleavage function, it was found to facilitate Pcp1 cleavage of Ccp1 by dislocating it from the IMM in an ATP-dependent manner in yeast. Hence, a novel mechanism of IMM proteases working together might have been discovered here [75]. The *i*-AAA protease is set up by Yme1 monomers in yeast and YME1L1 monomers in humans. As mentioned previously, Yme1/YME1L1 is mostly responsible for protein degradation in the IMS and found in a proteolytic hub together with PARL and OMA1. However, it has been shown that yeast Yme1 is the second enzyme after MPP cleaving polynucleotide phosphorylase (PNPase) during its maturation and import into the IMS, suggesting that Yme1 can also function in bipartite sequence driven protein import [76].

## Introduction

After the two described maturation steps carried out by 1) MPP and 2) IMMP1/2, PARL or an AAA-protease in the IMM, the IMS targeted protein is soluble in the IMS.

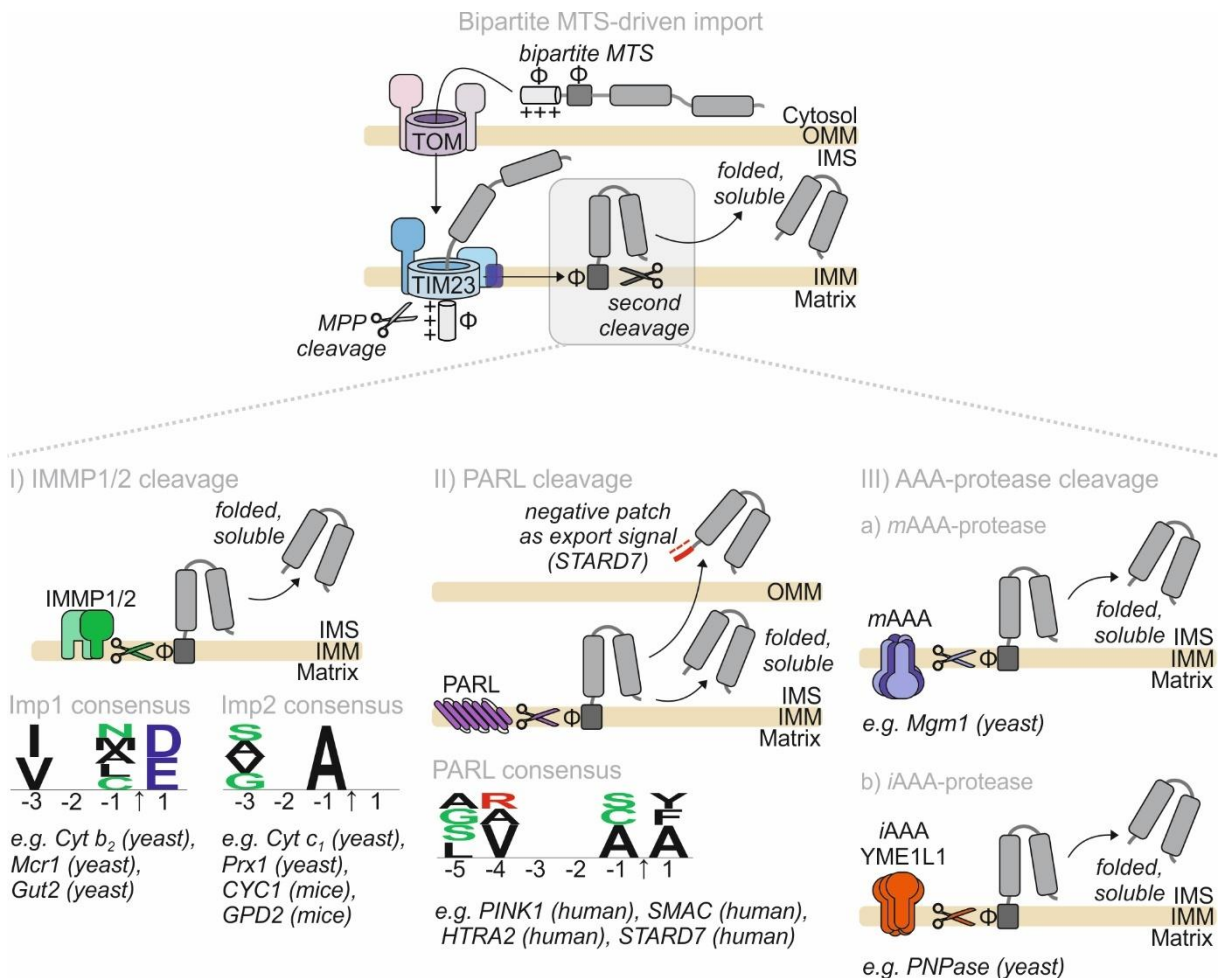


**Figure 2: Bipartite MTS-driven import into the IMS**

Protein precursors carrying a bipartite presequence for import first need to pass the TOM channel to enter mitochondria. Afterwards, they are translocated over the IMM by TOM23 until the hydrophobic stop-transfer signal stops translocation. MPP cleaves off the MTS part of the bipartite sequence. The hydrophobic domain downstream of the MTS is laterally released into the IMM and processed by different IMM proteases releasing a soluble IMS protein. Possible options are cleavage by IMMP1/2 (Imp1/2 in yeast) (I), by PARL (Pcp1 in yeast) (II) or an AAA-protease (III). I The IMMP1/2 complex is a heterodimer formed by IMMP1L (Imp1) and IMMP2L (Imp2). Preferences for Imp1 and Imp2 cleavage have been found in yeast and differ from each other [53-57]. II PARL (Pcp1) belongs to the rhomboid protease family. It is known to process important substrates like PINK1 or SMAC. A negative patch right after the bipartite sequence can act as an export signal after PARL cleavage, as it was shown for STARD7. A PARL consensus motif has been estimated by comparison of PARL substrates [65]. III AAA-proteases appear in two categories. The *m*-AAA-protease (a) is a heterohexamer with its active site facing the matrix. The *i*-AAA-protease, also known as YME1L1 (Yme1) (b), is a homohexamer with its active site facing the IMS. A consensus motif is not known yet [70].

### 1.2.2 Oxidation-dependent import

#### *Disulfide relay substrates*

About 50 of the around 150 IMS proteins known so far are imported into the IMS via the oxidative folding machinery of mitochondria, the disulfide relay, with its key players oxidoreductase mitochondrial import and assembly protein (MIA40) and sulfhydryl oxidase augments of liver regeneration (ALR), also called essential for respiration and viability 1 (Erv1) in yeast [77]. Disulfide

relay substrates are usually small proteins (maximum 20 kDa) with conserved cysteines that are arranged as twin CX<sub>3</sub>C or twin CX<sub>9</sub>C motifs. When folded, the proteins contain helix-loop-helix structures, in which the cysteines face each other and link the antiparallel helices, leading to a strong stabilization of the whole protein even in the reducing environment of the IMS [78, 79]. Besides that, non-classical substrates have been characterized that contain more complex disulfide arrangements or only use the disulfide relay for oxidative folding during or after import via a bipartite sequence. Examples for this special mechanistic combination are mitochondrial calcium uptake 1 and 2 (MICU1 and 2), ATP-binding cassette B8 (ABCB8) or ATPase 23 (ATP23) [80-82].

#### *Disulfide formation is important for structure and function*

The IMS is a compartment that hosts a high number of proteins that contain one or more disulfide bonds. They are involved in nearly all aspects of mitochondrial functioning and most of them are – or are predicted to be – substrates of the disulfide relay (Figure 3) [79, 83]. In a protein, disulfide bonds can have two purposes: they are either structural or functional.

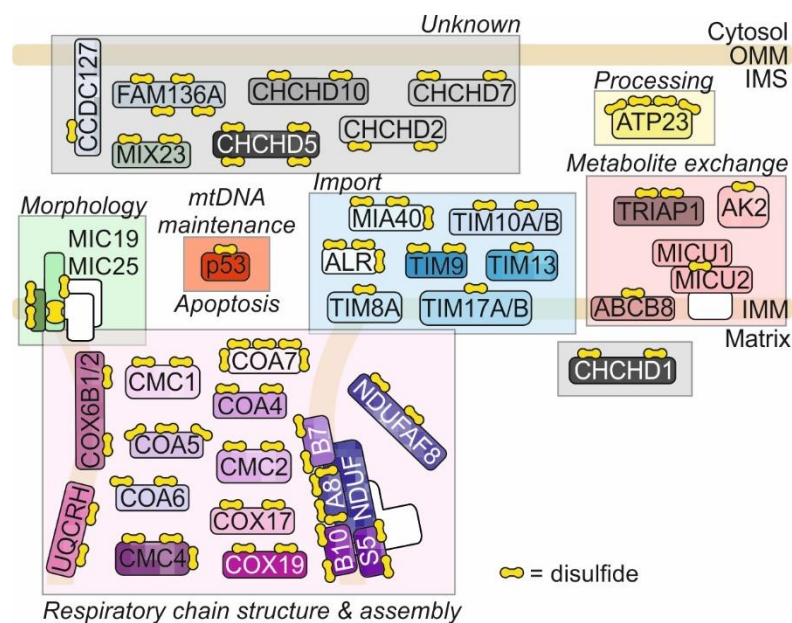


*Figure 3: Many disulfide containing proteins in the IMS undergo oxidation-dependent import*

The IMS hosts many different proteins that undergo or are predicted to undergo oxidation-dependent import. They contain one or more disulfides that are essential for their structure and function [83, 84]. Their functions include mitochondrial morphology, metabolite exchange, respiratory chain structure and assembly, protein import and processing. The function of some of these proteins are however still unknown.

Structural disulfides enhance the thermodynamic and mechanic stability of a protein as they help to keep it in a folded state [85]. Because of this, structural disulfides are often found inside of protein structures and do not undergo any modification or redox reaction. Structural disulfide-containing proteins are usually less temperature sensitive and less aggregation prone as they have lower susceptibility to denaturation and are less prone to be degraded. Structural disulfides can also exist across different subunits of a multimeric protein and hence support oligomerization, like it has been

## Introduction

shown for MICU1 and 2 or for ALR [81, 86]. In contrast, functional disulfides are less stable and easily accessible so they can participate in thiol-disulfide exchange reactions, which are necessary for redox-active proteins that are for example involved in catalysis or oxidative stress response [87].

### *MIA40 oxidizes precursors during import*

Like most other mitochondrial proteins, disulfide relay substrates are translated by cytosolic ribosomes and enter the mitochondria via the TOM complex in the OMM (detailed description in section 1.2.1). Similar to proteins with bipartite presequence, there is no defined recognition site known that targets precursors to TOM. They are either synthesized near the TOM pore or hold in an unfolded state and guided there by HSP70, HSP90 and HSP40 [88, 89].

After passing the TOM channel, precursors encounter the MIA40 (Figure 4 A). MIA40 is an oxidoreductase with chaperoning function [90]. Like many of its substrates, MIA40 contains a twin-CX<sub>9</sub>C motif located in a compact core domain and can also use the disulfide relay for import [91]. Yeast Mia40 is membrane anchored, whereas human MIA40 is in a complex with the membrane-bound apoptosis-inducing factor mitochondria-associated 1 (AIFM1), building a platform for protein import [92-94]. During import, MIA40 first acts as a receptor and initially binds the substrates via hydrophobic interactions. Substrates possess a mitochondrial IMS sorting sequence (MISS), also called IMS targeting signal sequence (ITS), a hydrophobic motif with which they can interact with a hydrophobic groove on the surface of MIA40's core domain [95, 96]. Interaction between the protein precursor and MIA40 aligns the correct substrate cysteines with the redox-active CPC-motif found at the active site of MIA40. Substrate cysteines have a hydrophobic environment, making them more reactive [97]. Together with the correct positioning, this allows for a nucleophilic attack on MIA40's CPC-motif resulting in a mixed disulfide intermediate between substrate and C55 in MIA40. The mixed intermediate is then resolved by a second nucleophilic attack by another substrate cysteine, leaving a reduced MIA40 and an oxidized substrate that is now trapped in the IMS [98-100]. If the interaction between the substrate and MIA40 does not result in productive oxidation, the mixed disulfide is resolved by MIA40's C53 and the unfolded protein is released back to the cytosol and degraded by the proteasome [98]. Importantly, the hydrophobic substrate-binding pocket of MIA40 is not only important for correct positioning of cysteines to prime the substrate for oxidation, but also mediates MIA40's chaperone-like activity by helping proteins fold [90, 96]. The three MIA40 functions as import receptor, oxidoreductase and chaperone can be exerted independent from each other. An illustrative example is the import and oxidative folding of ATP23. ATP23 is imported into the IMS in a MIA40-dependent manner, however this import is independent of its ten cysteines. Once inside the IMS, it is thought to interact with several MIA40 proteins at the same time to promote oxidation and folding [82].

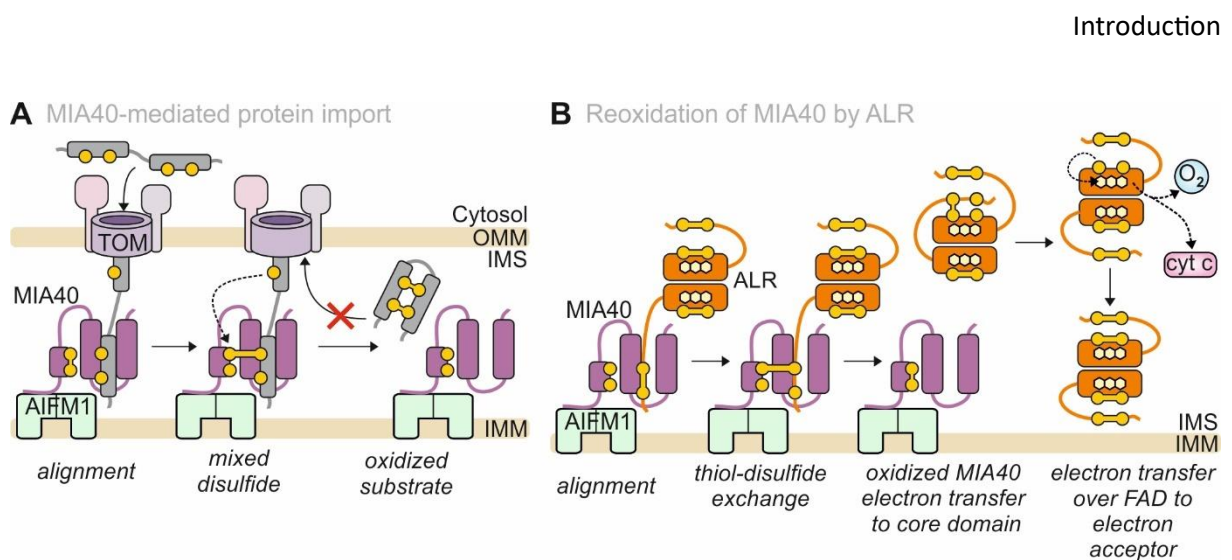


Figure 4: The disulfide relay

**A** Disulfide relay substrates contain conserved cysteines. During import, they pass the TOM channel and align in the hydrophobic groove of MIA40 via their MISS. Cysteines are coordinated in a way that a nucleophilic attack by a substrate cysteine leads to formation of a mixed disulfide. This intermediate is resolved by a second substrate cysteine, leaving MIA40 reduced and the substrate oxidized [95, 97]. **B** MIA40 is reoxidized by ALR. The distal disulfide of ALR aligns at MIA40's hydrophobic groove instead of a substrate to position cysteines for a thiol-disulfide exchange reaction. MIA40 is oxidized again. By clapping over its N-terminal arm to the other subunit, ALR shuttles the excess electrons to the core disulfide. From there they are transferred onto the final electron acceptor over the FAD cofactor. Cytochrome c (cyt c) is preferred, however molecular oxygen can be used too [101-105].

#### ALR reoxidizes MIA40

After oxidizing a substrate, the CPC motif in MIA40 is present in a reduced state and needs to be reoxidized for the next substrate interaction. This “regeneration” of MIA40 is mediated by ALR (Figure 4 B). ALR is a dimer. Each monomer consists of two domains, a core domain, and an 80 amino acid long N-terminal disordered domain. The core domain is a four-helix-bundle holding an flavin adenine dinucleotide cofactor (FAD). A fifth small helix adjacent to the adenine moiety of the FAD cofactor stabilizes its non-covalent binding. Additionally, there is a structural disulfide between C171 and C188 and a redox-active CEEC (C142-C145) motif that is located close to the FAD cofactor directly interacting with its isoalloxazine ring, enabling *de novo* disulfide bond formation. Dimerization of two subunits is mediated by hydrophobic interactions between the two core domains and further helped by two intermolecular disulfides between C95 of one and C205 of the other monomeric subunit. The N-terminal disordered domain contains another distal redox-active disulfide motif CRAC (C71-C74) [86, 102, 105, 106]. To interact with MIA40, one of the N-terminal “shuttle arms” of ALR non-covalently binds to the hydrophobic groove in MIA40 instead of a substrate. A nucleophilic attack on the oxidized CRAC motif originates from MIA40's C55, initiating a thiol-disulfide exchange similar to the one described for MIA40 and its substrates. In the end of this reaction, MIA40 is oxidized and the CRAC motif of ALR reduced [101, 107, 108]. In order to reoxidize the CRAC motif, the shuttle arm reaches over to the second ALR subunit and shuttles electrons onto the core CEEC motif of this subunit in another thiol-exchange reaction. The close proximity to the FAD cofactor allows reoxidation of the CEEC motif resulting in reduced FADH<sub>2</sub>. To reoxidize FADH<sub>2</sub>, electrons are transferred to oxidized cytochrome

## Introduction

*c* in a collision-type mechanism and finally fed into the respiratory chain (complex IV). ALR can also directly use molecular oxygen as electron acceptor, but cytochrome *c* is preferred to avoid formation of ROS [101-104]. In yeast, fumarate reductase Osm1 (osmotic sensitivity 1) has been found to act as anaerobic electron acceptor for Erv1 [109]. However, for humans such a mechanism has not been described and might not be relevant.

### 1.2.3 Affinity-driven import

A third possibility for protein import into the IMS besides bipartite sequence- and oxidation-driven import is affinity-driven import. Here, proteins use features like hydrophobic patches or conserved cysteines to interact with receptors inside the IMS (Figure 5). The different mechanisms belonging to the group of affinity-driven import are heterogenous and comparatively slow.

As mentioned previously, MIA40 can be imported by itself in the disulfide relay, however, another import pathway is preferred. An N-terminal unstructured region of MIA40 interacts with dimerized AIFM1 driving MIA40 import [84, 110]. After import, MIA40 remains in a complex with the AIFM1 dimer. MIA40 import is very slow, meaning that the MIA40 precursor spends a lot of time in the cytosol in an unfolded state and needs to be stabilized. MIA40's negatively charged C-terminus protects it from proteasomal degradation in the cytosol to allow for import of sufficient amounts of MIA40 into the IMS [110].

Cytochrome *c* needs cytochrome *c* heme lyase (CHL) for its import. It enters the IMS in an unfolded state and interacts with CHL in a non-covalent manner via parts of its N- and C-terminus. During cytochrome *c* folding, the heme cofactor is incorporated, a process that is important for cytochrome *c* stability. Deletion of CHL results in accumulation of the cytochrome *c* precursor in the cytosol [111-114].

Another example for affinity-driven import into the IMS are superoxide dismutase 1 (SOD1) and copper chaperone for SOD1 (CCS1). Both proteins rely on a CCS1-dependent pathway for import [115-117]. Mature CCS1 in the IMS acts as a receptor and folding interface for the CCS1 and SOD1 precursors. Both proteins acquire a disulfide bond during the import process, which is suggested to be at least partially dependent on local ROS levels.

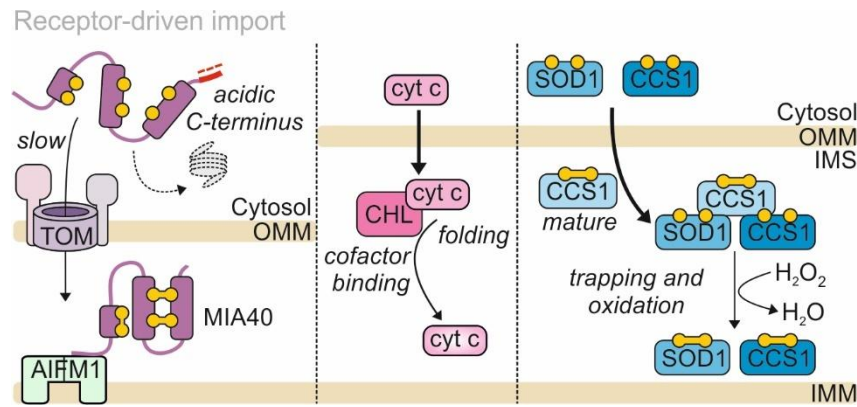


Figure 5: Receptor-driven import

MIA40, cytochrome c, SOD1 and CCS1 are examples for receptor-mediated IMS import. MIA40 is imported with help of the AIFM1 dimer. Cytochrome c uses CHL as IMS receptor. SOD1 and CCS1 both need oxidized CCS1 in the IMS to be imported. It acts as folding interface and the imported SOD1 and CCS1 both gain a disulfide bond.

### 1.3 Protein functions in the IMS

#### *The IMS is a hub for logistics*

The IMS is a crucial subcompartment for mitochondrial functions as it serves as a platform for important processes and harbors proteins with diverse roles. Due to its location between outer and inner membrane, it mediates the exchange with the mitochondrial matrix, but also communicates with the remainder of the cell over the OMM (Figure 6). For this reason, it can be seen as a logistic hub.

One important aspect in the context of logistics is the role of the IMS in protein distribution (Figure 6 A). It is involved in mitochondrial protein import, sorting, and degradation. Detailed aspects of protein import and folding in the IMS itself have been described in section 1.2. Besides its role in bipartite sequence-, oxidation-, and affinity-driven import, it is a stopover for matrix-localized proteins with classical MTS, and for precursors of membrane embedded proteins. Folding and membrane insertion of  $\beta$ -barrel proteins of the outer membrane is mediated by the SAM complex [118, 119]. Metabolite carriers residing in the IMM are inserted by the TIM22 complex [120, 121]. Precursors of both pathways are targeted to their respective insertion complexes by the chaperone system of the IMS, the small TIM proteins. Most work on this system has been done in yeast, showing that Tim9/Tim10 and Tim8/Tim13 form soluble hexamers that bind to the incoming precursors and escort them to SAM or TIM22 by using tentacle-like structures to keep them in an unfolded state [121-124]. When chaperoning systems or import pathways in the IMS fail and proteins misfold, they are degraded by IMS proteases like *i*-AAA-protease YME1L1 or HTRA2 to prevent aggregation and accumulation in the IMS [82, 125-130].

The IMS is not only involved in protein sorting, but also in the assembly of protein complexes (Figure 6 A). Respiratory chain complexes have a large number of subunits and cofactors that need to be coordinated for their correct assembly [131]. Complex I assembly is highly orchestrated with small NADH:ubiquinone oxidoreductase subunits (NDUFs) like NDUF5, NDUFB7 and NDUFB10 playing an

## Introduction

important role [94, 132]. Furthermore, some of the later steps of complex III assembly, like the attachment of cytochrome  $c_1$ , happen from the IMS site. Proteins like CX<sub>9</sub>C motif containing 1 (CMC1) stabilize the forming complex IV and cytochrome c oxidase copper chaperones COX11 and COX17 mediate copper insertion [133]. The MICOS complex is essential for mitochondrial morphology and consequently mitochondrial function. Its assembly is dependent on the IMS, as all subunits of MICOS need to be imported crossing the IMS and MICOS assembles on the IMS site of the inner membrane [134]. Another complex, which is formed in the IMS, is the mitochondrial calcium uniporter (MCU) that transfers calcium across the IMM [81].

Exchange between the IMS and the cytosol is mediated by voltage-dependent anion channels (VDACs) that let small ions and metabolites cross the OMM [19, 20]. VDACs are  $\beta$ -barrel proteins appearing in three isoforms (VDAC1,2 and 3) that let pass many different molecules. However, they are regulated and have a certain kind of selectivity. In general, their size does not allow molecules larger than 4 kDa to pass the channel. VDACs can be in a high conductance state with preference for anions or in a low conductance state with preferences for cations, for example calcium ( $\text{Ca}^{2+}$ ). The high conductance state is also the one allowing for rapid flux of ATP/ADP [19, 135, 136]. Besides that, more specialized transporters for important metabolites and cofactors like iron, porphyrins or iron-sulfur clusters have been identified [137-139].

The IMM on the other hand is much more selective in terms of permeability and contains a lot of different specialized carriers and transporters (Figure 6 A). The largest group of solute carriers and transporters in the IMM are proteins of the SLC25 family that transport all kinds of soluble molecules. The most prominent example is the ATP/ADP carrier that exports ATP from and imports ADP to the matrix. Other SLC25 family members mediate transport of amino acids like glutamate and aspartate, glycine, or arginine, transport inorganic ions like phosphate and many more [22, 140, 141]. A lot of these transport processes mediated by SLC25 proteins and other carriers are symports or antiports, which means that two different metabolites are exchanged simultaneously in the same direction or exchanged against each other. A well characterized example is the malate-aspartate shuttle, which serves to export oxaloacetate from the matrix to the IMS and ultimately the cytosol and to "import" NADH from cytosol to matrix. As there is no oxaloacetate carrier in the IMM, conversion to aspartate is used for export and conversion to malate to bring an  $\text{NAD}^+$  reducing factor into the matrix [142]. Another relevant group of metabolites crossing the IMS are metal ions, especially copper and iron. As mentioned previously, copper can be bound by the IMS proteins CCS1 and COX17 that shuttle it to SOD1 or complex IV, controlling copper levels and distribution of copper in the whole cell [143]. Iron is transported over the IMM to the matrix by mitoferrin (MFRN) 1 and 2 [139, 144, 145]. In the matrix, it is used for iron-sulfur cluster and heme biosynthesis. Both metabolites are exported into the IMS and

then into the cytosol after synthesis. Iron-sulfur clusters are exported from the matrix via ATP-binding cassette sub-family B member 7 (ABCB7) [146, 147], whereas heme is likely exported by feline leukaemia virus subgroup C receptor 1b (FLVCR1b) [138, 148]. Although it is not clear yet whether FLVCR1b is in the OMM or the IMM, it is predicted to contain an MTS.

Apart from small ions and metabolites, also lipids are transferred between the two mitochondrial membranes over the IMS. The lipid composition of both mitochondrial membranes is tightly regulated and crucial for mitochondrial function as it determines membrane architecture. Cardiolipin, phosphatidic acid, phosphatidylethanolamine, and phosphatidylinositol travel between the two mitochondrial membranes. Precursors for lipid synthesis like phospholipids, sphingolipids and cholesterol have to be imported into mitochondria from the cytosol and are transferred to the IMM via the IMS. These transfer processes are mediated by lipid-binding proteins or membrane contact sites [149, 150].

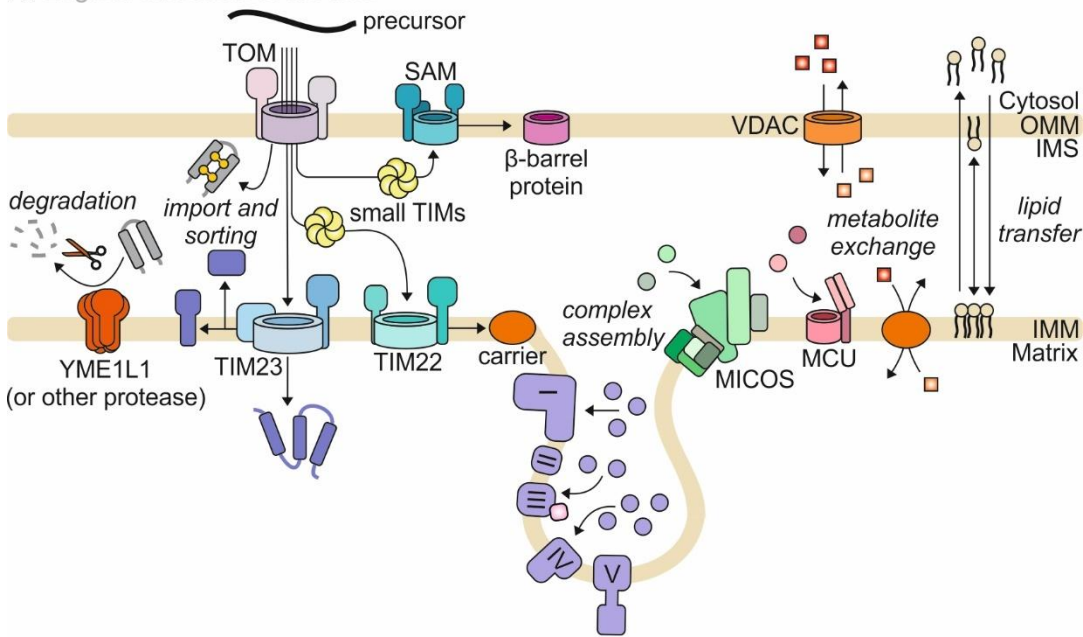
#### *Signaling from and through the IMS*

Due to its position, the IMS connects matrix and cytosol and is therefore an important signaling compartment (Figure 6 B). It integrates calcium signaling via the IMM spanning calcium uniporter MCU and its regulatory subunits MICU1, MICU2 and MICU3. Calcium can come from extracellular influx or from the endoplasmic reticulum (ER). When calcium levels in the cytosol rise, mitochondria can take up calcium to buffer cellular calcium levels. Calcium enters mitochondria over VDAC, where the MICUs sense and modulate MCU activity accordingly [6, 81, 151, 152]. Moreover, the IMS is part of cell death networks. When cell death is activated upon various stimuli like DNA damage, ER stress or growth factor deprivation, the OMM becomes permeabilized for proapoptotic factors that are released from the IMS. These factors include cytochrome c, Smac/DIABLO and HTRA2 [153] and their release goes along with cristae remodeling [154, 155]. In the IMS, significant amounts of ROS are generated. They either come from respiratory chain complexes releasing it into the cristae lumen, or from the peripheral IMS, where ROS is produced by NADPH oxidase 4 (NOX4), monoamine oxidases, p66shc and coproporphyrinogen oxidase (CPOX) [156-160]. The most abundant kind of ROS produced in the IMS are superoxide anions, which are converted to H<sub>2</sub>O<sub>2</sub> by SOD1. Notably, H<sub>2</sub>O<sub>2</sub> is toxic in higher concentrations and therefore can trigger apoptosis. However, H<sub>2</sub>O<sub>2</sub> also acts as an important signaling molecule that is released from the IMS at lower concentrations [14, 29]. Leaving the IMS, H<sub>2</sub>O<sub>2</sub> posttranslationally modifies thiols in different proteins to modulate their activity for metabolic adaptation. This involves activation or inhibition of cytosolic signaling proteins, activation of transcription factors that regulate production of anti-oxidant proteins and activation of proteins directly involved in redox homeostasis [161]. In addition, H<sub>2</sub>O<sub>2</sub> signaling induces a metabolic switch to enhance NADPH regeneration [162]. Within the IMS, H<sub>2</sub>O<sub>2</sub> can modulate proteins by oxidation of

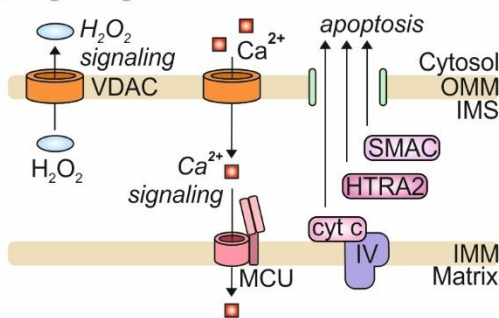
## Introduction

cysteines to form disulfide bonds, a process that has been observed for example for complex I subunits and that has been suggested to happen during import of CCS1 and SOD1 [117, 163].

### A Logistic functions in the IMS



### B Signaling in the IMS



### C Metabolism in the IMS

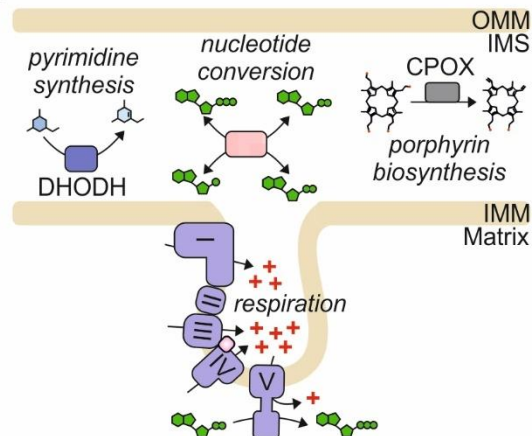


*Figure 6: Functions of IMS proteins*

**A** The IMS has important logistic functions. IMS proteins mediate protein import and sorting via TOM and TIM23, TIM22, SAM or MIA40 dependent import. Small TIMs help SAM and TIM22 substrates reaching their destination. Degradation of IMS proteins is controlled by different IMS or IMM proteases, for example YME1L1. Further, important protein complexes are assembled in the IMS. IMS proteins participate in assembly of the respiratory chain, the MICOS complex and the calcium transporter MCU. Metabolite and ion exchange is another process supported by the IMS. Lipids have to cross the IMS to traffic between IMM and OMM. This is important to maintain the correct lipid composition of both membranes. **B** The IMS has crucial functions for signaling. It integrates calcium signals from the cytosol and exports  $H_2O_2$ , which is produced in mitochondria and serves as signaling molecule in the cytosol. Besides that, it releases proapoptotic factors like cytochrome c, SMAC or HTRA2 upon strong cellular stresses to initiate cell death. **C** The IMS serves as a platform for metabolic processes. The cristae lumen as separated reaction room is essential for respiration. Additionally, nucleotide conversion steps happen. The IMS proteins AK2 and mCK convert nucleotides to support energy homeostasis. Lastly, IMS proteins catalyze single steps of complex biosynthesis pathways spanning multiple (sub-)compartments. For example, DHODH is involved in pyrimidine synthesis and CPOX is an enzyme of the porphyrin biosynthesis. Adapted from [164].

### *Metabolic processes in the IMS*

IMS proteins contribute to many metabolic pathways (Figure 6 C). One that has been mentioned many times in previous sections is of course the respiratory chain. Respiratory chain complexes reside in the cristae membrane and establish the proton gradient that is required for ATP production. The cristae lumen thereby hosts the protons. IMS proteins contribute to respiration by being part of respiratory complexes, shuttling electrons from complex III to IV (cytochrome c) or by feeding electrons into the respiratory chain [131, 132]. Glycerol-3-phosphate dehydrogenase (GPDH) transfers electron to ubiquinone, whereas ALR and sulfite oxidase (SUOX) transfer electrons to cytochrome c [101, 165-167]. Another important aspect of energy metabolism happening in the IMS is nucleotide conversion. Adenylate kinase 2 (AK2) recycles AMP with ATP to two ADP or converts two ADP to ATP and AMP and helps diffusion of adenine nucleotides in the cell [168, 169]. Mitochondrial creatine kinase (mCK) catalyzes a transphosphorylation reaction between creatine and ATP to produce phosphocreatine and ADP. One purpose of this reaction is to keep ATP to ADP ratio in mitochondria low to stimulate oxidative phosphorylation [170, 171]. Nucleoside-diphosphate kinase NME4/NDPK-D reversibly generates NTP and ADP from ATP and NDP [172]. Nucleotide conversion by these enzymes not only balances energy metabolism in mitochondria, but also regulates nucleotide exchange over the IMM and ensures activity of enzymes that use nucleotides as cofactor. Moreover, the IMS hosts single steps of multistep metabolic pathways that span over several compartments. SUOX acts in the end of degradation of the sulfur-containing amino acids methionine and cysteine [173]. Dihydroorotate dehydrogenase (DHODH) sits in the IMM facing the IMS and catalyzes the conversion of dihydroorotate to orotate during the de novo synthesis of pyrimidine [174]. Important is also IMS protein CPOX, which catalyzes the third last step in heme biosynthesis [5, 160].

## 1.4 Heme biogenesis

### 1.4.1 The essentiality of heme

The synthesis of heme, a protoporphyrin IX iron complex, is crucial for most organisms as heme is an essential cofactor for a variety of proteins and also an important signaling molecule. The group of hemoproteins is heterogenous with functions ranging from electron transfer to binding of gases [5]. A vital group of hemoproteins are globins. In the most prominent member of this family, hemoglobin, heme coordinates molecular oxygen and therefore enables its binding and transport. Cytochromes are another example for highly relevant proteins with a heme cofactor. Here, heme is important for electron transfer as the bound iron ion can shift between an oxidized ( $\text{Fe}^{3+}$ ) and a reduced ( $\text{Fe}^{2+}$ ) state [175]. Other hemoproteins are catalase and other types of peroxidases, and nitric oxide synthase (NOS). Catalase is one of the key antioxidant enzymes and detoxifies  $\text{H}_2\text{O}_2$  by decomposing it to water and molecular oxygen, a process that is enabled by the heme cofactor [176]. Other peroxidases also

## Introduction

bind a heme cofactor to reduce  $H_2O_2$  and catalyze oxidative reactions [177]. NOS produces nitric oxide (NO), an important cellular signaling molecule, for instance being involved in regulation of translation and posttranslational modifications [178, 179]. Moreover, heme is needed for respiration. Succinate dehydrogenase (Complex II) and all subunits of complex III have a heme cofactor. As member of the heme-copper oxidase superfamily, cytochrome c oxidase (complex IV) contains two heme groups, one associated to subunit COX1, the other to COX2 [180, 181]. Its cytochrome c oxidase assembly factor 7 (COA7) is also a heme-binding protein important for copper regeneration [182]. As signaling molecule, heme directly controls translation, translocation and assembly of proteins involved in oxygen sensing and impacts cell growth and differentiation, erythropoiesis, and neurogenesis. It also indirectly regulates protein activity by binding the iron regulatory protein (also called iron responsive protein; IRP) [148, 183, 184].

### 1.4.2 Heme biosynthesis

Heme biosynthesis is a complex multistep pathway. It comprises eight steps, which are performed in mitochondria and the cytosol (Figure 7 A, C). Heme biosynthesis does not only significantly contribute to diverse cellular functions, but is also an important factor in iron homeostasis, while producing potentially toxic intermediates. Therefore, it is regulated at different steps of the pathway.

#### *Step1: ALAS catalyzes the rate-limiting step of heme biosynthesis*

Heme biosynthesis starts in the mitochondrial matrix. Here, 5-aminolevulinic acid synthase (ALAS) condensates succinyl-CoA and glycine to 5-aminolevulinic acid (5-ALA). This reaction requires pyridoxal 5'-phosphate (PLP) as cofactor. Glycine can enter the matrix via SLC25A38 in the IMM, succinyl-CoA is already present in the matrix and comes from transformation of  $\alpha$ -ketoglutarate or succinate (Figure 7 A, C) [185-187]. ALAS is a highly conserved enzyme in nearly all organisms as it catalyzes the first biosynthesis step for all tetrapyrroles [5]. ALAS form a homodimer and appears in two isoforms in mammals. ALAS1 is ubiquitously expressed while ALAS2 is found exclusively in erythrocytes [188]. The production of 5-ALA by ALAS is considered the rate-limiting step of heme biosynthesis and is tightly controlled via different mechanisms. ALAS is regulated on a transcriptional and translational level. The ALAS1 promotor contains several regulatory elements. It has two nuclear respiratory factor 1 (NRF1) binding sites, two cAMP-responsive elements. Binding of the respective molecule can stimulate ALAS1 transcription and is influenced for example by oxidative stress or insulin levels [189-193]. Transcription of ALAS2 is only activated during erythroid cell differentiation. The ALAS2 promotor contains binding sites for erythroid-specific transcription factors, for example GATA binding factor 1 (GATA-1), erythroid Krüppel-like factor (EKLF) and nuclear factor erythroid 2 (NF-E2), but also for hypoxia inducible factor 1 (HIF-1) [194]. Apart from this, ALAS levels are also regulated on a translational level by iron. Iron responsive elements (IREs) have been identified and well characterized for the 5' untranslated region (UTR) of the ALAS2 mRNA [195-197], but the existence of a similar IRE on ALAS1 mRNA has been

suggested, too [198-200]. Under conditions of iron availability, IRE-binding protein 1 (IRP1) has aconitase activity whereas IRP2 is degraded. During heme deficiency, IRP1 loses its aconitase activity and IRP2 is stabilized so that both proteins can bind to the IRE on ALAS mRNA and prevent translation. Thereby, iron availability and porphyrin production can be coordinated [201]. Additionally, ALAS1 and ALAS2 are regulated on the protein level. They both contain a heme regulatory motif (HRM), which consists of three CP motifs. Two of them are localized in the ALAS MTS and one close to the N-terminus of the mature protein. Binding of heme to CP motif 1 and 2 impairs mitochondrial import of premature ALAS leading to degradation of the protein in the cytosol. CP motif 3 is still present in the mature ALAS protein. Binding of heme to this motif initiates ALAS degradation in the matrix by mediating its interaction with the protease CLPXP. For ALAS1, the protease LONP is also involved in heme-initiated degradation [201-206]. This system is very efficient, enabling extremely fast turnover of ALAS, which makes ALAS one of the proteins with the highest turnover rate in mitochondria [206, 207]. It constitutes an effective feedback regulation mechanism for ALAS depending on heme levels. Binding to the cofactor PLP causes structural changes in the ALAS active site allowing for substrate binding. In the ALAS1 homodimer, one PLP is bound, while ALAS2 has a PLP cofactor bound to both monomeric subunits. Therefore, PLP is crucial for ALAS function and might offer a second mode of ALAS regulation. It is not yet clear, how the cofactor insertion is mediated. In yeast, Hem1, the homologue of ALAS1, requires interaction with CLPX that acts as chaperone for efficient PLP incorporation. Additionally, PLP incorporation of Hem1 is dependent on a PLP transporter [208-210]. In vertebrates, PLP binding to ALAS has not been studied yet, but it could be an additional target of ALAS regulation.

#### *Steps 2-5: The cytosolic part of heme biosynthesis*

After ALAS catalyzed the production of 5-ALA in the mitochondrial matrix, heme biosynthesis continues in the cytosol. Here, ALA dehydratase (ALAD), also known as porphobilinogen synthase (PBGs), mediates the condensation of two 5-ALA molecules to one porphobilinogen (PBG), a monopyrrole (Figure 7 A, C). To reach ALAD, 5-ALA needs to cross IMM and OMM. A transporter for 5-ALA is not known yet, but one study suggests ABCB10 as transporter for 5-ALA over the IMM, as it has been shown to influence 5-ALA levels in the cytosol [211]. Still, it could not yet be experimentally proven that ABCB10 does transport 5-ALA [212]. SLC25A39 in the IMM has also been found to somehow influence heme metabolism, most likely at earlier stages of the heme biosynthesis pathway, however a direct connection or a specific substrate have not been shown [213]. Like ALAS, ALAD is evolutionary well conserved. It forms a homooctamer and needs a zinc ion for proper function [214]. For the cytosolic heme biosynthesis enzymes, distinct regulation mechanisms are not known. Nevertheless, ALAD is an iron-sulfur cluster containing enzyme whose activity is reduced upon loss of its iron-sulfur cluster presenting a link between general iron availability and ALAD activity [215]. After PBG synthesis, porphobilinogen deaminase (PBGD), also called hydroxymethylbilane synthase (HMBS), catalyzes the

## Introduction

synthesis of the linear tetrapyrrole hydroxymethylbilane (HMB). It is assembled by head-to-tail synthesis of four PBG molecules during which four molecules of ammonium are released (Figure 7 A, C). For synthesis of HMB, PBGD uses dipyrromethane as cofactor and foundation to build the tetrapyrrole on [216, 217]. Cyclisation of the linear HMB is mediated by uroporphyrinogen synthase (UROS) to form the asymmetric tetrapyrrole ring uroporphyrinogen III (UPPIII). The cyclisation process also involves an intramolecular rearrangement of the fourth ring (D) of the tetrapyrrole (Figure 7 A, C). UPPIII is the last universal intermediate, which can also be used for synthesis of other tetrapyrroles. When UROS activity is low, UPPIII can also spontaneously cyclize without inversion of the fourth ring, leading to uroporphyrinogen I, a molecule that cannot be used for heme biosynthesis [5, 148, 216, 217]. The homodimeric enzyme uroporphyrinogen decarboxylase (UROD) then sequentially decarboxylates the four carboxyl groups of the carboxymethyl side chains of each ring in UPPIII. By this, coproporphyrinogen III (CPPgenIII) and four molecules carbon dioxide are produced (Figure 7 A, C) [148, 217].

### *Step 6: CPOX continues heme biosynthesis in the IMS*

The next enzyme coproporphyrinogen oxidase (CPOX) catalyzes the third last step of heme biosynthesis. CPOX enters mitochondria via a bipartite sequence and is found soluble in the IMS, although over the years, there have been some suggestions that it might be loosely associated to the IMM or even remain bound to the IMM via the transmembrane domain upstream of its MTS [4, 202, 218-221]. To reach CPOX, its educt CPPgenIII is transported into mitochondria by an unknown mechanism. Eventually, import is mediated by ATP-dependent transporter ABCB6 as it was found to be necessary for proper heme biosynthesis and isolated mitochondria lacking ABCB6 could no longer import CPPgenIII [137, 222, 223]. Once CPPgenIII is in the IMS, it is converted to protoporphyrinogen IX (PPgenIX) by oxidative decarboxylation of two propionate side chains, one from ring A and one from ring B, to form vinyl groups. The decarboxylation happens stepwise via transient formation of the 3-carboxyl intermediate harderoporphyrinogen [224, 225]. For each decarboxylation step one molecule of molecular oxygen is required and one carbon dioxide molecule is produced. The reaction also sets free in total four electrons that most likely use molecular oxygen as acceptor leading to H<sub>2</sub>O<sub>2</sub> formation (Figure 7 A, C) [226-228]. No concrete mechanism has been identified so far for this complex reaction, however, there have been some theories around. CPOX consists of a flat seven-stranded  $\beta$ -sheet structure sandwiched from the top and bottom by  $\alpha$ -helices [228]. The active CPOX enzyme forms a homodimer, which is connected over a hydrophobic interface and hydrogen bonds. One monomer is rotated by 40° towards the second and each monomer contains an independent active site inside an electropositive cleft, which is imagined to be closed by two helices at the entrance, leaving a separated reaction room where a CPPgenIII molecule could fit in. Residues of the dimer interface and the cleft are conserved and most likely dimer interface residues influence the active site cleft as they are close

to these residues. A failure to dimerize would destabilize the active site conformation [227]. The crystal structure of human CPOX has a citrate bound in the proposed active site. With a total of three carboxyl groups, citrate is thought to mimic CPOX' substrate CPPgenIII with four carboxyl groups, hence revealing potential residues mediating substrate recognition and binding. It has been suggested that R262 mediates substrate recognition and H258 most likely forms a catalytic dyad with D282. Mutation of H258 to alanine in mice completely abolished CPOX function. Other possibly involved residues in the active site mediating substrate recognition and decarboxylation are S244, N260 and R332 as well as G406 and L407, which are thought to be relevant for correct substrate orientation [228]. Other studies showed that residues D400, R401, G402, T403 and K404 might play a role for the second decarboxylation step of harderoporphyrinogen (Figure 7 B) [229, 230]. The reaction that CPOX catalyzes must require a strong stereoselectivity, hence indicating a strictly constrained orientation of the substrate in the active site. Interestingly, it has been proposed that both decarboxylation steps of the reaction take place at the same active center, meaning that the harderoporphyrinogen intermediate would need to turn 90° counterclockwise in the cleft where the active site is located [228, 231]. It is not clear if such a turn would be possible inside a space limited area like the CPOX active center, however, porphyrins are very flexible and can switch between many conformations [232]. A regulation mechanism on protein level, for example during mitochondrial import like for ALAS, can be imagined, but no experimental evidence on the CPOX import mechanism or regulation exists yet [208]. However, CPOX is regulated on a transcriptional level. In non-erythroid cells, the CPOX promotor contains different binding sites involved in regulation of CPOX transcription. There are CACCC sites, a so-called CPRE element, an SP-1-like element and binding sites for CCAAT/enhancer-binding proteins (C/EBPs), which all regulate CPOX transcription upon binding of the respective transcription factors [233]. In erythroid cells, there are additional regulation motifs like GATA-1 binding sites [234]. CPOX seems to be especially important during cell differentiation, as it is strongly upregulated in differentiating cells and erythroid cells seem to have a higher demand for CPOX than other cell types, as they have more regulatory elements for this gene [234, 235]. For the yeast homologue of CPOX, Hem13, studies also show a transcriptional upregulation under heme-deprived conditions [236, 237]. Additionally, one study showed disturbed import of human CPOX into isolated rat mitochondria in presence of 20  $\mu$ M hemin, suggesting a heme-based regulation of CPOX import [238].

#### *Steps 7 & 8: The last steps of heme biosynthesis in the mitochondrial matrix*

In the penultimate step of heme biosynthesis, PPgenIX is oxidized to protoporphyrin IX (PPIX) by protoporphyrinogen oxidase (PPOX) under the use of three molecules of molecular oxygen and generation of three molecules  $H_2O_2$  (Figure 7 A, C). PPOX forms a homodimer with one FAD cofactor bound per subunit [239, 240]. The enzyme has a predicted internal MTS and a membrane binding region and associates to the inner membrane. Although it is under debate whether PPOX is found at

## Introduction

the IMS or the matrix site of the IMM, the most recent study suggests that it is bound to the IMM from the matrix side [4, 202, 241]. This means PPgenIX needs to cross the inner membrane. Proposed transporters for this matrix import of PPgenIX are the adenine nucleotide translocator (ANT) and the IMM transporter transmembrane protein 14C (TMEM14C). It was shown that mitochondrial ADP uptake was inhibited by heme, whereas PPIX uptake was inhibited by ADP, indicating a role for ANT in porphyrin transport over the inner membrane [242]. This seems contradictory to the proposed PPOX localization to the matrix site of the IMM, but possibly, ANT might also be able to transport PPgenIX. Besides that, PPIX levels and heme levels were found to be reduced in TMEM14C deficient murine erythroleukemia (MEL) cells whereas CPPgenIII accumulated, hinting at its function in transport of PPgenIX [243]. Not much is known about control of PPOX, however, a study in vertebrate erythroid cells demonstrated that PPOX activity is decreased in absence of CLPX [205]. The last step of heme biosynthesis is the insertion of ferrous iron into the PPIX ring by ferrochelatase (FECH) making it protoheme IX (heme b, the “common” heme) (Figure 7 A, C). Two protons are removed during iron insertion. FECH is a dimer bound to the IMM from the matrix site and contains one iron-sulfur cluster per monomer. FECH binds PPIX in an enclosed pocket where its active site is located and a conserved histidine (H263 in human) has been suggested to be involved in iron binding [18, 244, 245]. As mentioned already in section 1.3, iron is delivered to FECH by the iron transporters MFRN1 and 2 [139, 144, 145]. For use outside of mitochondria, heme is then proposed to be exported by FLVCR1b [5, 138]. FECH is the other major enzyme regulated to finetune heme biosynthesis. Its activity strongly depends on iron availability. Not only is iron a substrate of the FECH reaction, but FECH activity is also significantly decreased when it cannot incorporate an iron-sulfur cluster whose synthesis also needs iron [246-248].

### 1.4.3 Trafficking of porphyrins across the cell

With progression of porphyrin biosynthesis, porphyrin intermediates become more and more hydrophobic (Figure 7 D). Free movement of these molecules through the cell is hardly possible as they are not soluble in aqueous environment and can intercalate with lipid bilayers leading to accumulation in membranes and toxicity for the cell [217, 249]. They are also highly reactive and might autoxidize depending on the species and their environment. Hence, porphyrin intermediates need to be transported efficiently from enzyme to enzyme during heme biosynthesis. The transport of heme biosynthesis intermediates over mitochondrial membranes has been described above (section 1.4.2), however, defined handover processes from enzyme to enzyme within the same compartment and chaperoning proteins binding free porphyrins might be required.

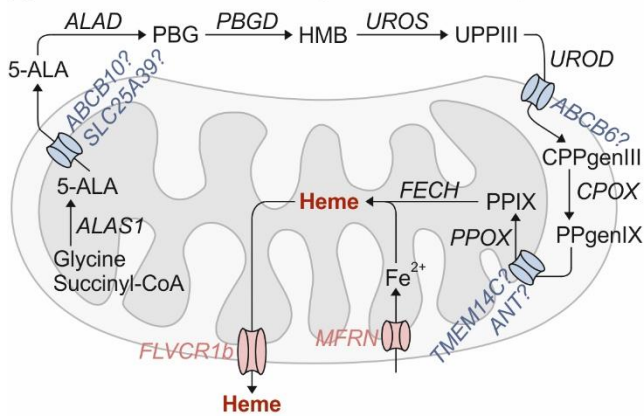
For heme, the last porphyrin in this row, it is known that due to its peroxidase activity and the potential of its iron to generate free radicals it is never actually free in the cell but bound to diverse chaperones

and heme-binding proteins [217]. For cytosolic heme, many heme-binding proteins (HBPs) and chaperones have been identified. These include 22 kDa HBP, (heme-binding protein 2) HEBP2, glutathione-S-transferase (GST), fatty acid-binding protein (FABP), PRX1, and glyceraldehyde phosphate dehydrogenase (GAPDH) [250-255]. Recent studies could show that PRX1 and GAPDH have dual roles, one of them being heme buffering or storage [254, 256]. A similar role in heme buffering can be suspected for the other HBPs although no data on this topic exists yet [257]. Interestingly, 22 kDa HBP binds to a wide range of porphyrin molecules [258] and also FABPs serve as chaperones for different hydrophobic ligands [259]. Consequently, there might be proteins that could hold and guide porphyrin intermediates during heme biosynthesis in the cytosol. The heme chaperone progesterone receptor membrane component 1 (PGRMC1) is localized not only in mitochondria, but also in the ER, nucleus, and cellular membrane, while the isoform 2 is in the ER [260-262]. Thus, it has been proposed that PGRMC1 and PGRMC2 transport heme directly from FECH in the matrix to other compartments of the cell [263].

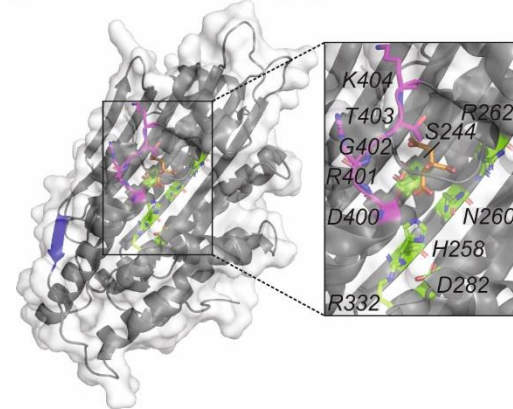
Direct handover from one enzyme to the next, like for heme from FECH to PGRMC1, seems to be the preferred mode of transport for porphyrin intermediates in the mitochondria. Prerequisite for this are protein-protein interactions and complex formation. Several independent studies reported various interaction partners of FECH whereas there is also one publication providing data for the existence of a heme metabolon, a super-complex of enzymes associated with heme biosynthesis and transport [264-268]. To summarize this data, work in MEL cells hints at an interaction between FECH and PPOX, which would facilitate transfer of the very hydrophobic PPIX. ALAS2 is a potential third interaction partner meaning that all matrix localized heme biosynthesis enzymes form a complex [239, 264]. Additionally, ABCB7, ABCB10, MFRN1 and the beta subunit of succinyl-CoA synthetase (SUCLA2) seem to be part of this metabolon. This could mediate efficient iron delivery to FECH and succinyl-CoA delivery to ALAS as well as 5-ALA export. Another interactor of FECH is MIC60 of the MICOS complex, indicating that FECH and its associated proteins are close to membrane contact sites to minimize the effort for transport of porphyrin intermediates over the mitochondrial membranes [269]. Other proposed components of the metabolon complex are VDAC2, TMEM14C, ANT2 and transferrin receptor protein 1 (TFRC), all of which are thought to be involved in transport of heme biosynthesis components, but strong experimental evidence is lacking [264, 268].

## Introduction

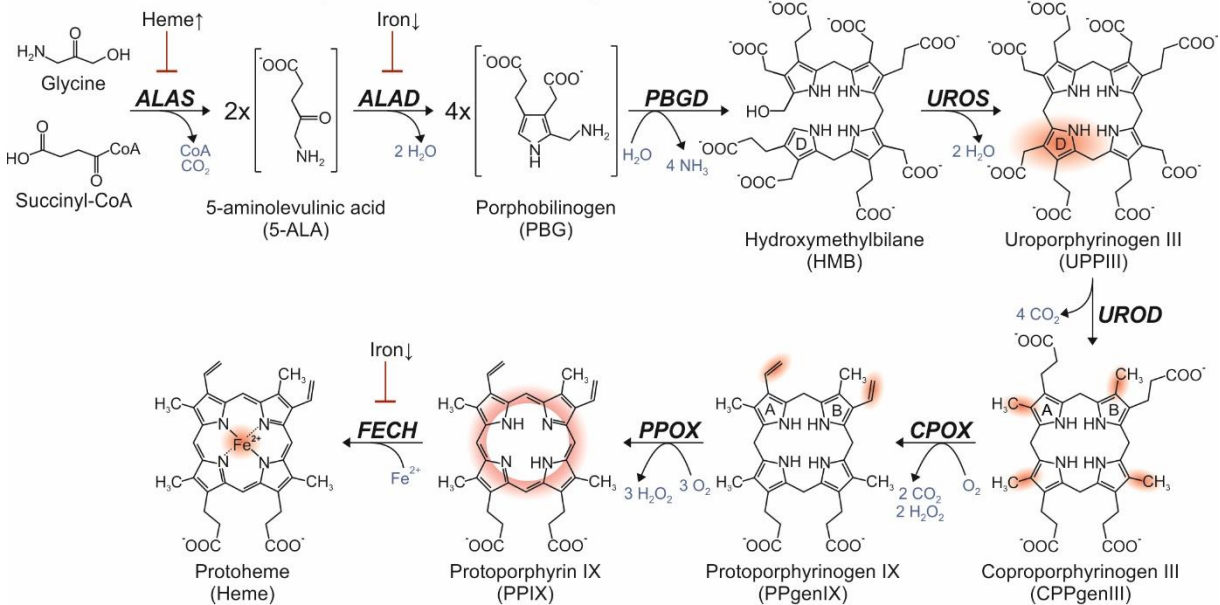
### A Overview over heme biosynthesis and transport



### B CPOX structure with proposed active site



### C Overview over heme biosynthesis reactions and regulation



### D Hydrophobicity scale of porphyrin intermediates

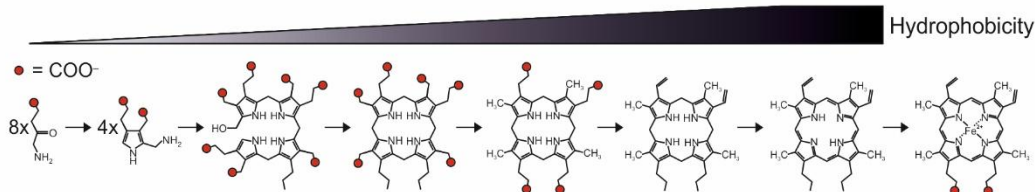


## Figure 7: Heme biosynthesis and function of CPOX

**A** Heme biosynthesis begins in the mitochondrial matrix with glycine and succinyl-CoA being condensed to 5-ALA by ALAS1. 5-ALA is exported into the cytosol, likely by IMM transporters ABCB10 or SLC25A39. The next biosynthesis steps by ALAD, PBGD, UROS and UROD are carried out in the cytosol. CPPgenIII is imported in the IMS supposedly by ABCB6 and transferred into PPIX by CPOX. PPIX is then transported into the matrix by a transporter. TMEM14C or ANT are possible candidates. The last two steps of heme biosynthesis happen in the matrix and are catalyzed by PPOX and FECH [148, 217]. **B** The proposed CPOX active site is located in a cleft in the CPOX monomer and built by S244, H258, N260, R262, D282 and R332 (green). The loop formed by D400, R401, G402, T403 and K404 (magenta) is suggested to be involved in substrate orientation [228-230]. Citrate (orange) is crystallized in the active center. The  $\beta$ -sheet mediating dimerization is shown in blue. PDB structure 2AEX [228]. **C** In the first step of heme biosynthesis glycine and succinyl-CoA are condensed to 5-ALA by ALAS, which is regulated directly by heme levels in a feedback mechanism. Two 5-ALA molecules are then combined to one monopyrrole, PBG, by ALAD. ALAD activity is dependent on iron availability because of its iron-sulfur cluster. PBGD builds the tetrapyrrole HMB from four PBG molecules. Afterwards, the ring at position D is inverted and the open HMB is closed by UROS producing UPP III. UROD decarboxylates the four carboxyl groups of the carboxymethyl

side chains of UPPgenIII resulting in CPPgenIII. The side chains of the rings A and B of CPPgenIII are then decarboxylated to PPgenIX by CPOX. PPOX further oxidizes PPgenIX to PPIX. In the ultimate step of heme biosynthesis, FECH inserts a ferrous iron into the porphyrin ring producing heme. FECH is regulated by iron availability [148, 216, 217]. **D** The hydrophobicity of the porphyrin intermediates increases throughout the heme biosynthesis pathway.

#### 1.4.4 Heme biosynthesis defects

Porphyria is the general term for hereditary metabolic disorders involving defects in heme biosynthesis. Each of the eight known porphyrias is characterized by defective activity of certain heme biosynthesis enzymes leading to the accumulation of cytotoxic porphyrin intermediates. As heme is a vital cofactor, disease causing mutations are usually heterozygous or do not completely abolish the functionality, but decrease it to low levels. Disease-causing mutations have been identified in all enzymes except for ALAS1. Depending on the affected cell type, porphyrias are either erythropoietic or hepatic. Characteristic symptoms for porphyrias are acute neurological dysfunctions and/or cutaneous photosensitivity [216, 270, 271]. Hepatic porphyrias are ALA dehydratase porphyria (ADP) caused by ALAD, acute intermittent porphyria (AIP) caused by PBGD, porphyria cutanea tarda (PCT) caused by UROD, hereditary coproporphyria (HCP) caused by CPOX, and variegate porphyria (VP) caused by PPOX. Erythropoietic porphyrias are X-linked protoporphyria (XLP) caused by ALAS2, congenital erythropoietic porphyria (CEP) caused by UROS, and erythropoietic protoporphyria (EPP) caused by FECH. An overview of all porphyrias including their underlying enzyme, symptoms and inheritance is presented in Table 1.

*Table 1: Overview over the eight different porphyrias*

Disorder	Enzyme	Erythropoietic	Hepatic	Neurological	Photosensitive	Inheritance
<b>XLP</b>	ALAS2	X			X	X
<b>ADP</b>	ALAD		X	X		R
<b>AIP</b>	PBGD		X	X		D
<b>CEP</b>	UROS	X			X	R
<b>PCT</b>	UROD		X		X	D
<b>HCP</b>	CPOX		X	X	X	D
<b>VP</b>	PPOX		X	X	X	D
<b>EPP</b>	FECH	X			X	R

X = X-linked; R = autosomal recessive; D = autosomal dominant. Adapted from [216].

#### *Hereditary coproporphyria*

As porphyrias related to mutations in CPOX and PPOX are the only ones leading to development of neurological dysfunctions and photosensitivity [216, 270, 272] and CPOX is of particular interest for this work, hereditary coproporphyria and some related mutations are discussed in detail, although a discussion of all 92 so far known disease-causing CPOX mutations (Human Gene Mutation Database (HGMD)) is not possible [273]. Hereditary coproporphyria is characterized by high levels of coproporphyrin III (CPPgenIII), the oxidized form of CPPgenIII, or harderoporphyrin, the oxidized form of harderoporphyrinogen, that are excreted by patients. The latter is a special form of the disease named harderoporphyrin [274]. Mutations leading to development of harderoporphyrin often affect amino

## Introduction

acids 400 to 404 of CPOX, the region that is thought to have a role in orientation and turning of harderoporphyrinogen. One of the mutations that has been described very often in this context is K404E [229, 230, 275-277]. Other studies show a similar effect for R401W or report a deletion of amino acids 403 to 406, which caused chronic cutaneous photosensitivity [278, 279]. Larger deletions might affect CPOX tertiary and quaternary structure, for example a deletion from amino acid 392 to 418 prevents CPOX dimerization [228]. Other mutations that will most likely affect CPOX dimerization are W427R, H327R and R328C [279-282]. The mutation H327R is a special case because it not only might affect dimerization, H327 is also predicted to interact with W399, which is likely involved in decarboxylation of harderoporphyrinogen [229, 280]. Another important group of mutations that need to be mentioned are deletions of larger parts of the CPOX gene, sometimes complete exons. Obviously, this strongly impairs CPOX structure and disturbs its function [219]. Mutations that do not impair the CPOX active site or CPOX dimerization or delete larger parts of the structure are usually ones which result in a premature stop codon or disturb parts of CPOX' tertiary structure [279].

### *Model systems to study defects in heme biosynthesis*

Besides the examination of patients, ways to study hereditary coproporphyrin, harderoporphyrin and other porphyrias are model systems, for example mouse models or chemical treatments that affect heme biosynthesis enzymes. Three mouse strains with CPOX mutations are published so far. The CPOX mutation W373X (W384 in human) leads to a premature stop codon and a homozygous mutation is embryonically lethal at E9.5, while heterozygous mice display a mild HCP phenotype [283]. Similarly, a mouse strain with the mutation R380L (R389 in mice), which affects a well conserved region of CPOX, reduced CPOX activity by 85% [284]. The third CPOX mutation did not result in HCP, but in anemia (intron 4 mutation leading to many different splice variants) [285]. In terms of pharmacological treatments, no CPOX inhibitor has been developed yet, however inhibitors for other heme biosynthesis enzymes are established. Itaconyl-CoA is a competitive inhibitor for ALAS2 and inhibition can be rescued by supplementing with the ALAS product 5-ALA [286]. Succinylacetone (SA) is a potent inhibitor of ALAD, which had been discovered early and used for heme synthesis inhibition ever since [287, 288]. PPOX inhibition can be achieved by treatment with the competitive inhibitor acifluorfen (AF) [289, 290]. N-methylprotoporphyrin (NMPP) is a substrate analogue for FECH and inhibits it efficiently [291, 292]. Of course, heme biosynthesis can also be impaired by inhibitors targeting related enzymes and pathways, for example transporters involved in porphyrin intermediate or iron trafficking or proteins involved in heme biosynthesis enzyme biogenesis. Curiously, a recent publication demonstrated an influence of MitoBlock-6 (MB-6) treatment on heme biosynthesis [293]. The heme biosynthesis proteins ALAS1 and PPOX were upregulated and heme biosynthesis rate and iron levels were disbalanced [293-295]. MB-6 is an inhibitor of ALR, one of the key players of the disulfide relay, but none of the heme biosynthesis enzymes or other proteins involved in heme biosynthesis are known or

predicted disulfide relay substrates, hinting at a novel interconnection between heme biosynthesis and disulfide relay.

### 1.5 Aims of this work

#### *First aim*

The role of sulfhydryl oxidase ALR in the oxidative folding machinery of mitochondria, the disulfide relay, has been well established over the last decade. Here it reoxidizes and “recycles” oxidoreductase MIA40 in a thiol-disulfide exchange and feeds electrons to cytochrome c [101, 103, 105-107]. When comparing the disulfide relay with the oxidative folding machinery of the ER, there are several remarkable parallels. The key players of disulfide formation are members of the oxidoreductase family of protein disulfide isomerases (PDIs), which can interact with different electron acceptor proteins, the most prominent being the sulfhydryl oxidase ER oxidoreductin 1 (ERO1) [87, 296]. ALR and ERO1 employ a similar intramolecular electron transfer mechanism to shuttle electrons over their FAD cofactor to an electron acceptor. But in contrast to ERO1, which can interact with all of the over 20 members of the PDI family, MIA40 is the only known interactor of ALR (Figure 8 A). Nevertheless, evidence exists that ALR might have functions apart from MIA40 reoxidation. Unpublished data from our lab revealed several years ago that Erv1, the yeast homologue of ALR, is able to directly oxidize MIA40 substrates *in vitro*, showing that ALR does not display substrate specificity towards MIA40. Moreover, recent data demonstrated that siRNA mediated knockdown (KD) of ALR did not phenocopy KD of MIA40. A proteome of ALR or MIA40 depleted human embryonic kidney cells (HEK293) showed that particularly the IMS proteome displayed very different phenotypes for the different KDs (Figure 8 B). Equal observations could be made for growth of the different KDs on glucose. Cells lacking ALR exhibited more severe proliferation defects than cells lacking MIA40 (Figure 8 C). In addition, analysis of gene dependencies based on information from the DepMap database revealed a strong co-dependency for disulfide relay genes *CHCHD4* (MIA40 gene) and *AIFM1*, whereas the correlation between ALR gene *GFER* and *CHCHD4* or *AIFM1* was much lower (Figure 8 D) [297, 298]. In a ranking of the top 100 co-dependencies of the respective gene, *CHCHD4* and *AIFM1* represented their respective top hit, whereas *GFER* was only on position 92 for *CHCHD4* and on position 19 for *AIFM1*. For these reasons, the first aim of this work was to confirm that ALR has roles beyond the disulfide relay, to identify potential novel interaction partners and to characterize the nature of this interaction.

## Introduction

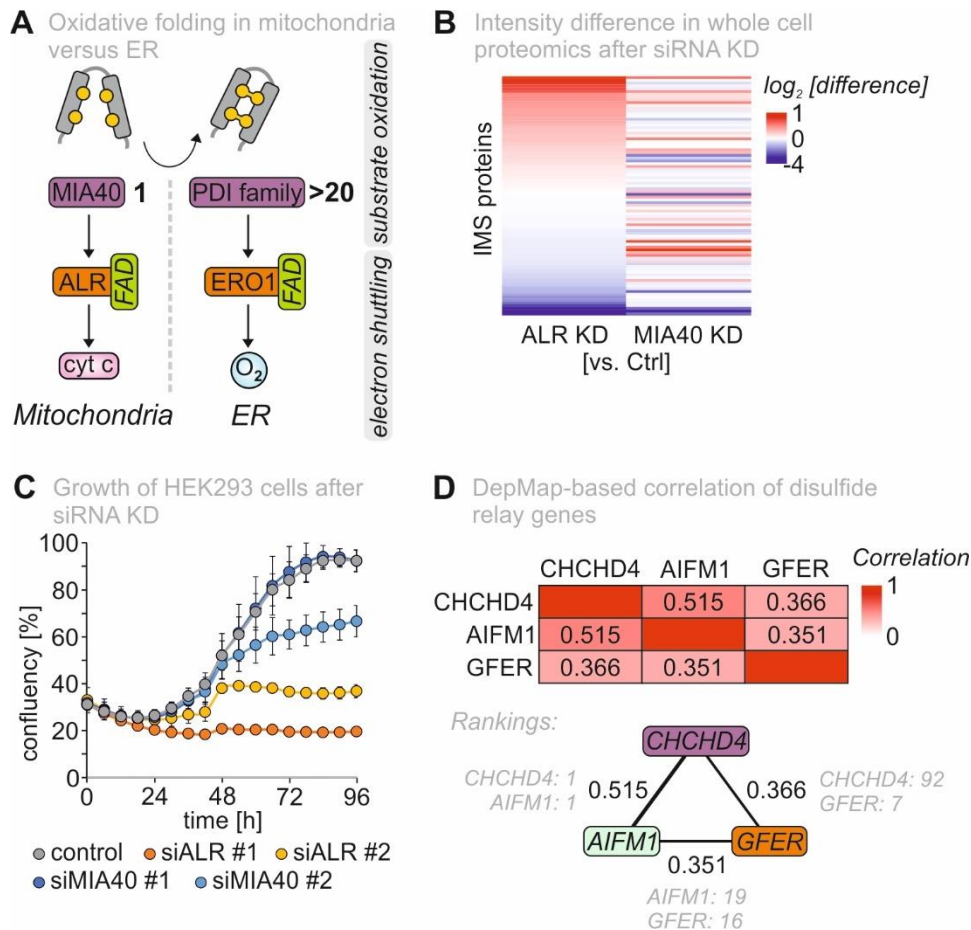


**Figure 8: ALR might have functions beyond the disulfide relay**

**A** Mitochondria and the ER both have an oxidative folding machinery displaying common features as the involvement of an oxidoreductase for substrate oxidation and the subsequent reoxidation of the oxidoreductase by a sulfhydryl oxidase with FAD cofactor. ER sulfhydryl oxidase ERO1 can interact with over 20 different proteins, whereas the known interactors of ALR are limited to one. **B** Whole cell proteomics of HEK293 cells depleted of ALR or MIA40 via siRNA show that the change of IMS proteins in comparison to control cells does not display the same pattern in ALR KD vs. MIA40 KD. Plotted is the average of the  $\log_2$  of the intensity difference between the respective KD and a scrambled siRNA control, calculated from four individual samples of each group. **C** Growth of ALR depleted HEK293 cells is more severely impaired than growth of cells depleted of MIA40. **D** The correlation between the disulfide relay gene *CHCHD4* (MIA40 gene), *AIFM1* and *GFER* (ALR gene) based on data from the DepMap database is shown [297]. Correlations from DepMap are Pearson correlations based on Chronos dependency scores from the CRISPR (DepMap Public 24Q2+Score, Chronos) dataset [298]. The rankings describe the position of the respective gene in the top 100 Co-dependencies list, for example, *AIFM1* is the gene that correlates most with *CHCHD4*, whereas *GFER* is only at place 92 in correlating with *CHCHD4*.

### Second aim

In interactome datasets, heme biosynthesis protein CPOX appears as novel interactor of ALR. CPOX Heme biosynthesis is an essential process for life, which is why enzymes of the heme biosynthesis pathway have been extensively studied. For CPOX, a crystal structure has been solved and its submitochondrial localization has been suggested [4, 202, 218, 228]. However, little is known about CPOX biogenesis, regulation or its catalytic mechanism and a potential involvement of ALR in these aspects. In the course of this work, my second goal was to examine the role of CPOX' conserved cysteines and the purpose of ALR interaction for its function, biogenesis, and regulation.

## 2. Results

### 2.1 CPOX is a novel interactor of ALR

#### 2.1.1 ALR has functions beyond the disulfide relay

ALR has been well characterized as sulfhydryl oxidase of the disulfide relay, where it reoxidizes oxidoreductase MIA40 in a thiol-disulfide exchange and shuttles electrons via an intramolecular transfer mechanism over its FAD cofactor onto cytochrome c [101, 103, 107]. The thiol-disulfide exchange is a stepwise process, in which ALR forms a mixed disulfide intermediate with its substrate MIA40, which is then resolved by the substrate's second cysteine. This leaves the previously reduced protein oxidized and the ALR CRAC motif reduced [108] (Figure 9 A). Notably, comparison with the oxidative folding machinery of the ER and recent experimental evidence comparing ALR and MIA40 depletion suggests that this thiol-disulfide exchange initiated by ALR could be a general mechanism applied to more interaction partners than only MIA40 (Figure 8). To find out, whether ALR interacts with other proteins than MIAA40, a radioactive affinity-precipitation experiment was performed that enables visualization of potential disulfide-linked intermediates. For this, HEK293 cells expressing ALR-Strep or a Mock control were radioactively pulsed, lysed, and Strep-tagged protein was precipitated. Samples were compared under non-reducing conditions keeping potential disulfide-linked intermediates intact and reducing conditions that would resolve potential disulfides (Figure 9 B). Indeed, under non-reducing conditions, most ALR was visible in its dimeric state, which is disulfide-linked. Additionally, higher molecular weight bands were visible that were absent in the reduced samples. In turn, under reducing conditions, ALR was mostly present in its monomeric state and a lot of bands, often at lower molecular weight, appeared in comparison to non-reducing conditions, representing previously disulfide-linked intermediates that were then separated. In sum, this experiment showed that ALR has more than one interaction partner. To gain deeper insight into the spectrum of potential ALR interactors, interactome datasets were generated using different affinity tags, lysis conditions and detection methods (Figure 9 C-E). Prior to lysis for the experiments, cells were treated with NEM to prevent thiol-disulfide exchange and thereby conserve disulfide-linked interactions. The data revealed that ALR interacts with proteins in outer and inner mitochondrial membrane as well as proteins from the IMS. Most of the significant hits found after native lysis were also detected under denaturing conditions, suggesting covalent interaction of ALR with most of the newly found interactors (Figure 9 C, D). A total of six ALR interactome datasets was available for analysis and identification of reliable interaction candidates, including four label-free and two SILAC (stable isotope labeling by amino acids in cell culture) experiments. As interactome datasets tend to show some false-positive results, only proteins, which appeared as significant hit in at least four of the six datasets, were considered reliable (Figure 9 E). Besides MIA40, that also fulfilled a role as positive control in this set of experiments, and ALR itself, six novel interactors of ALR were identified this way.

## Results

Two of these novel interaction partners, AK2 and CPOX, were significant hits in each of the present datasets making them the most confident hits of the analysis. Their interaction with ALR could be confirmed in a native IP experiment that was analyzed via Western blot. The IMS protein SMAC served as negative control (Figure 9 F). In conclusion it can be noted that ALR has potential functions beyond the disulfide relay becoming evident by interacting with these six novel interactors: mitochondrial adenylate kinase AK2, heme biosynthesis protein CPOX, mitochondrial outer membrane protein insertase MTCH2, apoptosis-inducing factor and MIA40 interaction partner AIFM1, the receptor subunit of the inner membrane translocase complex TIM50 and the OMM porin VDAC2 (Figure 9 G) [39, 94, 228, 299-301].

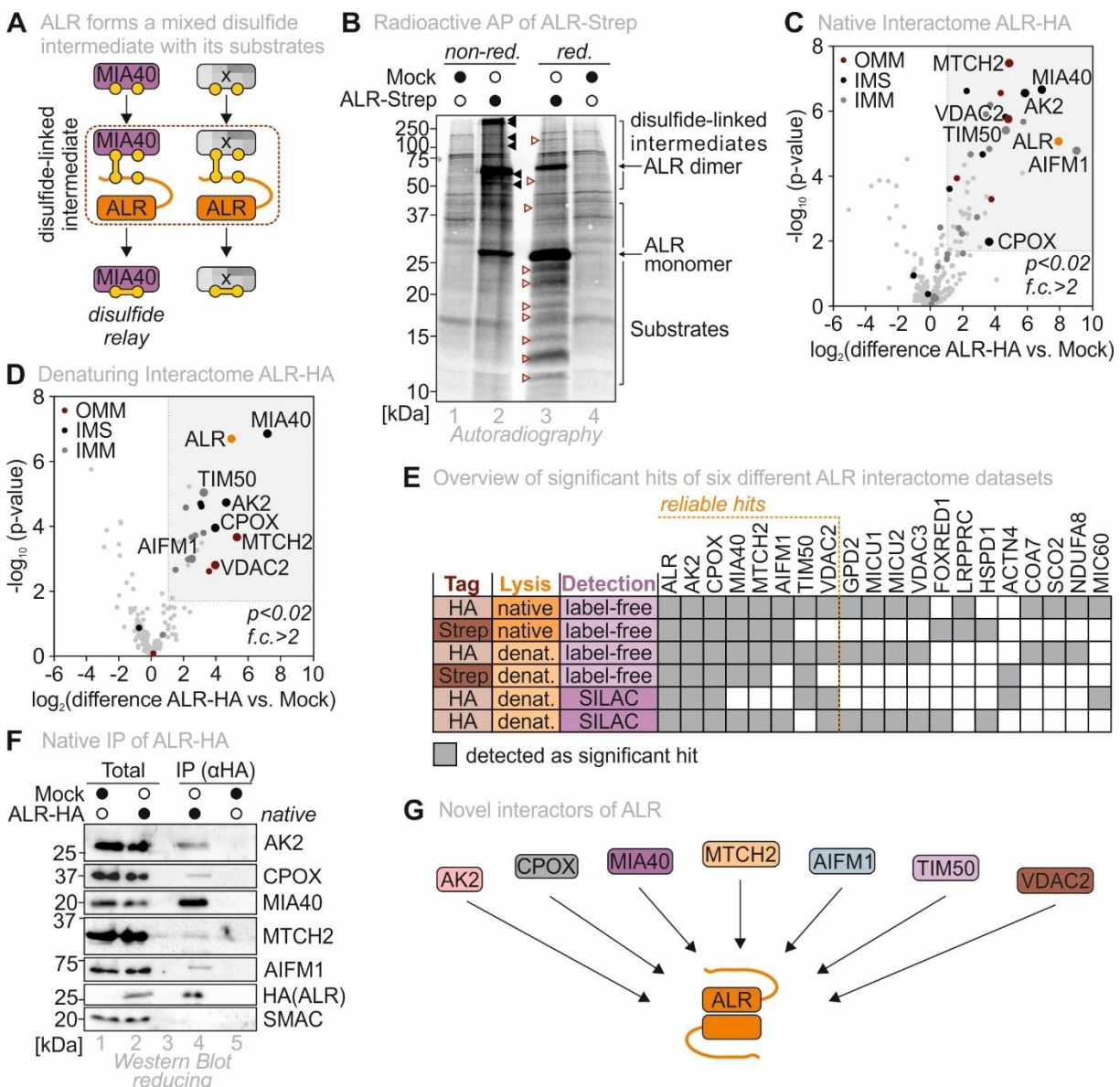


**Figure 9: ALR has functions beyond the disulfide relay**

**A** ALR forms a mixed disulfide with its substrate MIA40 during a thiol-disulfide exchange reaction, leaving previously reduced MIA40 oxidized. Potentially, this mechanism is universal and can be transferred on other interaction partners. For simplicity reasons, only one ALR subunit is depicted. **B** Radioactive APs of ALR-Strep versus a Mock control were performed and non-reducing and reducing conditions were compared in an

autoradiography. Black, filled arrowheads indicate bands of disulfide-linked intermediates. Dark red, unfilled arrowheads indicate unbound substrates. **C** The native interactome of ALR-HA shows significant hits from OMM (dark red), IMS (black) and IMM (dark grey). ALR itself is marked in orange. Hits with a p-value lower than 0.02 and a fold change (f.c.) higher than two were considered significant. **D** The denaturing interactome of ALR-HA shows significant hits from OMM (dark red), IMS (black) and IMM (dark grey). ALR itself is marked in orange. Hits with a p-value lower than 0.02 and a fold change higher than two were considered significant. **E** Significant hits (grey boxes) from a total of six ALR interactome datasets were compared. The datasets differed in terms of tag, lysis conditions and detection method. Listed are proteins appearing as a hit in at least two of six datasets. A threshold of four out of six was set for a reliable hit (orange dotted line). **F** Western blot analysis of a native IP of ALR-HA confirming interaction partners identified in E. **G** ALR has six novel interactors except MIA40.

### 2.1.2 ALR interacts with CPOX covalently

Six novel interaction partners were found in the ALR interactome screen and porphyrin biosynthesis protein CPOX was one of the two most confident hits (Figure 9 E). However, this is not the only reason making CPOX an interesting interaction candidate to follow up on. Literature hints at a link between heme biosynthesis and the disulfide relay, particularly ALR. Treatment of rat hepatocellular carcinoma cells with ALR inhibitor MB-6 had an impact on heme biosynthesis proteins with a strong upregulation of ALAS1, which is a sign of heme deficiency and impaired heme biosynthesis [293]. In addition, hepatocyte-specific ALR knockout (KO) in mice resulted in the liver turning completely white two weeks after birth, exactly when the full ALR KO was achieved, an observation that might also be associated to a heme biosynthesis defect [302]. Consequently, the interaction between ALR and CPOX was investigated in detail in the course of this work.

In order to define the interaction of ALR with CPOX, it was first verified again under different conditions. Native and denaturing IP experiments with HA-tagged ALR were performed, using Western blot as readout. CPOX and ALR interacted under both, native and denaturing, lysis conditions (Figure 10 A, B), confirming a covalent interaction between the two. MIA40 and the cysteine-free HCLS1 associated protein X-1 (HAX1) were employed as positive and negative controls. In a native IP of CPOX-HA, ALR could be co-precipitated, supporting the previous observations (Figure 10 C). HAX1 served as negative control. As there is no other known interaction partner of CPOX, a positive control in this experiment is lacking. Taken together, ALR and CPOX interact covalently, matching the proposed mode of action of ALR, forming disulfide linked intermediates with its interaction partners.

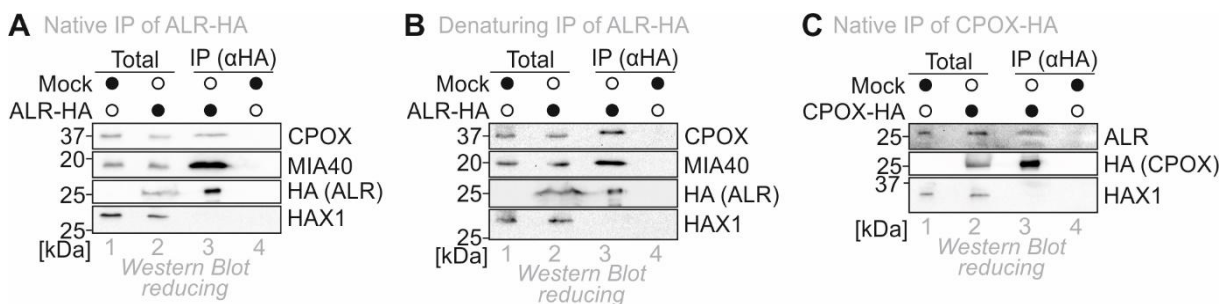


**Figure 10: ALR covalently interacts with CPOX**

**A** Native IP of ALR-HA with MIA40 as positive and HAX1 as negative control. **B** Denaturing IP of ALR-HA with MIA40 and HAX1 as positive and negative controls. **C** Native IP of CPOX-HA with HAX1 as negative control.

## Results

### 2.1.3 ALR interacts with CPOX via specific cysteines

When investigating an interaction between ALR and a substrate protein, cysteines play an essential role, as they are target for ALR's sulfhydryl oxidase activity. Having a look at human CPOX, 14 cysteines can be found, 10 of them in the mature protein. Six cysteines in CPOX are well conserved among higher eukaryotes, indicating their importance for the protein even though the function of CPOX cysteines has not been described yet (Figure 11 A). To first answer the question, whether the interaction between CPOX and ALR was indeed dependent on CPOX cysteines, CPOX-HA wildtype (WT) and a cysteine free ("10CA") version of CPOX were co-expressed with ALR-Strep on a HEK293 CPOX KO background (Figure S 1 A). The CPOX KO is important to avoid heterodimer formation with endogenous CPOX and will be extensively described later (section 2.2.1). Before the actual experiment, mitochondrial localization of the CPOX constructs was confirmed by immunofluorescence (Figure S 2). In a denaturing affinity precipitation (AP), it turned out that the WT version of CPOX could be efficiently co-precipitated with ALR-Strep, whereas no interaction was detected between ALR and the 10CA variant. The positive control MIA40 showed strong interaction with ALR-Strep in both AP experiments. HAX1 served as negative control (Figure S 1 B). Together, this data implies that the ALR-CPOX interaction is dependent on CPOX cysteines.

When looking at the position of the cysteines in the CPOX crystal structure, four of the six conserved cysteines attract particular attention [228]. C164 and C192 as well as C304 and C357 form "pairs", as they are only around 4 Å apart from each other (Figure 11 B). Such a small distance between two cysteines can in principle allow for disulfide bond formation, making them interesting to further examine in the context of interaction with ALR. Like for the 10CA mutant, behavior of the variants C164,192,304,357A (from now on called "4CA"), C164,192A, C304,357A and C164,304A, was compared to CPOX-HA WT (Figure 11 C). Again, mitochondrial localization of the 4CA variant, a representative for all four employed mutants, was confirmed prior to the experiments (Figure S 2). Strikingly, in a denaturing AP CPOX 4CA could not be co-precipitated with ALR, while interaction with WT CPOX was still observed. This shows that the interaction of CPOX with ALR is indeed mediated by the respective cysteines (Figure 11 D, H). When performing the same experiment with the three two-cysteine mutants, CPOX-HA C164,192A was still co-precipitated with ALR, but quantification showed that it interacts three times less with ALR than the WT (Figure 11 E, H). When C304 and C357 were mutated, the interaction between ALR and CPOX was impaired even more and only a faint interaction band was still detected (Figure 11 F). The quantification showed that it was decreased by six-fold (Figure 11 H). The C164,304A variant, in which both cysteine pairs are disturbed, nearly phenocopied the 4CA variant and showed a very weak interaction with nearly no visible interaction band (Figure 11 F, H). This preliminary data allows to hypothesize that both cysteine pairs, C164-C192 and C304-C357, have a role in interacting with ALR, as loss of either of the cysteine pairs resulted in a decrease of the ALR-CPOX

interaction. C304-C357, however, seems to be more important for this interaction than C164-192. When cysteines from both pairs were mutated simultaneously, the strongest decrease in interaction with ALR was observed. Hence, ALR seems to interact with CPOX via specific cysteines, preferentially via C304-C357 (Figure 11 I).

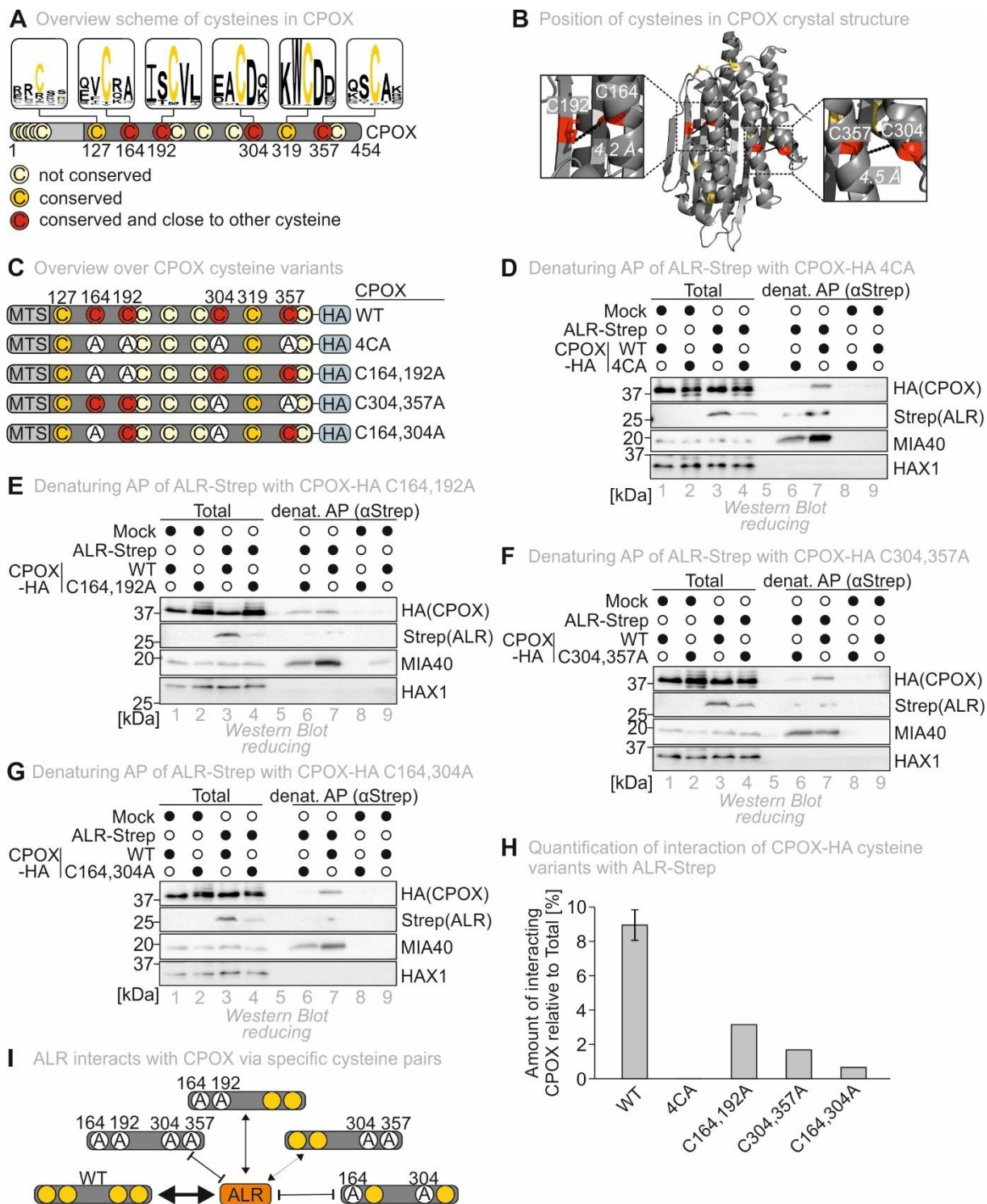


Figure 11: ALR interacts with CPOX via specific cysteine pairs

**A** Human CPOX has many cysteines (light yellow), six of which are conserved (dark yellow). Four of these conserved cysteines (red) are found close to another cysteine in the CPOX tertiary structure (see also **B**). **B** In the CPOX crystal structure (PDB: 2AEX [228]), four conserved cysteines are arranged in “pairs” less than 5 Å apart of

## Results

each other (red). **C** CPOX-HA WT and CPOX-HA variants targeting the cysteine pairs as found in **B** were expressed HEK293 Flp-In<sup>TM</sup> T-Rex<sup>TM</sup> CPOX KO cells. The variants included C164,192,304,357A, C164,192A, C304,357A and C164,304A. **D** Denaturing AP of ALR-Strep with CPOX-HA WT or 4CA, where both cysteine pairs are mutated. **E** Denaturing AP of ALR-Strep with CPOX-HA WT or C164,192A, where the first cysteine pair is mutated. **F** Denaturing AP of ALR-Strep with CPOX-HA WT or C304,357A, where the second cysteine pair is mutated. **G** Denaturing AP of ALR-Strep with CPOX-HA WT or C164,304A, where both cysteine pairs are mutated. **H** Quantification of CPOX-HA cysteine variant interaction with ALR-Strep. It was calculated, how much protein interacted with ALR relative to the loaded Total. WT: n=4, all other variants: n=1. **I** ALR interacts with CPOX via specific cysteines, preferentially over C304-C357. MIA40 and HAX1 served as positive and negative controls in **B-G**.

As described before, in a thiol-disulfide exchange with ALR, one cysteine of a substrate's cysteine pair attacks the oxidized ALR CRAC motif forming a mixed disulfide and the second substrate cysteine resolves this disulfide-linked intermediate again. If one of the substrate cysteines is missing, interaction might either not happen, or the disulfide-linked intermediate can still be formed but might be trapped until it is resolved by the second ALR cysteine or glutathione (GSH), like it was shown for unproductive MIA40-substrate intermediates [98, 101, 107, 164]. To further pinpoint which CPOX cysteine initiates the interaction with ALR, single cysteine mutants of CPOX, C164A, C192A, C304A and C357A (all with mitochondrial localization; Figure 12 A, Figure S 2), were tested in the same experimental setup as used before. Surprisingly, all single cysteine variants of CPOX interacted with ALR under denaturing conditions (Figure 12 B-F). Interactions were neither impaired nor increased, revealing no trapping mutant. This raises doubts about the specific relevance of these four cysteines, in particular C304 and C357, for the ALR interaction. It cannot be completely clarified why the single cysteine mutants still showed WT-like ALR interaction. Trying to explain this observation, it must be considered that, when one cysteine pair is disturbed, interaction of CPOX with ALR is still possible over the respective other cysteine pair. The ALR-CPOX interaction seems to be completely abolished only when both cysteine pairs are affected by mutations (Figure 11 D, G, H). Also, nothing is known yet about interaction of ALR with other substrates except MIA40, so it is not clear how quickly an unproductive mixed disulfide would be resolved by ALR, GSH or other influences in the IMS, meaning that trapping mutants like they are known for MIA40 might not exist for ALR substrates. If an unproductive mixed disulfide was resolved as fast as a productive one, an interaction comparable to WT CPOX could still be detected. Further, data on C357 is preliminary and cannot be considered reliable until reproduction. Together, the data on CPOX single cysteine mutants does not provide information about which cysteine initiates the thiol-disulfide exchange reaction, but does also not contradict previous findings.

In summary of all experiments on the ALR-CPOX interaction, it can be noted that this interaction depends on four distinct CPOX cysteines, even though their individual contribution could not be finally determined yet.

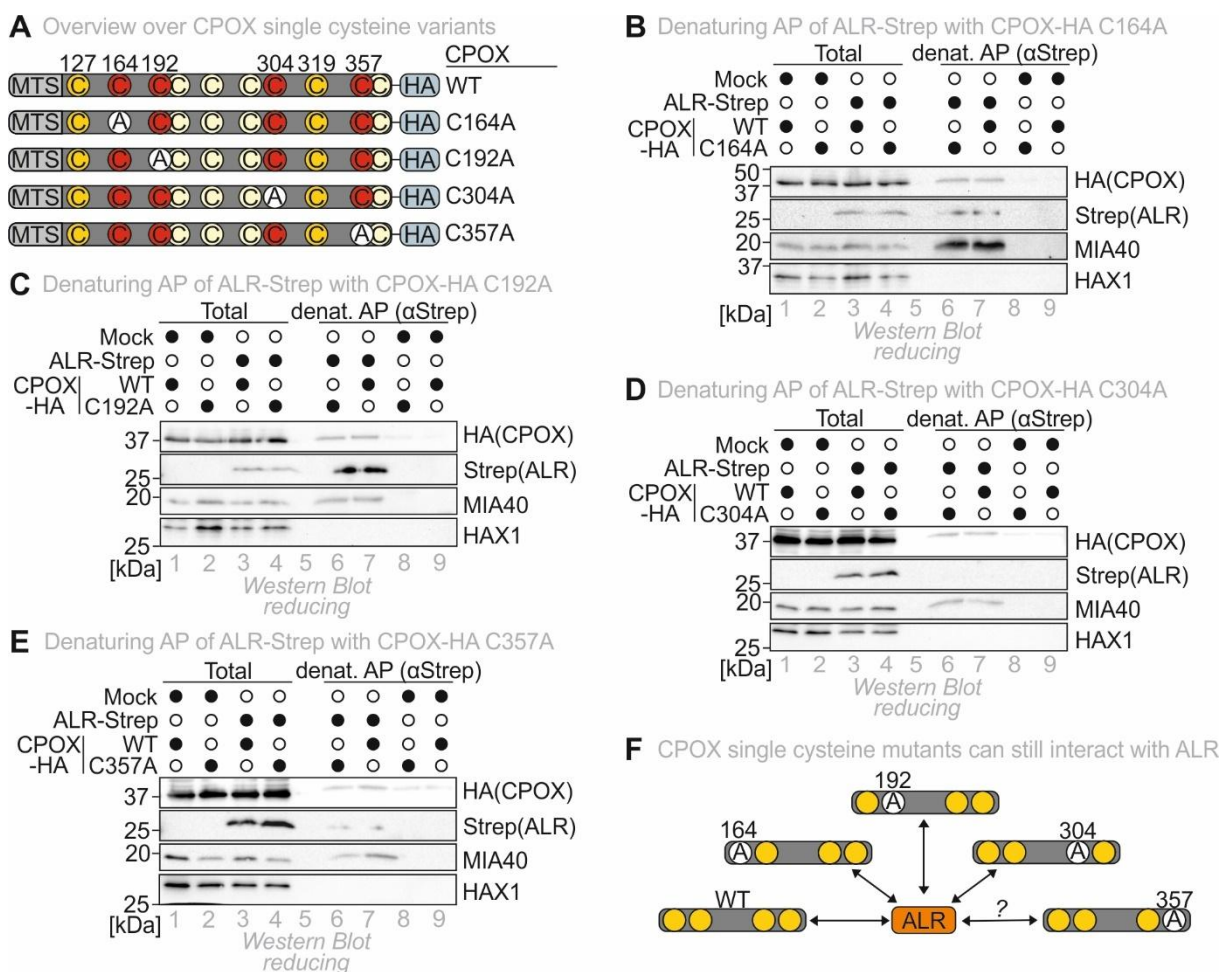


Figure 12: Single cysteines variants of CPOX interact with ALR

**A** CPOX-HA WT and CPOX-HA single cysteine variants targeting C164, C192, C304 and C357 were expressed on a CPOX KO background. **B** Denaturing AP of ALR-Strep with CPOX-HA WT or C164A. **C** Denaturing AP of ALR-Strep with CPOX-HA WT or C192A. **D** Denaturing AP of ALR-Strep with CPOX-HA WT or C164A. **E** Denaturing AP of ALR-Strep with CPOX-HA WT or C304A. **F** The tested CPOX single cysteine mutants C164A, C192A, C304A and C357A could interact with ALR comparable to the WT.

#### 2.1.4 CPOX contains oxidized cysteines

The interaction between ALR and CPOX was found to be dependent on specific cysteines, however, this is no direct confirmation that ALR introduces disulfides in CPOX. To test whether CPOX contains oxidized cysteines, an inverse redox shift assay was performed (Figure 13 A). In this assay, cultured cells are incubated *in situ* with NEM, a thiol-reactive agent that modifies free cysteines adding small mass, to protect free thiols from further modification. Afterwards, trichloroacetic acid (TCA) is added to lyse the cells and precipitate the protein. TCA also reversibly protonates reactive thiols and therefore traps a proteins' redox state [303, 304]. Subsequent treatment with the reductant Tris(2-chlorethyl)phosphate (TCEP) opens disulfides and allows for modification of previously oxidized cysteines by the larger thiol-modifying agent mm(PEG)<sub>12</sub> that adds more molecular mass to the protein and changes its chemical properties. This means, the more oxidized a protein is, the higher it runs on SDS-PAGE (fully oxidized means fully modified), whereas completely reduced proteins only show a small shift up (minimal shift).

## Results

In the inverse shift assay, endogenous CPOX from HEK293 cells was detected at around 37 kDa when it was not modified and only a slight difference could be observed between the unmodified and the minimally shifted band. When fully oxidized and thereby maximally shifted, CPOX was observed at a molecular weight of about 50 kDa. Under steady-state conditions, CPOX was detected at an intermediate molecular weight between these two bands, suggesting that CPOX is partially oxidized in the cellular context (Figure 13 B). The CPOX redox status does not appear to be cell type specific, as endogenous CPOX from HepG2 cells behaved similarly to the HEK293 sample (Figure 13 C). A shift assay is not a quantitative experiment, therefore, the degree of CPOX oxidation cannot be determined precisely. Still, the intermediate oxidation status of CPOX at steady state, observed in the middle of minimal and maximal shift, allows to speculate that CPOX might contain two disulfides. As the cysteine-dependent interaction of CPOX with ALR was confirmed by previous experiments, ALR might promote introduction of at least one disulfide in CPOX.

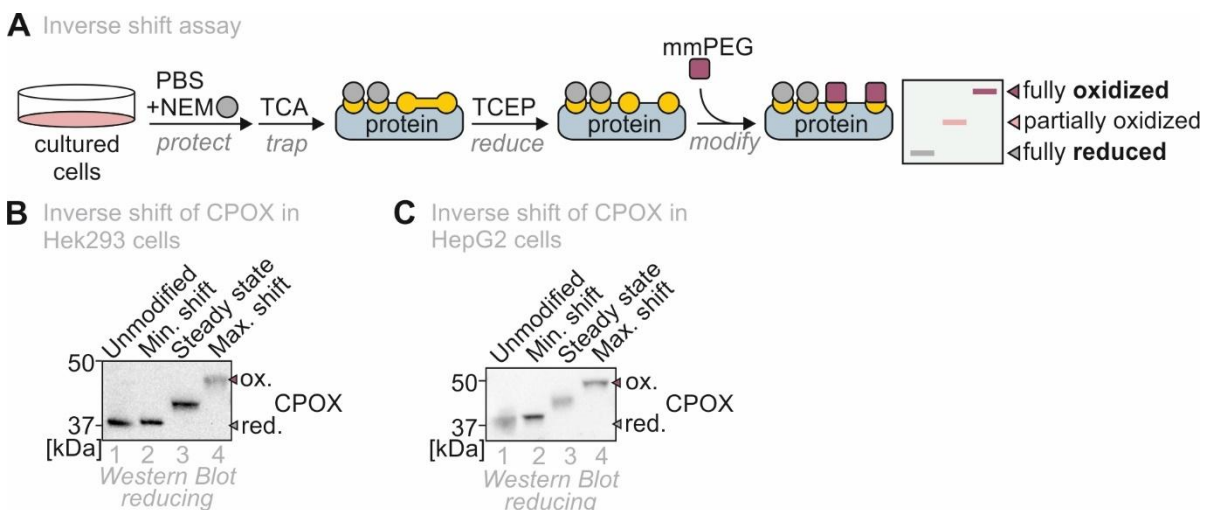


**Figure 13: CPOX contains oxidized cysteines**

**A** In an inverse shift assay, cells are incubated with NEM to protect free thiols before being denatured and precipitated by TCA. TCA also traps the redox status of proteins. Oxidized cysteines are then reduced by TCEP, making them available for modification with maleimides like mm(PEG)<sub>12</sub>, adding molecular mass. The more oxidized a protein is, the higher it will run on SDS-PAGE after the assay. **B** Inverse shift assay of endogenous CPOX from HEK293 cells. **C** Inverse shift assay of endogenous CPOX from HepG2 cells. ox. = oxidized, red. = reduced.

Next, it needed to be checked if the CPOX-HA WT construct would behave like the endogenous protein to make sure that the tag and the overexpression did not influence its redox status. An inverse shift of CPOX-HA WT showed that it had a semi-oxidized steady state like the endogenous form. The CPOX 10CA variant lacking all cysteines did not shift, as no modification is possible without cysteines (Figure 14 A). Interestingly, the 10CA variant showed a double band on Western blot, not only in the inverse shift experiment, but also on all other Western blots (Figure S 1). When analyzing the different CPOX cysteine mutants in inverse shift experiments, the 4CA variant was observed to still shift, but to a lesser extent than the WT as the steady state of 4CA was only slightly above its minimal shift. Hence, it can be assumed that the CPOX 4CA variant does not contain disulfides anymore. Nevertheless, the inverse

shift assay cannot distinguish between disulfides and other cysteine modifications, so CPOX still might contain a differently modified cysteine (Figure 14 B).

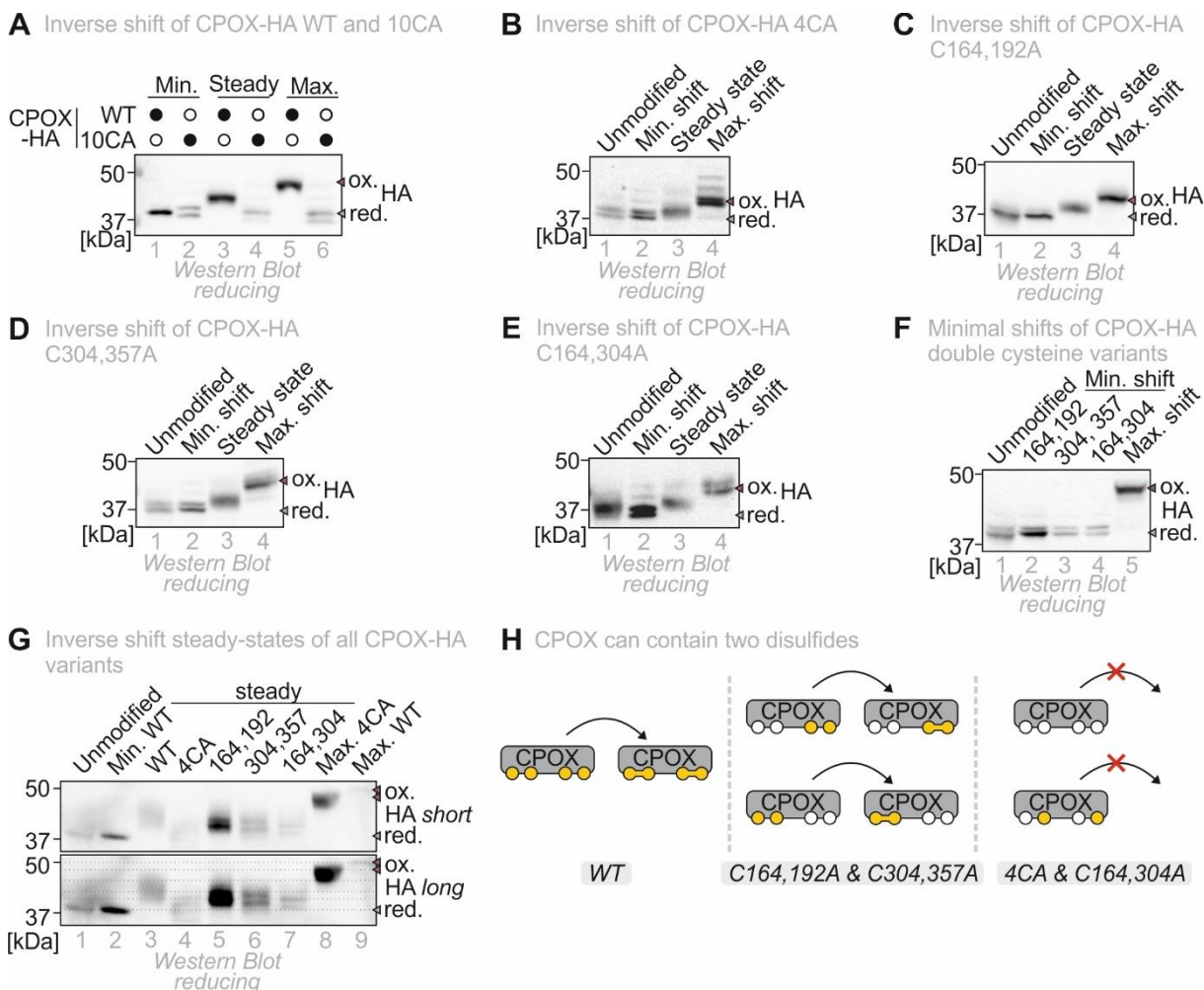


**Figure 14: CPOX contains one or two disulfide bonds**

**A** Inverse shift of CPOX-HA WT in comparison to the cysteine-free 10CA variant. **B** Inverse shift of CPOX-HA 4CA. **C** Inverse shift of CPOX-HA C164,192A. **D** Inverse shift of CPOX-HA C304,357A. **E** Inverse shift of CPOX-HA C164,304A. **F** Minimal shifts of CPOX-HA C164,192A, C304,357A and C164,304A next to each other. Unmodified and maximal shift samples are C164,192A. **G** Steady states of CPOX-HA WT, 4CA, C164,192A, C304,357A and C164,304A next to each other. The unmodified control is CPOX-HA WT. **H** WT CPOX can establish two disulfide bonds. In C164,192A and C304,357A, one of these disulfide bonds cannot be built. In 4CA and C164,304A, formation of both disulfides is impaired. ox. = oxidized, red. = reduced.

As next step, the redox status of the different double cysteine mutants was determined. They all shifted to an intermediate steady state, so the shifting pattern was comparable to the WT (Figure 14 C-E), but judging from individual blots, it was difficult to compare them. For this purpose, minimal shift and steady state samples of all double cysteine mutants were loaded next to each other. All minimal shift samples could be detected at a similar molecular weight (Figure 14 F). Notably, the running behavior of steady state samples of CPOX-HA 4CA and the three double cysteine mutants differed (Figure 14 G). As expected, steady states of the cysteine mutants ran below the steady state of CPOX-HA WT. CPOX 4CA had the lowest steady state, being closest to the minimal shift control. CPOX-HA C164,192A and C304,357A, the constructs in which one cysteine pair was mutated at a time, shifted to the same extent

## Results

showing an intermediate redox state below the WT and above the 4CA. This means that they contain more oxidized cysteines than the 4CA variant but less than the WT. In contrast, the steady state of CPOX C164,304A, where one cysteine from both potential disulfides is mutated, did not run next to the other double cysteine variants, but was comparable to 4CA, suggesting that it is lacking the same number of oxidized cysteines.

Taken together, the data proposes that CPOX can form disulfides between C164-C192 and C304-C357, which are both found in the WT under steady-state conditions (Figure 14 H). Whether each of these disulfides or only C304-C357, which plays the major role in ALR-CPOX interaction, is usually introduced by ALR is not clear, as an interaction of CPOX with MIA40 has been detected already (Figure S 3). Therefore, MIA40 might as well have an influence on the redox state of CPOX. Remarkably, CPOX 4CA, C304,357A and C164,304A displayed the same double band as the 10CA variant. A possible underlying reason for this pattern will be discussed in the second part of this work.

### 2.2 CPOX cysteines are critical for its stability during processing in the IMS

#### 2.2.1 CPOX KO is characterized by a distinct phenotype

ALR and CPOX were shown to interact via specific cysteines to introduce a disulfide in the first part of this work, the relevance of these cysteines and potential disulfides for CPOX, however, remained elusive. To investigate the function of CPOX cysteines, tools were needed that allow determining functionality of different CPOX (cysteine) variants. In a first step, a HEK293 Flp-In™ T-Rex™ CPOX KO cell line was generated using the CRISPR/Cas9 system targeting the first exon of the CPOX gene (Figure 15 A). It is important to study respective CPOX variants on a KO background to avoid the influence of endogenous CPOX on the experimental outcome. CPOX KO cells showed no change in ALR or MIA40 levels, but displayed strongly elevated levels of ALAS1 on Western blot and in a whole cell mass spectrometry analysis (Figure 15 B-D). Mass spectrometry revealed ALAS1 as the only heme biosynthesis enzyme that was strongly upregulated upon lack of CPOX. The other enzymes were not significantly changed, but FECH showed a slight non-significant increase (Figure 15 D). ALAS1 is the major regulator of heme biosynthesis and upregulated under heme deprivation [202-206]. Therefore, upregulation of ALAS1 indicates heme depletion in CPOX KO cells (Figure 15 E). In line with this, FECH, is the second major regulator of heme biosynthesis, explaining why it is also slightly upregulated [246-248]. Complementation of CPOX KO with a CPOX-HA WT construct brought levels of ALAS1 and FECH back to control levels of HEK293 cells without CPOX KO (Figure 15 D). This shows, that ALAS1 levels can be used as a readout for CPOX functionality.

Besides assessment of ALAS1 levels, which is only an indirect readout for CPOX functionality, a direct readout method was established. CPOX decarboxylates CPPgenIII stepwise to PPgenIX and both are

quickly oxidized by oxygen in the air after cell lysis (Figure 16 A). The oxidized versions of CPPgenIII and PPgenIX, CPPIII and PPIX, can then be measured via high-performance liquid chromatography (HPLC) from cell lysates and are distinguishable because of their different retention times (Figure 16 B). The HPLC measurements of lysates from normal HEK293 and CPOX KO cells detected an accumulation of CPOX educt CPPgenIII (measured as CPPIII) in CPOX KO cells but not in HEK293, as it cannot be converted to PPIX anymore.

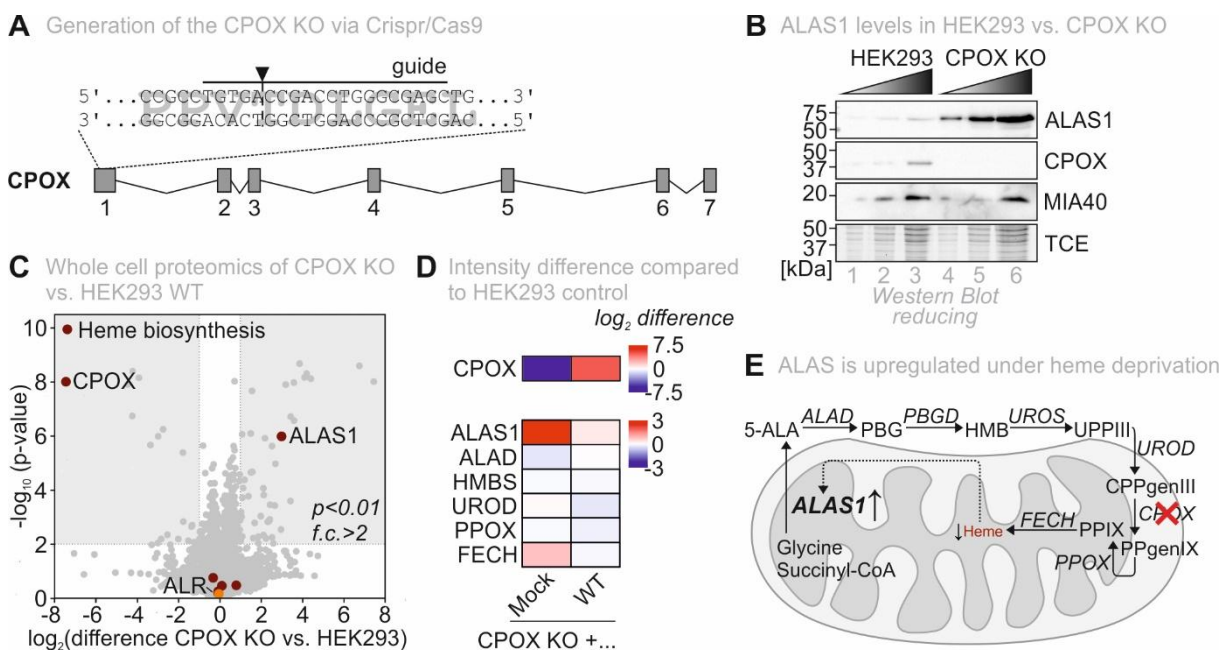


Figure 15: CRISPR/Cas9 mediated CPOX KO shows elevated ALAS1 levels

**A** A CRISPR/Cas9 mediated KO of CPOX was generated targeting gRNA to a region in exon 1 of the CPOX gene. **B** Western blot of lysates from normal HEK293 and CPOX KO cells. MIA40 acts as IMS control. TCE staining acts as loading control. **C** Volcano plot of whole cell proteomics of CPOX KO vs normal HEK293 cells. Heme biosynthesis proteins are highlighted in red. ALR is highlighted in orange. Hits were considered significantly changed when  $p < 0.01$  and  $f.c. > 2$ . **D** The heatmap shows the  $\log_2$  intensity difference of a CPOX KO cell line expressing a mock plasmid or CPOX-HA WT compared to standard HEK293 cells for heme biosynthesis proteins. **E** ALAS1 is upregulated under heme deprived conditions to compensate for heme loss.

PPIX on the other hand was low in both samples (Figure 16 C, F). When growth of CPOX KO cells was compared to standard HEK293 cells and a CPOX-HA WT complementation, no difference was observed on glucose (Figure 16 D). In contrast, after shifting cells to galactose on day 0, proliferation of CPOX KO was strongly impaired in comparison to HEK293 cells, but could be rescued by complementation with CPOX-HA WT (Figure 16 E). With galactose as carbon source, cells cannot perform glycolysis and need to fully rely on respiration for ATP production. As complexes II, III and IV of the respiratory chain all require a heme cofactor for functionality, it is most likely that CPOX KO cells show a proliferation defect on galactose due to heme depletion (Figure 16 F) [180, 181].

## Results

Taken together, CPOX KO cells exhibit three different measurable phenotypes, elevated ALAS1 levels, CPPgenIII accumulation and a growth defect upon galactose shift, which can be used to understand the relevance of certain cysteines for CPOX functionality.

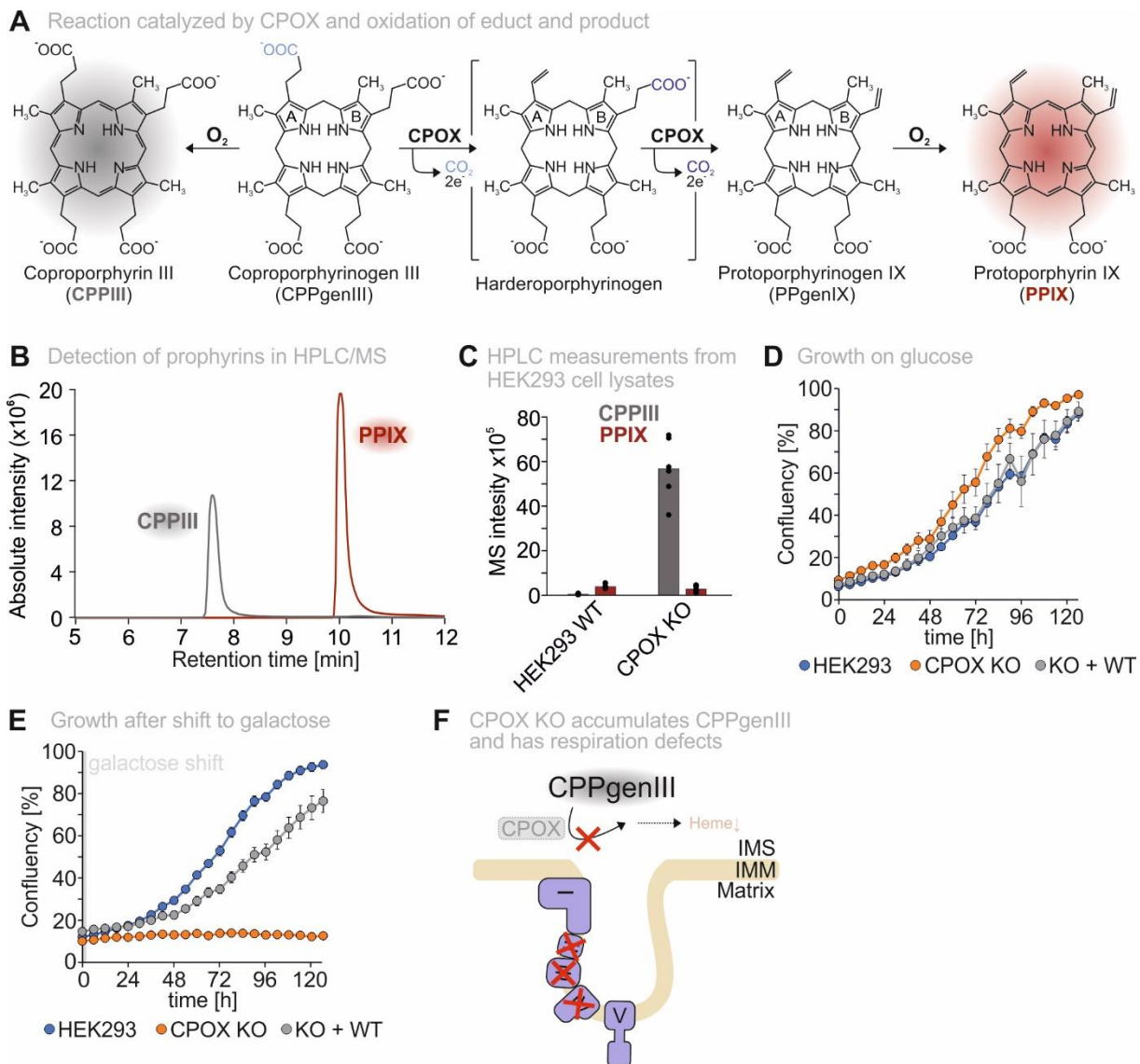


**Figure 16: CPOX KO cells accumulate CPPgenIII and show growth defect after galactose shift**

**A** CPOX decarboxylates CPPgenIII in a two-step mechanism to PPgenIX. During this process, the intermediate harderoporphyrogen is produced. Outside of a cell, CPPgenIII and PPgenIX can be oxidized by molecular oxygen in the air to CPPIII and PPIX. **B** CPPIII and PPIX levels can be measured via HPLC/MS and distinguished because of their different retention times. **C** HPLC measurements of CPPIII and PPIX from lysates of HEK293 and CPOX KO cells. Measurements were performed by Dylan Stobbe and Jan Jirschitzka. **D** Growth of HEK293, CPOX KO and CPOX KO + CPOX-HA WT cells on glucose was measured for 120 h. **E** HEK293, CPOX KO and CPOX KO + CPOX-HA WT cells were shifted from glucose to galactose at timepoint 0 (light gray) and growth was measured for 120 h. **F** In CPOX KO cells, CPPgenIII accumulates and heme production is not functional anymore. This leads to respiration defects as complex II, III and IV require heme cofactors for function.

### 2.2.2 The two CPOX cysteine pairs are not equally relevant for its function

To get a first impression, whether the lack of cysteines influences CPOX function, ALAS1 levels, CPPgenIII levels and growth after galactose shift were measured for CPOX KO cells expressing the cysteine-free 10CA variant of CPOX. ALAS1 levels in the 10CA complementation were still upregulated,

indicating that heme availability was not sufficient due to CPOX dysfunctionality (Figure S 1 C). Levels of CPPIII, the oxidized version of CPPgenIII, were strongly increased, showing that cysteine-free CPOX does not efficiently convert CPPgenIII to PPgenIX (Figure S 1 D). The CPOX 10CA variant could also not rescue cell growth after galactose shift. Only a small improvement compared to the CPOX KO was visible, probably because the presence of a cysteine-free CPOX protein is still better for overall fitness of the cell than a complete absence (Figure S 1 E). Consequently, CPOX cysteines are generally relevant for its function.

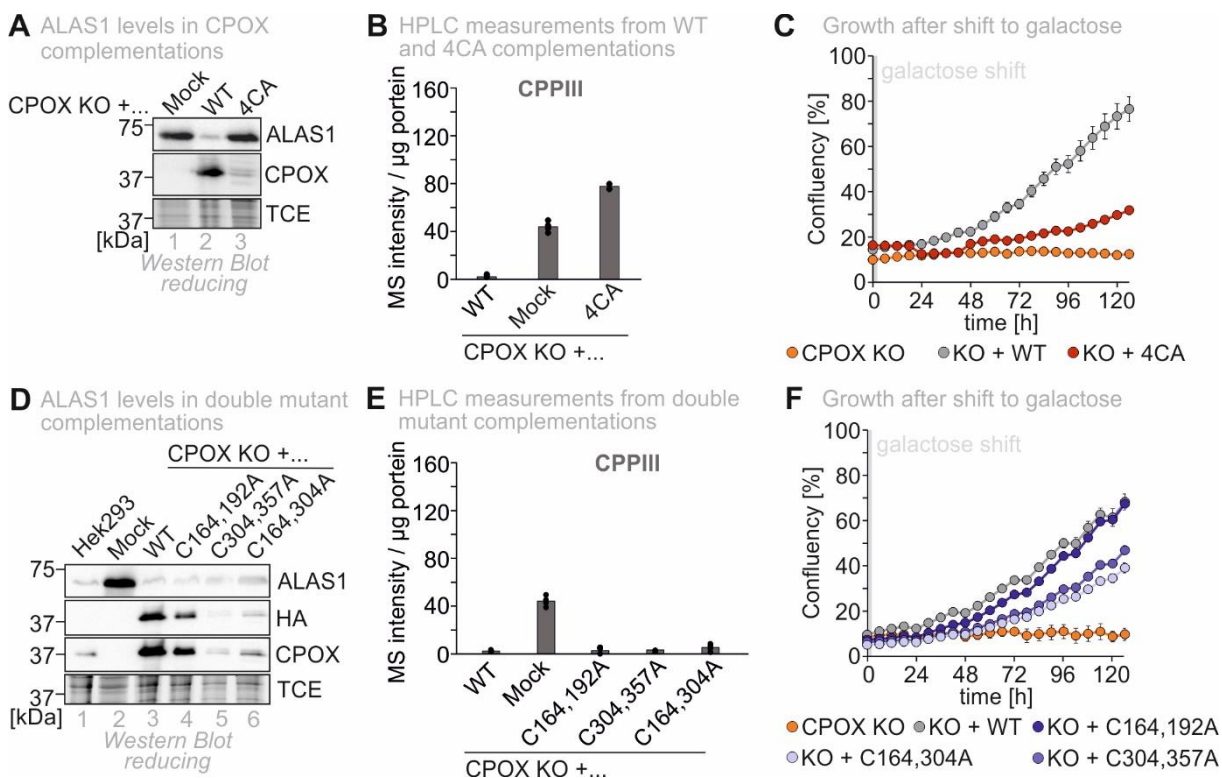


**Figure 17: The cysteine pair C304-C357 is required for optimal CPOX functionality**

**A** Western blot of cell lysates from CPOX KO cells complemented with a mock control, CPOX-HA WT or CPOX-HA 4CA. TCE acts as loading control. **B** HPLC measurement of CPPIII from cell lysates of CPOX KO cells complemented with CPOX-HA WT, Mock or CPOX-HA 4CA. Signal intensities were normalized to protein level. **C** CPOX KO, CPOX KO + CPOX-HA WT and CPOX KO + CPOX-HA 4CA cells were shifted from glucose to galactose at timepoint 0 (light grey) and growth was measured for 120 h. **D** Western blot of cell lysates from HEK293 cells and CPOX KO cells complemented with a mock control, CPOX-HA WT, C164,192A, C304,357A or C164,304A. TCE acts as loading control. **E** HPLC measurement of CPPIII from cell lysates of CPOX KO cells complemented with CPOX-HA WT, Mock, C164,192A, C304,357A or C164,304A. Signal intensities were normalized to protein level. **F** CPOX KO cells and CPOX KO cells complemented with C164,192A, C304,357A or C164,304A were shifted from glucose to galactose at timepoint 0 (light grey) and growth was measured for 120 h. Measurements in **B** and **E** were performed by Dylan Stobbe and Jan Jirschitzka.

Next, it was investigated whether specifically the cysteines mediating the interaction with ALR were also the ones relevant for CPOX functionality. Comparison of CPOX KO cells complemented with CPOX-HA WT and 4CA showed that also the 4CA variant, like the 10CA variant, was not functional. In contrast to WT, 4CA was not able to rescue the increased ALAS1 levels of CPOX KO cells and accumulated CPPgenIII (Figure 17 A, B). It could also not be strongly overexpressed like the CPOX-HA WT even though

## Results

expression was induced with the same high amount of doxycycline (1 µg/ml). Moreover, growth of CPOX KO complemented with CPOX-HA 4CA after shift to galactose looked very similar to the 10CA complementation and was only weakly improved compared to the KO (Figure 17 C). To learn more about the influence of the two individual cysteine pairs on CPOX function, ALAS1 and CPPgenIII levels and growth after galactose shift were also measured for C164,192A, C304,357A and C164,304A. All three double cysteine mutants could decrease ALAS1 to a normal level and did not accumulate CPOX educt CPPgenIII (Figure 17 D, E), showing their functionality. Remarkably, C164,192A reached an expression level comparable to the WT construct, whereas C304,357A and C164,304A were present at lower levels, like the 4CA mutant (Figure 17 A, D). In line with this observation, only C164,192A complementation could rescue growth as efficiently as the WT. The two other double cysteine mutants showed better proliferation than the 4CA complementation, but still only reached around 45% instead of 70% confluency after 120 h (Figure 17 F). All in all, the lower protein levels and missing ability to fully complement for loss of endogenous CPOX further indicate a different relevance of the two cysteine pairs for CPOX, showing that C304-C357 is more important than C164-C192.

### 2.2.3 Lack of a certain CPOX cysteine pair impacts CPOX processing and stability

So far, it could be reported that specific CPOX cysteines impact its functionality but seem to contribute to a different extent. Still, how these cysteines exert their influence on CPOX functionality required further investigation. Knowledge about CPOX maturation, homeostasis, regulation, and its catalytic mechanism is limited. CPOX is imported into the IMS via a long bipartite presequence consisting of an MTS followed by a cleavable transmembrane (TM) domain [218]. A well conserved negative amino acid stretch is located right after this transmembrane domain (Figure 18 A). A similar negative stretch has recently been found to mediate export of the dually localized protein STARD7 from mitochondria to cytosol after its import and processing has been completed in mitochondria [66]. In addition to this attention-drawing presequence structure, it is known that most mitochondrial proteins acquire their disulfides during import [99, 164]. Therefore, an influence of CPOX cysteines on import and processing in the IMS could be imagined and was examined in the following section.

To investigate CPOX import and follow its processing, pulse chase experiments were performed (Figure 18 B). In short, cells were starved from sulfur-containing amino acids and then pulsed with medium containing cysteine and methionine that contain heavy sulfur (<sup>35</sup>S). The radioactively labeled amino acids were incorporated in newly synthesized proteins during this timeframe, whose maturation could then be followed over time after the radioactivity had been washed out. In the end, the protein of interest was precipitated to get a clean sample for analysis by autoradiography. In a pulse chase of endogenous CPOX, it was already visible that CPOX undergoes at least three different processing steps before reaching its mature form that then accumulates over time (Figure 18 C). This demonstrates a

more complex processing for CPOX than for other known bipartite presequence containing proteins [50, 55, 64, 66, 73].

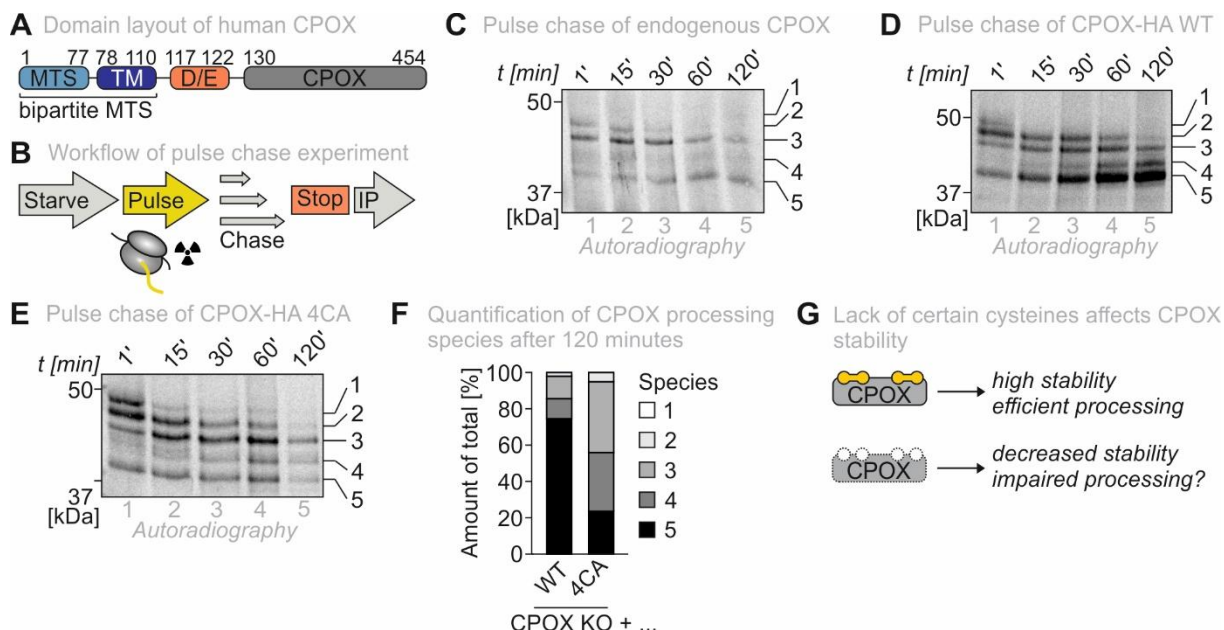


**Figure 18: CPOX processing is complex and affected by cysteines**

**A** CPOX has a bipartite presequence consisting of MTS and transmembrane domain, which is followed by a conserved negative amino acid stretch. **B** In a pulse chase experiment, cells are starved from sulfur-containing amino acids and then pulsed with radioactively labeled cysteine and methionine with  $^{35}\text{S}$ . Radioactive amino acids are incorporated into nascent polypeptide chains. Afterwards, radioactivity is washed out and labeled protein can be chased over time. **C** Pulse chase of endogenous CPOX from HEK293 cells. **D** Pulse chase of CPOX-HA WT on CPOX KO background. **E** Pulse chase of CPOX-HA 4CA on CPOX KO background. **F** It was quantified to how many percent the different CPOX processing species contribute to the total amount of protein at 120 minutes. Quantifications were done for CPOX-HA WT ( $n=6$ ) and 4CA ( $n=3$ ). **G** The lack of certain CPOX cysteines (C164, C192, C304 and C357) impairs CPOX stability and might also affect its processing.

As endogenous protein is less efficiently enriched in pulse chase experiments than overexpressed protein and samples from endogenous protein tend to give weaker signal intensity, CPOX-HA overexpression constructs were used to further study its import. In a pulse chase of CPOX-HA WT, five species were clearly visible (Figure 18 D). The first species was only still visible at the 1-minute timepoint and could be detected at a molecular weight of around 50 kDa, the molecular weight of the full length CPOX precursor before processing. As it was quickly transformed into the second species, the second species most likely represents CPOX after losing its MTS due to MPP cleavage. Assuming a cleavage step in the CPOX TM domain as part of bipartite sequence processing, species 3 or 4 must be produced by an IMM protease. Species 5, the mature form of CPOX, was stabilized over time and not further processed. To analyze the influence of the four potentially disulfide-forming cysteines as well as the general influence of cysteines on CPOX maturation, pulse chase experiments of CPOX-HA 4CA and the cysteine-free 10CA variant were performed (Figure 18 E, F, Figure S 1 F, Figure S 4 A-C). Processing of the cysteine mutants looked overall comparable to the WT as they showed five processing species including mature CPOX. However, the mature form of the CPOX cysteine mutants did not

## Results

accumulate. Instead, it seemed to be degraded as the intensity of the respective band declined over time and overall protein levels also seemed to decrease. In contrast, the processing intermediates, particularly species 3, appeared to be more prominent, mostly due to a shift in intensity ratios of the individual bands as a consequence of the less intense mature form (Figure 18 F). Notably, an impairment of processing of the CPOX cysteine mutants cannot be excluded and might contribute to the increased abundance of the CPOX precursors. As CPOX-HA 10CA completely phenocopied the 4CA variant, the observed destabilization and potentially impaired processing can be attributed to the lack of C164, C192, C304 and C357 (Figure 18 G).

Before proceeding to concentrate on the contribution of the individual cysteine pairs C164-C192 and C304-C357 to CPOX processing and stability, the general CPOX import and maturation process was further investigated. For this purpose, a CPOX construct without MTS was designed. The exact length of the CPOX presequence is not known and had been estimated to be around 110 amino acids long in import experiments [218, 219]. However, recent studies on N-termini of mitochondrial proteins not only found presequence lengths of around 110, but also of 88 amino acids for human CPOX [305-308]. Amino acid 88 lies within the predicted CPOX transmembrane domain and hence would fit with bipartite sequence processing, which is why CPOX-HA  $\Delta$ 1-88 was chosen for analysis [218, 309]. Immunofluorescence confirmed its exclusively cytosolic localization (Figure S 2). In a pulse chase experiment, CPOX-HA  $\Delta$ 1-88 showed just one prominent band at the height of species 4, which was stable and not modified over time, suggesting that in the IMS, species 4 is already lacking the major part of its presequence (Figure 19 A). Next, CPOX-HA WT was analyzed in a pulse chase experiment upon overexpression in IMMP1/2 double KO (DKO) cells, as the IMMP complex is one of the two proteases most often processing bipartite presequences (Figure 19 B). Indeed, CPOX processing was arrested at species 3, showing that IMMP1/2 mediates the cleavage from species 3 to species 4. This becomes even more apparent when looking at the quantifications of the individual CPOX processing species after 120 minutes, where no mature CPOX is present and 3 is the most abundant species in the IMMP1/2 DKO (Figure 19 C). CPOX is most likely already soluble after IMMP1/2 cleavage, as IMMP1/2 is known to cleave the TM domain close to the IMS site. The remaining amino acids might not be sufficient to hold CPOX attached to the IMM anymore. To test if CPOX is released from the IMM by IMMP1/2, carbonate extractions were performed. Here, isolated mitochondria are fractionated by incubation with sodium carbonate buffer followed by ultracentrifugation. This procedure allows to separate soluble from membrane bound or aggregated protein (Figure 19 D). Under normal conditions, CPOX is completely soluble like the IMS control MIA40 and unlike YME1L1, the IMM bound control, which were tested in parallel. In the IMMP1/2 DKO, only incompletely processed CPOX that runs higher than the mature form is in the pellet fraction, meaning without IMMP processing, it is membrane bound (Figure 19 E). In the supernatant soluble fraction, the mature form of CPOX still dominates,

although there is some impurity of incompletely processed CPOX. Probably, cells adapted to loss of IMMP1/2 and other IMM proteases can take over to produce mature CPOX, but less efficiently.

Taken together, it was demonstrated that CPOX import is mediated by a bipartite presequence, which undergoes four cleavage steps during import into the IMS. The first processing step is carried out by MPP, the third one releasing CPOX into the IMS is performed by the IMMP1/2 complex. Other proteases involved in CPOX processing and the contribution of the negative amino acid stretch are yet to be identified (Figure 19 F).

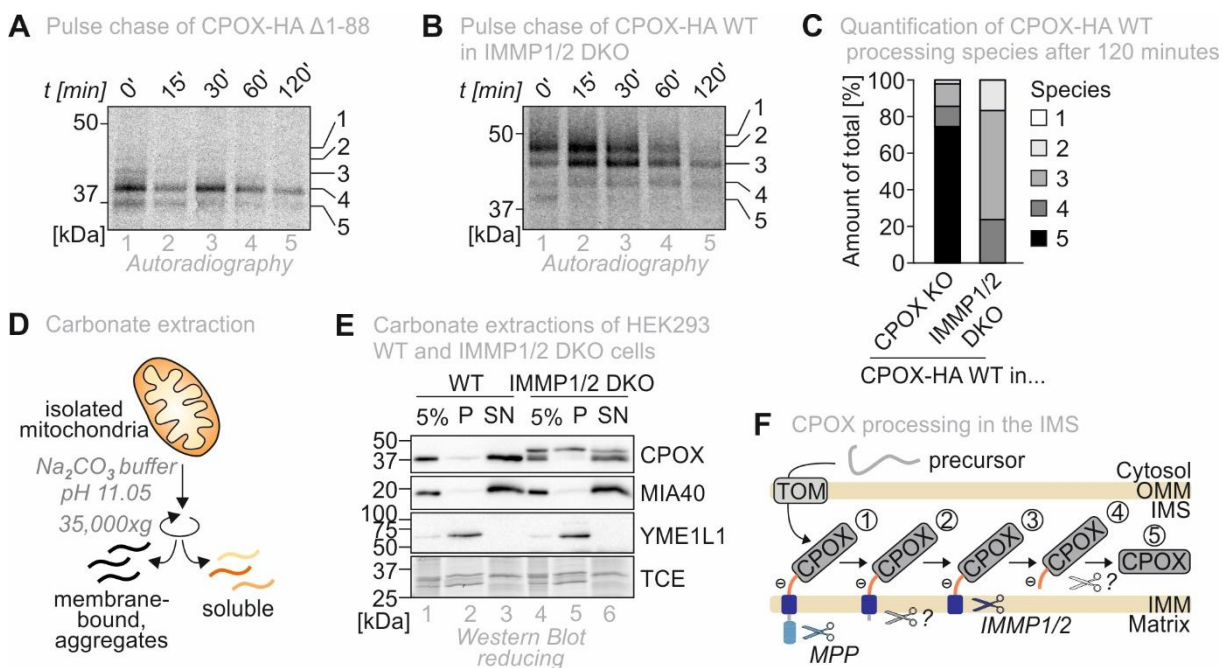


**Figure 19: CPOX enters mitochondria via a bipartite presequence and is processed by the IMMP1/2**

**A** Pulse chase of CPOX-HA  $\Delta$ 1-88 (without MTS) on CPOX KO background. **B** Pulse chase of CPOX-HA WT in IMMP1/2 DKO cells. **C** For CPOX-HA WT on CPOX KO (n=6) and IMMP1/2 DKO (n=1) it was quantified to how many percent the different CPOX processing species contribute to the total amount of protein at 120 minutes. **D** In a carbonate extraction, isolated mitochondria are incubated in sodium carbonate buffer to permeabilize membranes. Membrane bound and aggregated protein can then be separated from soluble protein via ultracentrifugation. **E** Carbonate extraction of mitochondria from HEK293 WT or IMMP1/2 DKO cells expressing CPOX-HA WT. MIA40 acts as soluble IMS control and YME1L1 as membrane-bound control. TCE staining is the loading control. P=pellet, SN=supernatant. **F** CPOX is imported into mitochondria via a bipartite presequence. After the full-length precursor (1) entered mitochondria over TOM, it is inserted into the membrane and MPP cleaves off the MTS (2). A further cleavage step happens (3), before IMMP1/2 cleaves within the TM, releasing CPOX (4). A last unknown modification, maybe associated with CPOX' negative patch, happens to produce mature CPOX (5).

Next, the individual impact of the potentially disulfide-forming cysteine pairs C164-C192 and C304-C357 on CPOX maturation and stability was assessed. For this purpose, the CPOX-HA double cysteine mutants C164,192A, C304,357A and C164,304A were analyzed in pulse chase experiments. Consistent with data presented earlier in this work, the lack of C164-C192 had a relatively weak effect on CPOX stability (Figure 20 B, Figure S 4 D). Mutation of C304 and C357, on the other hand, decreased the level of mature protein compared to WT and C164,192A, indicating that C304-C357 is more important for CPOX stability than C164-C192 (Figure 20 C, E, Figure S 4 E). The destabilization of CPOX was further

## Results

enhanced when both cysteine pairs were affected by mutations. The CPOX construct C164,304A displayed the strongest stability impairment, showing a phenotype comparable to CPOX-HA 4CA and 10CA (Figure 20 D, E, Figure S 4 F). In addition, precursor bands of the destabilized CPOX double cysteine mutants C304,357A and C164,304A seemed more prominent than precursor bands of CPOX WT. This observation might be caused by a shift in intensity ratios of the observed bands due to decreased intensity of the mature band. Additionally, there could be an influence of the missing cysteines on CPOX processing, which might further contribute to destabilization and degradation of CPOX.

In Western Blot analyses of certain CPOX-HA cysteine mutants, including 10CA, 4CA, C304,357 and C164,304A, that have been presented earlier in this thesis, a double band pattern and low overall protein levels were observed, but have not yet been addressed (refer to Figure 14, Figure 17, Figure 20, Figure S 1). The above identified decrease in stability of the respective mature CPOX variants might reflect in this double band pattern and the low steady state protein levels. Normally, mature CPOX is highly abundant and its intense band would overshadow the last precursor band running only slightly higher on Western blot. For the constructs that are destabilized in their mature form, this does not happen, revealing the second band. Earlier in this work, it was observed that particularly the 4CA and the C164,304A variants of CPOX are less oxidized than the other variants. Consequently, lack of the ability to form a certain disulfide could be the underlying reason for their observed stability problems.

To gain further insights into the connection between the CPOX redox status and its processing and stability, oxidation of newly synthesized CPOX was analyzed in oxidation kinetic experiments. For an oxidation kinetic, a radioactive pulse chase is not directly followed by precipitation of the protein of interest, but by a TCA precipitation and a redox shift experiment. Hereby, the thiol-reactive probe is directly added to the protein, free thiols are modified and oxidized cysteines are protected. Therefore, reduced protein runs at a higher molecular weight on SDS-PAGE than the oxidized form. In oxidation kinetics of CPOX-HA WT and 4CA, their oxidation was followed over time and compared to an unmodified and a TCEP-reduced control and among each other. CPOX-HA WT was fully oxidized within the first 30 minutes and then stayed in its oxidized form. CPOX-HA 4CA, in contrast, remained reduced over the tested 120 minutes, confirming that there is no disulfide bond formation in this cysteine variant (Figure 20 F, G). Hence, there is a correlation between CPOX oxidation and stability suggesting that missing disulfide bond formation between C304 and C357 in CPOX cysteine mutants could be the reason for destabilization of mature CPOX form.

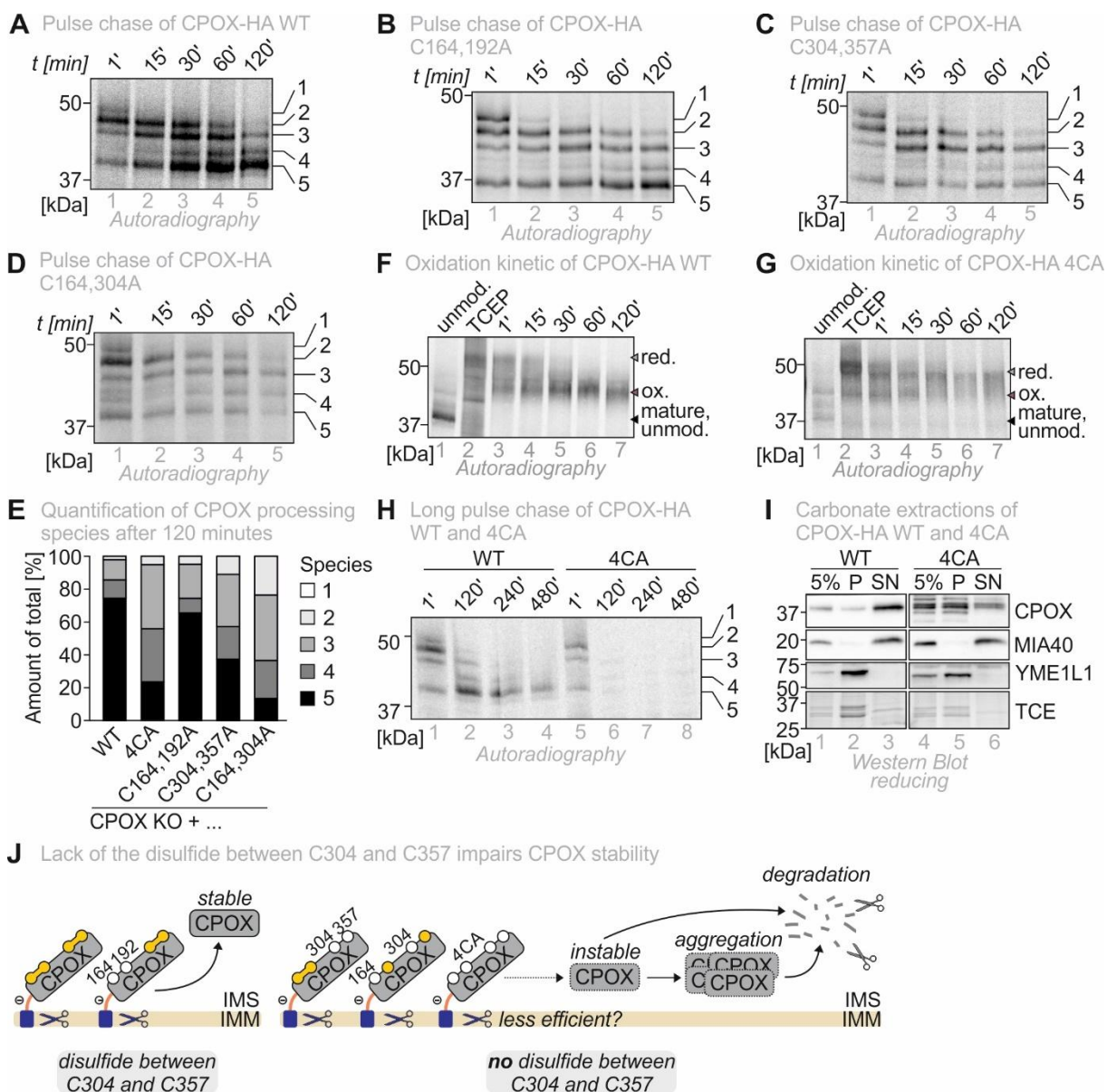


**Figure 20: Lack of the disulfide between C304 and C357 impairs CPOX stability**

**A** Pulse chase of CPOX-HA WT on CPOX KO background. **B** Pulse chase of CPOX-HA C164,192A on CPOX KO background. **C** Pulse chase of CPOX-HA C304,357A on CPOX KO background. **D** Pulse chase of CPOX-HA C164,304A on CPOX KO background. **E** It was quantified to how many percent the different CPOX processing species contribute to the total amount of protein at 120 minutes. Quantifications were done for CPOX-HA WT (n=6), 4CA (n=3), C164,192A (n=3), C304,357A (n=3), C164,304A (n=2). **F** Oxidation kinetic of CPOX-HA WT. TCEP is the reducing control. The unmodified and TCEP samples were chased for 120 minutes. **G** Oxidation kinetic of CPOX-HA 4CA. TCEP is the reducing control. The unmodified and TCEP samples were chased for 120 minutes. **H** Long pulse chase of CPOX-HA WT and 4CA over 480 minutes. **I** Carbonate extraction of mitochondria from CPOX KO cells expressing CPOX-HA WT or 4CA. MIA40 acts as soluble IMS control and YME1L1 as membrane-bound control. TCE staining is the loading control. P=pellet, SN=supernatant. **J** CPOX-HA WT and C164,192A are released into the IMS as a stable protein. In contrast, CPOX-HA 4CA, C304,357A and C164,304A that lack the disulfide between C304 and C357, are instable and aggregation prone, leading to their degradation. Less efficient processing of these variants might contribute to their destabilization.

Along these lines, stability of CPOX-HA WT and the 4CA mutant was compared in a 480-minute-long pulse chase experiment. Here, mature CPOX WT was mostly stable over the whole chase time, whereas CPOX 4CA was almost completely absent already after 120 minutes, further showing that it was

## Results

destabilized (Figure 20 H). To further investigate how missing disulfides affect CPOX stability and to test, whether the lack of cysteines and disulfides, respectively, has an influence on CPOX processing, carbonate extractions of CPOX-HA WT and 4CA were performed (Figure 20 I). Several observations could be made. The majority of CPOX-HA 4CA accumulated in the pellet fraction and only a smaller proportion was soluble. Interestingly, a clear band corresponding to the size of the IMMP1/2-uncleaved CPOX was present in the pellet fraction and the total of CPOX-HA 4CA, but not in the soluble fraction. This indicates a relevance of CPOX cysteines C164, C192, C304 or C357 for CPOX processing by IMMP1/2, as the IMMP1/2 uncleaved precursor form of CPOX is still membrane bound. However, a large proportion of CPOX-HA 4CA in the pellet was cleaved to a similar extent as the soluble protein, suggesting that it is not anymore membrane bound but rather aggregated. A complete lack of cysteines did not alter this phenotype (Figure S 1 G). Thus, removal of aggregates might be the cause for decreased levels of mature CPOX lacking certain cysteines (Figure 20 J).

All in all, data on CPOX maturation, including oxidation, and stability suggests that CPOX variants without the ability to establish a disulfide bond between C304 and C357 are more aggregation prone and less efficiently processed by IMMP1/2, which impairs their stability but not their functionality (Figure 20 J, compare also Figure 17 D-F). The other disulfide, C164-192, hereby plays a minor role, but its lack additionally aggravates the phenotype.

### 2.2.4 Cytosolic CPOX is not dependent on cysteines

The four CPOX cysteines of interest, C164, C192, C304 and C357, that are crucial for its stability and processing in the IMS, are well conserved in higher eukaryotes with IMS localized CPOX forms. The CPOX homologue in *Saccharomyces cerevisiae* (from now on only referred to as “yeast”), Hem13, however, neither contains conserved cysteines, nor are its three cysteines arranged in a way that allows disulfide formation. It also does not have an MTS but is localized to the cytosol (Figure 21 A). Therefore, the yeast homologue of ALR, Erv1, which is localized to the IMS, can most likely not interact with Hem13 (Figure 21 B). Nevertheless, the tertiary structure of CPOX is extremely well conserved among all species, which becomes apparent in an overlay of the structures of human CPOX and Hem13 from yeast (Figure 21 C). Consequently, there seems to be a correlation between the presence of cysteines and the subcellular protein localization, indicating that CPOX cysteines and disulfide formation are only relevant for mitochondrial but not for cytosolic versions of CPOX. To test this hypothesis, CPOX KO cells were complemented with a cytosolic variant of CPOX, CPOX-HA  $\Delta$ 1-88, or with yeast Hem13-HA, which also displayed cytosolic localization (Figure S 2). Both cytosolic variants were fully functional, as they could efficiently rescue the ALAS1 phenotype and growth after galactose shift and were able to transfer CPPgenIII to PPgenIX without accumulation of the educt (Figure 21 D-F). However, cells expressing

CPOX-HA  $\Delta$ 1-88 or Hem13-HA showed accumulation of the CPOX product PPgenIX (measured as PPIX, Figure 21 F).

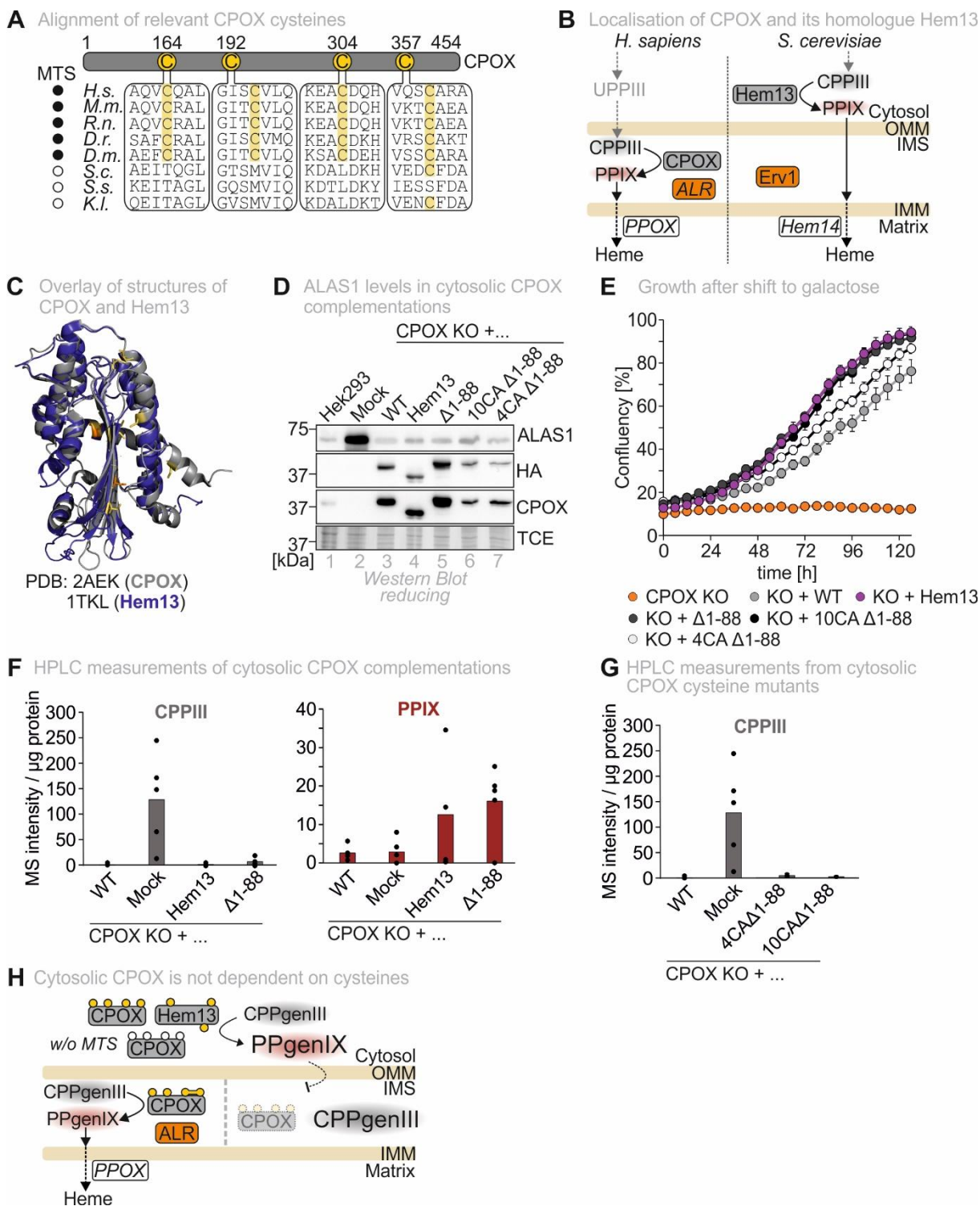


Figure 21: Activity of cytosolic CPOX is not dependent on cysteines

**A** Alignment of CPOX homologues from different species shows that the CPOX cysteines of interest, C164, C192, C304 and C357 in human, are well conserved among species in which the protein has mitochondrial localization, but not among species where it is cytosolic (different yeasts). **B** In humans and other higher eukaryotes, CPOX is found in the IMS together with ALR. In *S. cerevisiae* and other yeast strains, CPOX homologue Hem13 is in the cytosol, whereas ALR homologue Erv1 is in the IMS. **C** Overlay of crystal structures from CPOX (PDB: 2AEX) and Hem13 (PDB: 1TKL) [227, 228]. **D** Western blot of cell lysates from HEK293 cells and CPOX KO cells complemented

## Results

with a mock control, CPOX-HA WT, Hem13-HA, CPOX-HA  $\Delta$ 1-88, 10CA  $\Delta$ 1-88 or 4CA  $\Delta$ 1-88. TCE acts as loading control. **E** CPOX KO cells and CPOX KO cells complemented with CPOX-HA WT, Hem13-HA, CPOX-HA  $\Delta$ 1-88, 10CA  $\Delta$ 1-88 or 4CA  $\Delta$ 1-88 were shifted from glucose to galactose at timepoint 0 and growth was measured over 120 h. **F** HPLC measurement of CPPIII from cell lysates of CPOX KO cells complemented with CPOX-HA WT, Mock, Hem13-HA, or CPOX-HA  $\Delta$ 1-88. **G** HPLC measurement of CPPIII from cell lysates of CPOX KO cells complemented with CPOX-HA WT, Mock, 4CA  $\Delta$ 1-88 or 10CA  $\Delta$ 1-88. **H** IMS localized CPOX requires presence of disulfides for stability, otherwise, CPPgenIII accumulates. Cytosolic CPOX variants and Hem13 do not need cysteines as they do not encounter processing or destabilizing influences in the IMS. However, when cytosolic CPOX versions are expressed, PPgenIX accumulates because it cannot easily cross the OMM. Measurements in **F** and **G** were done by Dylan Stobbe and Jan Jirschwitzka.

PPgenIX produced in the cytosol needs to cross both mitochondrial membranes to reach PPOX/Hem14 (Figure 21 B) although it is a very hydrophobic and relatively large molecule and can therefore not freely move through the cell. Nonetheless, a small proportion of PPgenIX must have still reached the next enzyme in heme biosynthesis, PPOX, in the mitochondrial matrix as cytosolic CPOX and Hem13 did not show growth defects on galactose. The next step in finding out whether cytosolic CPOX requires cysteines or not was to complement CPOX KO with a cytosolic version of the 4CA mutant, CPOX-HA 4CA  $\Delta$ 1-88, and even with a cysteine-free cytosolic CPOX version, CPOX-HA 10CA  $\Delta$ 1-88. Both cytosolic cysteine mutants of CPOX could fully complement for CPOX loss in the tested conditions, which were ALAS1 levels, growth on galactose and CPPgenIII/CPPIII levels (Figure 21 D, E, G), underlining that CPOX cysteines are not relevant in the cytosol.

In conclusion, it was demonstrated that cytosolic CPOX variants do not require cysteines (or disulfides) for proper function, presumably because they do not undergo the same maturation process as IMS localized CPOX, which needs disulfides for efficient processing and stabilization. However, cells expressing cytosolic CPOX variants accumulate the porphyrin intermediate PPgenIX, which might act as an inducer of oxidative stress or sensitize cells for other kinds of stresses.

### 3. Discussion

#### 3.1 ALR could impact several mitochondrial processes

The sulfhydryl oxidase ALR has been well characterized in its function to reoxidize oxidoreductase MIA40 in the disulfide relay via a thiol-disulfide exchange mechanism. In addition, the ALR homologue in yeast and plants, Erv1, was shown to be able to directly oxidize IMS proteins in the absence of MIA40 *in vitro*, but work on MIA40-independent Erv1 activity *in vivo* is lacking [101, 310]. The possibility for human ALR to interact with other substrates except MIA40 was never addressed. In this thesis, six novel interactors of ALR have been defined with high confidence and one of them, CPOX, has been further characterized, revealing ALR functions beyond the disulfide relay (Figure 9 E-G). For the other newly identified ALR interaction partners, the way and purpose of the ALR interaction remains yet to be investigated. All novel ALR interactors share their conserved cysteines as a common feature. When comparing MIA40 substrates to ALR substrates, it can be noted that ALR generally seems to interact with proteins of higher molecular mass than MIA40. With a size of 15 kDa, MIA40 is the smallest known interactor of ALR. All other novel ALR interactors are larger than 25 kDa (with exception of the less confident NDUFA8). In contrast, most MIA40 substrates are smaller than 20 kDa [79, 311]. Additionally, MIA40 substrates are mostly soluble IMS proteins, whereas four of the seven reliable interactome hits of ALR localize to the outer or inner membrane.

Interestingly, some of the ALR interactors were also shown or proposed to be MIA40 substrates. One of these proteins is adenylate kinase AK2. AK2, like CPOX, is a highly confident hit appearing in all available interactome datasets of ALR (Figure 9 E). AK2 contains three conserved cysteines, C40, C42 and C92. During its import into the IMS via the disulfide relay, interaction with MIA40 is initiated over C40 and a disulfide is introduced between C40 and C42. Subsequently, an intramolecular shuffling of the disulfide bond is proposed to happen, as the IMS localized mature AK2 contains a disulfide between C42 and C92 instead of C40 (PDB: 2C9Y) [312]. However, it is unknown how the isomerization of this disulfide is achieved. Internal isomerization, an isomerase function of MIA40 or proofreading by GSH were suggested to mediate the disulfide switch. The interactome data on ALR provides an additional possible mechanism, as ALR could be responsible for the disulfide isomerization of AK2 (Figure 22 A). An interaction between the hydrophobic stretch in ALR's shuttle arm surrounding the CRAC motif and the MISS of AK2 might thereby contribute to the correct positioning of the involved cysteines. Another newly defined interaction partner of ALR is AIFM1. In contrast to AK2, AIFM1 is not a substrate, but an important component of the disulfide relay. In its dimeric form, AIFM1 interacts with MIA40 to support its import and afterwards forms a stable complex with MIA40 that serves as an interaction platform for MIA40 with its substrates [84, 94]. AIFM1 is also a pro-apoptotic factor, which is released into the cytosol upon cell injury. From there it then translocates to the nucleus promoting caspase-independent

## Discussion

cell death [313, 314]. Interaction of AIFM1 with ALR could not only be detected in four out of six ALR interactome datasets presented in this thesis, but also in three native AIFM1 interactome datasets that have been performed and published by our lab [315]. Therefore, AIFM1 is a very reliable hit. AIFM1 cysteines are not oriented in a way that they could form an intramolecular disulfide, whereas disulfide bond formation between two monomers during AIFM1 dimerization also seems unlikely [316]. A possible explanation for the observed interaction of AIFM1 and ALR could be an indirect interaction of ALR and AIFM1 over MIA40. However, an indirect interaction contradicts the precipitation of AIFM1 with ALR under denaturing conditions, where only covalent interactions remain stable. Interestingly, a study from 2015 reported the cysteine-dependent interaction between AIFM1 and thioredoxin-1 (TRX1) in the cytosol of HEK293 cells. Here, the interaction with TRX1 prevented AIFM1-mediated DNA damage and apoptosis induction under non-stress or mild stress conditions by preventing interaction of AIFM1 with other proteins involved in DNA fragmentation [317]. Two of the three AIFM1 cysteines were required to establish the interaction with TRX1, whereas no specific cysteine of AIFM1 was needed. A comparable kind of interaction could be imagined between AIFM1 and ALR. One or more ALR molecules might be able to bind individual AIFM1 cysteines, for example to modulate binding of AIFM1 to other interactors or to prevent translocation of AIFM1 into the cytosol under mild stress conditions (Figure 22 B). Another novel interactor of ALR is MTCH2. MTCH2 is localized to the OMM and inserts  $\alpha$ -helical OMM proteins using a hydrophilic groove within the membrane [301]. Human MTCH2 contains 11 cysteines that are all conserved among mammals. Analysis of the AlphaFold structure and the predicted membrane orientation of MTCH2 reveals that most of these cysteines are accessible from the IMS site. Assuming some flexibility of the structure, disulfides might be established between C160-C163, C249-C255 and/or C49-C297. In principle, C296 and C297 could also form a vicinal disulfide. This form of disulfide is observed rarely and only a small number of proteins with a vicinal disulfide is known yet, however it is possible [318]. None of the cysteines that are a potential ALR target are adjacent to the hydrophilic cavity that inserts MTCH2 substrates, hence an interaction with ALR is unlikely to influence insertase activity of MTCH2. As a relatively large part of MTCH2 is predicted to reach into the IMS, disulfides could have a stabilizing influence on this part of the protein. They might also induce a conformational change in the IMS part of MTCH2, which could promote interactions with other proteins (Figure 22 C). The ALR interaction partner TIM50 is a single-span IMM protein that acts as a receptor of the TIM23 complex [39]. It contains four cysteines that are all conserved among mammals. Two cysteines of TIM50, C133 and C236, are found in close proximity in the predicted AlphaFold model. These cysteines are not localized near the presequence-binding groove that was proposed for the TIM50 homologue in yeast [319]. Although the sequence identity between human and yeast TIM50 is only 31.6%, the overall structure is similar. A potential disulfide bond between C133 and C236 would link a long unstructured loop to another mostly unstructured region of the protein.

This might be relevant to keep the overall shape of TIM50 intact (Figure 22 D). Consequently, a structural role for this potential disulfide can be suggested. The last high-confident interaction partner of ALR that was identified in the interactome screen is the porin VDAC2, which allows small molecules to cross the outer membrane [136, 300]. VDAC2 contains nine cysteine residues that are all conserved among mammals. Seven of these cysteines face the IMS. The residues C8 and C13 are localized on a flexible arm on the IMS site of VDAC2 that can reach into the inside of the barrel. The other cysteines are positioned on the edges surrounding the entry of the pore. In the predicted AlphaFold model, C13 and C133 are the cysteine residues with the smallest distance. However, their localization on the flexible arm of VDAC2 could allow for C8 or C13 to form a disulfide bond with all five cysteines on the IMS site of VDAC2. Such a disulfide could orientate the flexible arm of VDAC2 inside the pore and partially clog it, thereby increasing selectivity and gating (Figure 22 E). Unpublished data from our lab described an altered VDAC2 redox status upon siRNA-mediated depletion of ALR. Additionally, disulfide-mediated dimer formation of VDAC2 was observed under oxidative stress conditions. Cysteines C8 and C13 could be identified as the residues involved in dimerization. Thus, it is also possible that ALR promotes disulfide-induced dimerization of VDAC2.

Interaction of ALR with all high-confidence interactors discussed above, eventually with the exception of AIFM1, seems to be covalent and based on a mixed disulfide intermediate. Formation of a mixed disulfide is the canonical way of interaction between ALR and its substrates, but cannot explain non-covalent interactions between ALR and other proteins. As described earlier in this work, ALR employs a complex intramolecular electron transfer mechanism to shuttle electrons from a substrate to cytochrome c [101, 107, 108]. In the usual case, these electrons originate from oxidation of substrate cysteines. However, it might also be possible for ALR to act as an electron acceptor for electrons that are released during enzymatic reactions, given that ALR was close to the active site. Correct orientation of the ALR CRAC motif could be achieved by hydrophobic interactions between ALR's shuttle arm and the respective enzyme. Such a role of ALR as an additional electron acceptor in the IMS would be beneficial to avoid overproduction of ROS. Still, experimental data supporting this idea is so far lacking.

In conclusion, ALR seems to impact many different mitochondrial pathways via interaction with its various substrates and the resulting introduction of disulfide bonds. Thereby, ALR could be indirectly involved in nucleotide conversion, protein import and distribution, metabolite transport, heme biosynthesis and more.

## Discussion

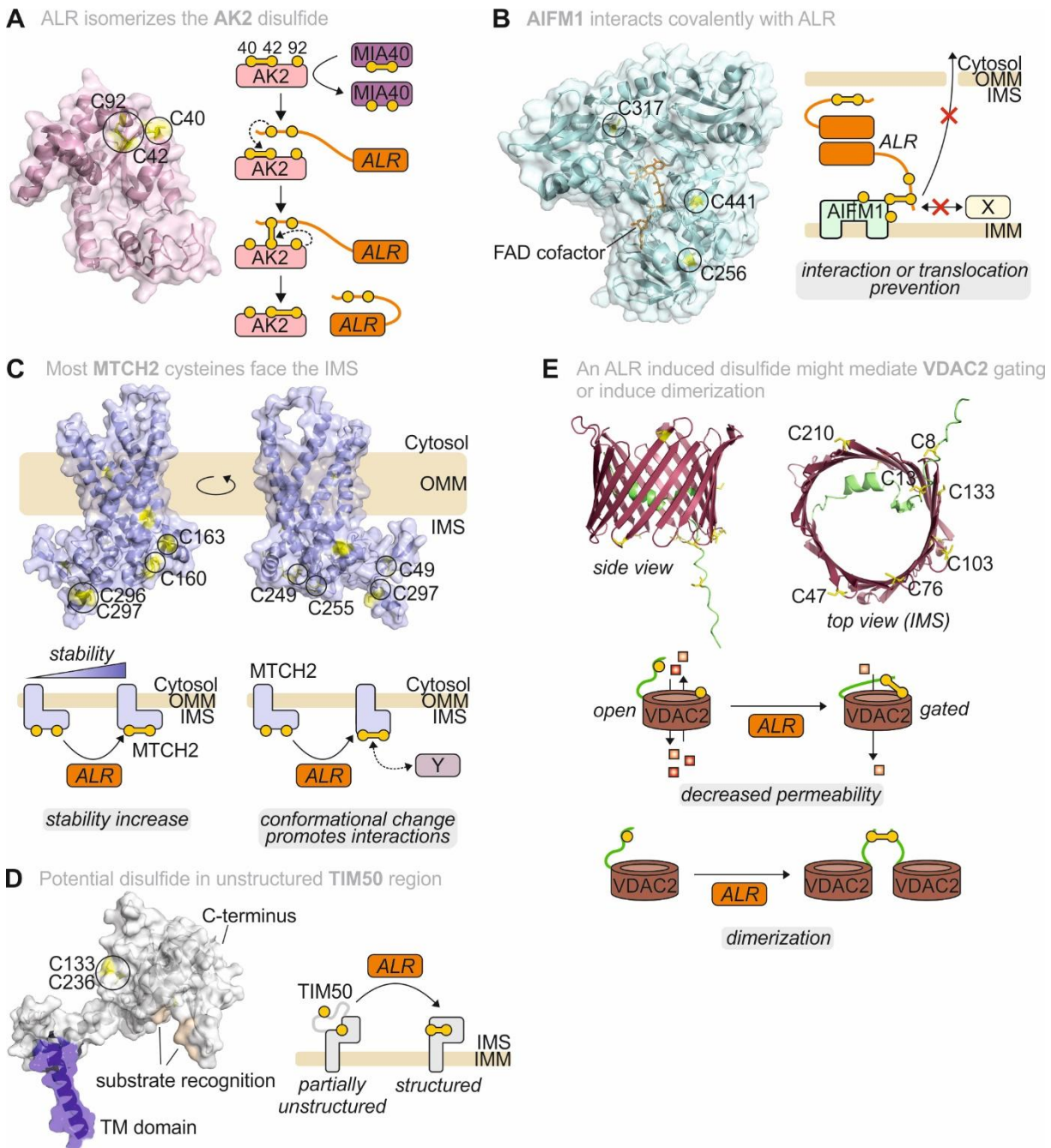


**Figure 22: Possible ways of ALR interaction with novel substrates**

**A** During import via the disulfide relay, AK2 gains a disulfide between C40 and C42, which is afterwards isomerized to a disulfide between C42 and C92 (PDB: 2C9Y) [312]. As ALR was shown to interact with AK2, isomerization of the disulfide could be mediated by ALR. **B** The cysteines of AIFM1 are distributed over the protein with no potential disulfide to be identified (PDB: 4LII). Interaction of ALR with AIFM1 could prevent interaction with other proteins or AIFM1 translocation into the cytosol under mild stress conditions, thereby preventing early apoptosis induction. **C** MTCH2 contains 11 conserved cysteines (yellow), most of them being exposed to the IMS. ALR could introduce disulfides between C160-C163, C249-C255, C296-C297 or C49-C297. Due to their distance to the substrate binding cleft, they are presumably involved in stabilization or interaction with additional IMS proteins and do not affect the MTCH2 insertase function. **D** TIM50 contains four conserved cysteines, two of which are localized in close proximity. Both cysteine residues are positioned in unstructured parts of TIM50 and exposed to the IMS. A disulfide introduced by ALR could restrict free movement of these regions and help to preserve the compact shape of TIM50. TIM50's transmembrane domain is shown in blue. The proposed substrate recognition area is light brown. **E** Seven of the nine cysteines (yellow) in VDAC2 face the IMS, five on the edge of the channel and two on a flexible arm (green) reaching from inside of the channel into the IMS. An ALR induced disulfide bond

could connect the flexible arm of VDAC2 with the edge of the channel to decrease VDAC2 permeability and increase gating. Alternatively, ALR could promote disulfide-induced VDAC2 dimerization.

### 3.2 ALR induced disulfides are important for CPOX stabilization in the IMS

Disulfides can have two major implications for proteins. On one hand, they can influence a protein's activity by regulation (e.g. ERO1) or by direct participation in its activity cycle (e.g. MIA40). On the other hand, disulfides can increase the stability of proteins [87, 100]. In this work, the impact of disulfides on heme biosynthesis protein CPOX was investigated. It could be shown that CPOX requires at least one structural disulfide to preserve its stability and prevent it from aggregation and degradation in the IMS. Data suggests that this structural disulfide is introduced by sulfhydryl oxidase ALR, which was previously only known for its role in the disulfide relay [101, 106, 107]. In contrast to mitochondrial CPOX, cytosolically localized CPOX does not seem to require disulfides for stability and function (Figure 23). As CPOX was shown to be fully active in the cytosol independent from the presence of disulfides or cysteines in general, its overall fold does not seem to be affected.

ALR induced disulfide stabilizes CPOX in the IMS

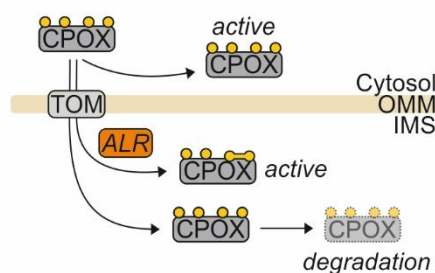


Figure 23: An ALR induced structural disulfide stabilizes CPOX in the IMS

In the IMS, CPOX needs an ALR-induced disulfide to preserve its stability and prevent it from degradation. Without the disulfide, it is degraded. On the other hand, cytosolic CPOX does not require disulfides for stability and is fully active.

Although cytosol and IMS share similarities with respect to their small molecule composition, they differ in their protein and lipid composition and in availability of space, as the IMS is a small and densely packed compartment [27, 164]. Moreover, cytosol and IMS differ in their temperature due to mitochondrial heat production [320, 321]. Heat in mitochondria is generated through the activity of the respiratory chain in the IMM of cristae and the associated proton leak. Proton leak is defined as a flux of protons into the matrix without being coupled to ATP production, which is an important mechanism involved in the thermal balance of organisms, especially for endotherms [322, 323]. Respiratory chain complexes are concentrated in cristae and mitochondria are engulfed by a double membrane, which might limit the spread of heat throughout the cell. Thus, it can be assumed that mitochondria operate at higher temperatures than the surrounding cell environment to maintain a temperature of around 37°C in the organism [321]. Data from studies with different temperature-sensitive fluorescent sensors show the presence of a temperature gradient across human cells and

## Discussion

suggest a mitochondrial operation temperature between 38°C and 50°C, whereas most studies agree on a temperature between 38°C and 43°C [321, 324-330]. Structural disulfides are known to increase the stability of a protein and make it less susceptible to denaturation, hence preventing aggregate formation, for example under heat stress conditions [85]. This is a likely reason why CPOX requires a stabilizing disulfide in the IMS, but not in the cytosol (Figure 24). Heat stress is a general challenge for mitochondrial proteins, but there are tissues that have increased heat production in comparison to others [323]. Adipose tissue and skeletal muscle both harbor specific uncoupling proteins (UCPs) that are located in the IMM and regulate proton re-entry into the matrix [331]. Brown adipose tissue is known for its non-shivering thermogenesis, the ability to produce heat without muscle activity. High rates of heat production are here enabled by UCP1 (also named SLC25A7). Further, it was shown that also white adipose tissue can express UCP1 and thereby increase heat production upon cold stimuli [332]. In skeletal muscle, heat production is suggested to be mediated by UCP3 (also known as SLC25A9) and increased upon exercise [333, 334]. Therefore, in muscle and adipose tissue the requirement of thermostability of proteins is supposedly higher than in other tissues.

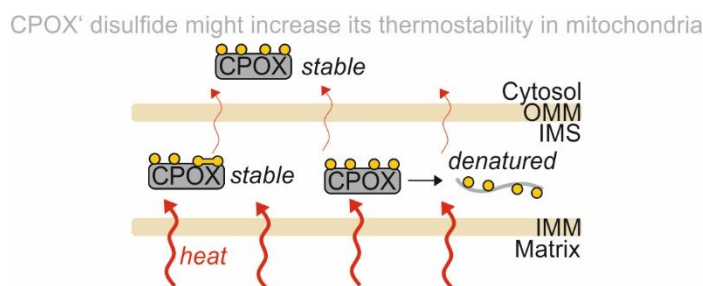


*Figure 24: CPOX' second cysteine pair increases its temperature stability*

The CPOX disulfides bond between C304 and C357 might stabilize it against increased temperatures in the mitochondrial IMS.

### 3.3 The complex CPOX maturation and its role for regulation and quality control

Heme biosynthesis enzyme CPOX is imported via a bipartite presequence, an import pathway which includes one cleavage step for removal of the protein's MTS and one cleavage step within the protein's transmembrane domain after import to release it into the IMS [202, 217-219]. In the course of this thesis, it was observed that CPOX undergoes multi-step processing during mitochondrial import, showing that CPOX maturation is a more complex process than proposed by previous publications (Figure 25 A) [4, 202, 217-221]. Analysis of CPOX import revealed four different cleavage steps required for production of the mature protein. Use of different protease KO cell lines identified the IMM1/2 complex as the mediator of CPOX cleavage within the transmembrane domain of its bipartite presequence, enabling release into the IMS.

### First and second step of CPOX processing

Following CPOX maturation chronologically, the first processing step is the removal of the CPOX MTS by MPP after translocation of this part of the protein into the matrix via TIM23 (Figure 25 A). In pulse chase experiments on CPOX maturation, MPP cleavage was observed to be fast, as there was no remaining full-length CPOX precursor after the first 15 minutes of chase. Speculating about the protease promoting the second step of CPOX processing, after MPP and before IMMP1/2 cleavage, the mitochondrial intermediate peptidase (MIP) is a plausible candidate. MIP is a soluble monomeric metalloprotease in the mitochondrial matrix that removes an octapeptide from the N-terminus of its substrates after MPP cleavage [53, 335-338]. This cleavage removes destabilizing amino acids from the N-terminus of substrate proteins, thereby increasing their half-lives [335]. A study in yeast showed that MIP homologue octapeptidyl aminopeptidase 1 (Oct1) can process Prx1 in the mitochondrial matrix [58]. Notably, Prx1 has also been identified as Imp2 substrate. The authors demonstrated a dual localization for Prx1 in the matrix and the IMS of mitochondria, where only the matrix proportion of Prx1 was cleaved by Oct1, while the IMS localized part of Prx1 was processed by Imp2 (Figure 25 B).

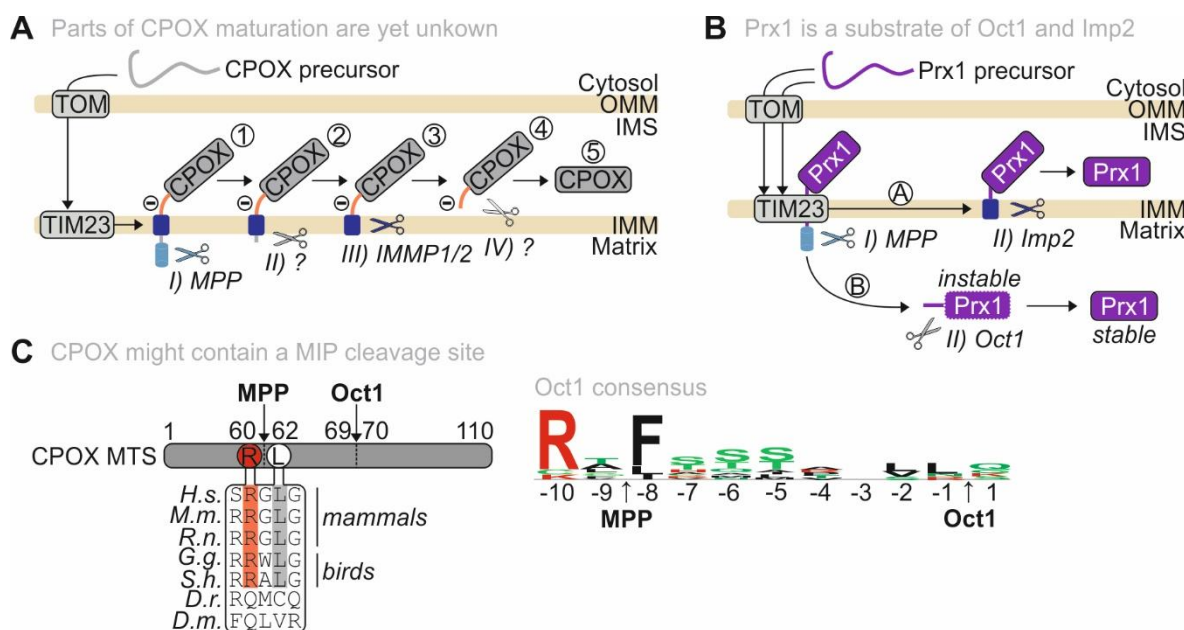


Figure 25: CPOX processing might involve MIP cleavage

**A** CPOX processing involves cleavage by four proteases. However, only MPP and IMMP1/2 are known to be involved in CPOX maturation. The other two proteases remain elusive. **B** Yeast protein Prx1 displays dual localization in IMS and matrix. During import, Prx1 MTS is removed by MPP. Afterwards, Prx1 can be integrated into the IMM, where it is released from into the IMS by Imp2 (option A). Alternatively, Prx1 is fully translocated into the matrix, where Oct1 removes an octapeptide to produce mature, stable matrix-localized Prx1 [58]. **C** CPOX might contain a MIP cleavage site. It contains residues conserved in mammals and birds, which would fit to the consensus sequence that was determined for Oct1 in yeast. Figure of consensus motif adapted from [335].

Although CPOX is exclusively found in the IMS, this observation supports the idea that IMMP1/2 substrates could also be cleaved by MIP. Therefore, CPOX was analyzed for a potential MIP cleavage site. The yeast homologue of MIP, Oct1, has been shown to preferentially cleave substrates possessing an R at position -10 and an F, L, or I at position -8 as determined by comparison of the 14 known Oct1

## Discussion

substrates [339, 340]. Prediction with the iMLP tool suggested a length of 63 amino acids for the CPOX MTS [341], whereas the transmembrane domain of CPOX is predicted to span from amino acid ~70 to ~100, depending on the source or tool employed (comparison between Jalview [309], TMHMM 2.0 Transmembrane domain prediction [342, 343] and [218]). Remarkably, CPOX fulfills the requirements for a MIP cleavage site with an R at position 60 and an L at position 62, which are conserved among mammals and birds and would correspond to the positions -10 and -8, assuming MIP cleavage between amino acid residues 69 and 70 (Figure 25 C). Hence, MIP is a promising candidate mediating the second CPOX maturation step, suiting with current knowledge and predictions on CPOX MTS length and transmembrane domain position within the bipartite sequence. MIP processing prior to IMM1/2 cleavage might be beneficial for CPOX. Removal of destabilizing residues from CPOX' N-terminus could stabilize the IMM-anchored CPOX precursor from the matrix site of the membrane until its release into the IMS.

### *IMMP catalyzes the third CPOX processing step*

The third maturation step of CPOX within its transmembrane domain is catalyzed by the IMM1/2 complex (Figure 26 A). IMM processing is rather slow in comparison to cleavage by other mitochondrial proteases like PARL [65, 66, 81]. A good example underlining the different cleavage kinetics of PARL and IMM relative to protein folding is presented by Saita *et al.* [66]. In this work, processing of STARD7 by PARL was analyzed. PARL processes STARD7 during its import rather fast. Therefore, a proportion of STARD7, which has not been fully translocated into the IMS by the TOM complex yet, can retranslocate back into the cytosol explaining STARD7's dual localization in cytosol and IMS. When STARD7 was equipped with the presequence of IMM1L substrate MICU1 instead of its own presequence, STARD7 was processed by IMM1L resulting in an exclusively mitochondrial localization. This observation implies that IMM1L cleavage is slower than PARL cleavage, as it allows for complete import and folding of the substrate protein, trapping it in the IMS, before release from the IMM is mediated. Appropriately, IMM1/2 cleavage seems to be the rate-limiting step during CPOX maturation (Figure 26 A). Of all CPOX processing intermediates (species 1-4), the IMM1/2 substrate band (species 3) was the most prominent one. Processing of this precursor was still not completed after 120 minutes (see Figure 18, Figure 20, Figure S 4). It can be assumed that IMM cleavage is only initiated, when the IMM1/2 substrate, in this case CPOX, is fully imported and/or folded, preventing its retranslocation back to the cytosol. Folding kinetics of proteins are generally dependent on the size of the molecule and the complexity of its tertiary structure [344]. Already identified IMM1/2 substrates vary strongly in size, which indicates that IMM1/2 might need to sense its substrate's folding state. It has already been shown that other mitochondrial proteases are able to sense the folding state of their substrates. Relevant examples are AAA-proteases, which have been implicated not only in protein degradation but also in protein processing. In yeast, *i*-AAA protease Yme1 was found

to sense the folding state of solvent-exposed domains of substrates via the amino-terminal region of its AAA domain [125]. Another study in yeast identified a similar mechanism for the *m*-AAA protease and its substrate mitochondrial ribosomal subunit protein MrpL32 [345]. MrpL32 contains a CxxC-X<sub>9</sub>-CxxC motif that can bind a metal ion, which is important for protein stability. In case of mutations in the cysteine motif, the protein is not matured by *m*-AAA protease, but degraded (Figure 26 B). Interestingly, a comparable asseveration was made in this thesis. When CPOX' stabilizing disulfide between C304 and C357 was disturbed, IMMP1/2 cleavage of CPOX appeared to be less efficient, potentially because IMMP1/2 might be able to recognize this disulfide bond as a sign for complete folding of CPOX (Figure 26 C). This could result in a time-dependent competition between processing by IMMP1/2 and degradation.

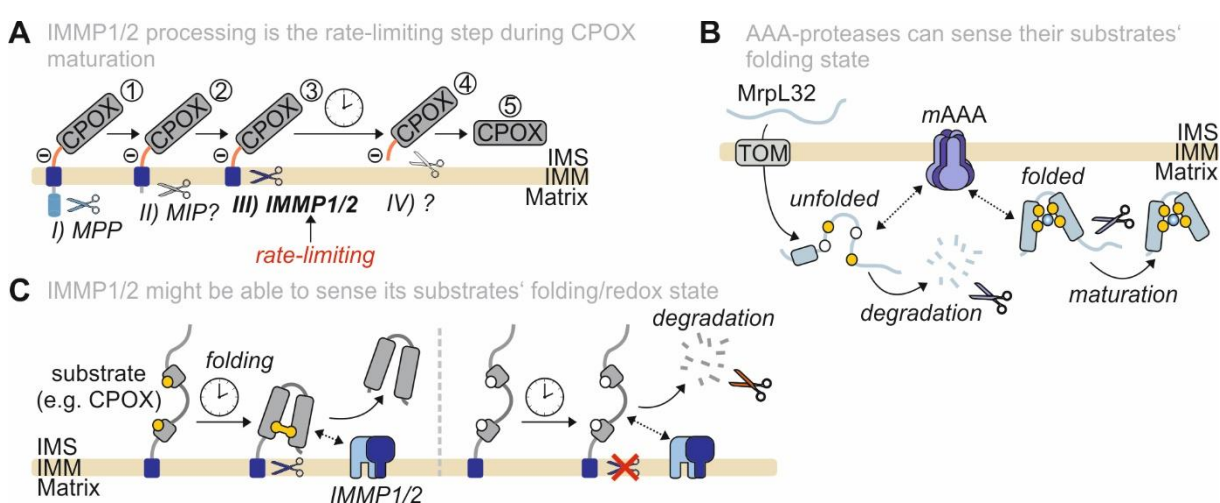


*Figure 26: Some mitochondrial proteases can sense their substrates folding state*

**A** IMMP1/2 processing is particularly slow compared to other proteases, making it the rate-limiting step during CPOX maturation. **B** AAA-proteases can sense their substrates' folding state. In yeast, the *m*-AAA-protease senses the folding state of MrpL32 to decide whether it is matured or degraded. MrpL32 folding and stability requires cysteine-dependent metal ion incorporation [345]. **C** The IMMP1/2 complex might sense the folding or redox state of substrates like CPOX to ensure complete folding prior to release into the IMS. If folding takes too long, degradation of the substrate might be initiated.

#### *Fourth step of CPOX processing – generating mature CPOX*

Only speculations can be formulated on CPOX fate after release from the IMM. Remarkably, the IMMP1/2-cleaved version of CPOX, which lacks the first 88 amino acids, is most widely detected in N-terminomic datasets [305-308]. A CPOX version lacking around 110 amino acids, corresponding to the size of mature CPOX, is also found, but not in all studies. Nevertheless, Western blot analyses of cell lysates from HEK293 and HepG2 cells done in the course of this study showed that under normal conditions, the mature form of CPOX is the predominant form. CPOX  $\Delta$ 1-88 was only present in the cell in low levels and its visibility on Western blot improved under conditions where the mature CPOX was destabilized by cysteine mutations. As mature CPOX and CPOX  $\Delta$ 1-88 show very similar running behavior on SDS-PAGE as their molecular weight only differs minimally, the high intensity signal of mature CPOX tends to overshadow the signal of the  $\Delta$ 1-88 form. More experiments are needed to identify

## Discussion

the protease involved in the terminal step of CPOX maturation, however there are several possibilities how mature CPOX could be produced.

It is highly probable that the mature form of CPOX can only be produced by cleavage of CPOX  $\Delta$ 1-88, as no mature CPOX is produced in an IMMP1/2 DKO cell line. Several proteases are worth considering for this cleavage (Figure 27 A). The soluble IMS protease ATP23 has so far only been studied in yeast and only one substrate, Atp6, is known yet. Atp23 processes Atp6 before it promotes Atp6 assembly into the F<sub>1</sub>F<sub>0</sub>-ATP synthase complex. Atp23 therefore displays a proteolytic and a chaperoning function [82, 128, 346, 347]. Due to lack of knowledge on ATP23 substrate recognition, participation in CPOX maturation cannot be excluded. Another IMS protease is HTRA2 (also called OMI). HTRA2 is a serine protease with chaperone-like activity, which is involved in mitochondrial protein quality control degrading misfolded proteins. It is also involved in apoptosis, as it can translocate into the cytosol, where it degrades members of the inhibitors of apoptosis (IAP) family [348-351]. Assuming that CPOX folding is complete at its last precursor stage, cleavage by HTRA2 seems unlikely. Although rarely observed, the last CPOX processing step might be again mediated by the IMMP1/2 complex, particularly considering the distinct specificity of the two IMMP subunits whose active centers are both orientated towards the IMS. For Imp1 substrate mitochondrial genome required 2 (Mgr2) in yeast, it is suggested that Imp1 cleaves an IMS exposed part, indicating that Imp1 can exert cleavage activity also outside of the inner membrane [55]. OMA1, YME1L1 and PARL are less likely candidates for promotion of the last CPOX maturation step, as depletion of either of these proteases did not impact CPOX running behavior on SDS-PAGE (Figure S 5 and unpublished data). For OMA1 and YME1L1, this finding fits to current knowledge. OMA1 remains inactive until activation upon mitochondrial stress, whereas YME1L1 is mostly involved in degradation of misfolded proteins [352-355]. Although PARL KO showed no influence on CPOX' molecular weight on Western blot, PARL is still an interesting protease to look at in the context of CPOX processing. The reason is a conserved negative stretch in CPOX, which spans from amino acid 116 to 122 and is hence located directly at the N-terminus of mature CPOX (Figure 27 B). Such an accumulation of conserved negative residues in proteins is rare and expected to have a relevant function. Notably, a similar negative stretch has been shown to mediate interaction and sorting of PARL substrate STARD7 in human [66]. In yeast, a prominent and well conserved negative stretch in Mgm1 upstream of the Pcp1 cleavage site mediated recognition of it by Pcp1 and also by human PARL, which was expressed in a  $\Delta$ *pcp1* strain [356]. Besides this potential role in PARL recognition, the negative stretch in CPOX might promote electrostatic interactions with positively charged parts of other proteins (Figure 27 C). Possible targets for an interaction with CPOX could be porphyrin intermediate transporters. Such an interaction would facilitate the handover of the hydrophobic, potentially cytotoxic porphyrin intermediates and provide an explanation why CPOX is sometimes described as loosely associated to the IMM [220, 221]. Although the relevance of the negative amino acid motif for

CPOX is still unclear, it is assumed to impact an IMS specific process, as CPOX and its cytosolically localized homologue Hem13 share common features only from CPOX' M130 on that corresponds to the initial methionine of Hem13 (Figure 27 B).

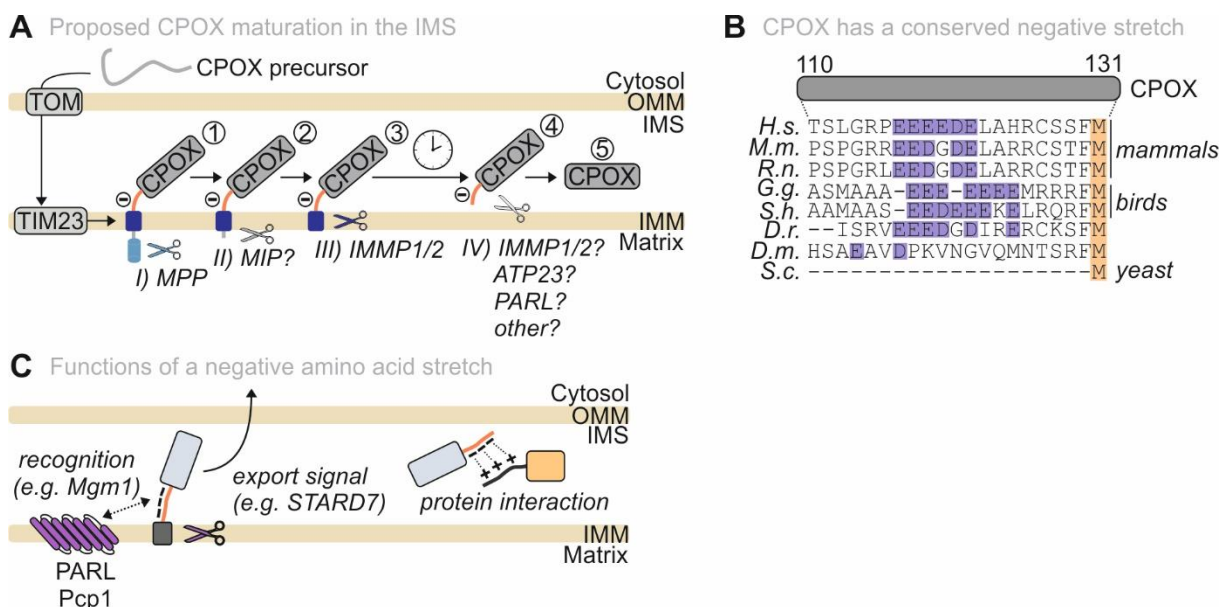


Figure 27: CPOX' conserved negative stretch might influence its last processing step

**A** CPOX is matured through a multi-step processing. After import over TOM and TIM23, MPP removes the MTS from the full-length CPOX precursor. In the second step, MIP might remove an octapeptide from the CPOX' N-terminus. Afterwards, IMMP1/2 releases CPOX into the IMS. IMMP1/2 cleavage is slow and thought to be the rate-limiting step during CPOX processing. It is not clear, how mature CPOX is produced. The last cleavage could be mediated by different proteases. Likely candidates are ATP23, PARL or again the IMMP1/2 complex. **B** CPOX contains a conserved negative amino acid stretch following the transmembrane domain of its bipartite MTS. Accumulation of negative residues in this region is conserved, particularly in mammals and birds. **C** A negative amino acid stretch in proteins has been shown to serve as recognition motif of certain PARL/Pcp1 substrates and can also act as export signal after PARL processing [66, 356]. Besides that, a negative stretch could mediate contact with other proteins via electrostatic interactions.

Another option to consider is that CPOX  $\Delta$ 1-88 and CPOX  $\Delta$ 1-110 might represent alternative isoforms instead of precursor and mature protein. The presence of different CPOX isoforms would explain the detection of both CPOX versions by N-terminomics and sometimes also by Western blot [305-308]. In this scenario, the longer CPOX isoform would either originate from an additional cleavage step of one proportion of the CPOX pool by a fourth protease or from alternative processing by the IMMP1/2 subunits IMMP1L and IMMP2L. Alternative processing by IMMP1/2 does also not contradict the observed arrested CPOX processing at stage 3 in IMMP1/2 DKO cells. For other mitochondrial proteins like OPA1, alternative processing leading to isoforms of different lengths with different functions has been described already [357]. For OPA1, a combination of longer and shorter isoforms is required for mitochondrial fusion. Importantly, the idea of two CPOX isoforms is speculative and would imply decreased stability of the CPOX  $\Delta$ 1-88 variant in comparison to CPOX  $\Delta$ 1-110 to fit to the data presented in this thesis (see Figure 19, Figure 20). Moreover, a potential purpose for the requirement of two

## Discussion

different CPOX isoforms cannot be formulated on the basis of current knowledge about CPOX, making this hypothesis the less probable one.

### *The complex CPOX processing might be constitute new aspect of heme biosynthesis regulation*

The multi-step processing that CPOX undergoes is complex and rare among mitochondrial proteins. Observing the different cleavage events and corresponding kinetics, the question about the purpose of this maturation pathway is raised. CPOX import and processing is slow, not only due to the individual maturation steps (e.g. IMMP1/2 cleavage), but also because instead of the usually two-step maturation of proteins with bipartite presequence, CPOX requires four. Another protein with a complex maturation pathway is SUOX. Like CPOX, SUOX contains a long bipartite presequence and is released into the IMS by the IMMP1/2 complex. The slow processing allows SUOX to bind its first cofactor, the molybdenum cofactor (Moco), which is needed to trap SUOX in the IMS and prevent retranslocation into the cytosol. Moco binding to SUOX is also prerequisite to integrate its second cofactor heme [358]. CPOX is a cofactor-free enzyme. Instead, it requires disulfides for stability. CPOX processing might be slow enough to allow for concurrent disulfide bond formation in CPOX mediated by ALR. Besides that, heme biosynthesis needs to be tightly regulated at different points. Regulation mechanisms on transcriptional, translational or protein level or in cofactor binding are existing for at least four of the eight heme biosynthesis enzymes. CPOX' multi-step maturation enables control of CPOX levels via all involved proteases and provides enough time to allow for quality control. In case of incorrect folding and/or missing disulfide formation, CPOX can be degraded before it is released into the IMS. Degradation of CPOX is likely initiated by YME1L1, which is the most prominent protease involved in protein degradation in the IMS [69, 125, 355].

### 3.4 Mitochondrial CPOX localization avoids protoporphyrinogen IX accumulation

The CPOX protein and its mitochondrial localization are well conserved among higher eukaryotes. The CPOX homologue in yeast, Hem13, on the other hand, shares the same fold, but does not contain an MTS, making it a cytosolic protein (Figure 28). Nevertheless, the here presented work shows that Hem13 as well as cytosolic variants human CPOX were able to fully complement for CPOX loss in human cells independent of their cysteine content, presumably as long as their fold is intact. The relevance of cysteines for IMS and cytosolically localized CPOX has already been discussed in section 3.1. There is, however, still the open question about the purpose of CPOX' evolutionary relocalization from cytosol to IMS considering that CPOX was observed to be functional in both compartments. Notably, this question can be partially answered by data from this thesis. The CPOX product PPgenIX is highly hydrophobic and not soluble in aqueous environment (Figure 7 D). Free PPgenIX is therefore not able to move through the cell independently. Chaperoning proteins are required to prevent PPgenIX from

binding to any hydrophobic surface instead. PPgenIX can therefore hardly be transported over OMM and IMM into the matrix to encounter the next enzyme PPOX. Only a small part of PPgenIX might reach PPOX for porphyrin production, whereas the rest accumulates in the cytosol. HPLC measurements revealed, that CPOX KO cells complemented with Hem13 or cytosolic CPOX could efficiently convert CPPgenIII to PPgenIX, but displayed PPgenIX accumulation (Figure 21 F, H). Conclusively, PPgenIX transport to PPOX seems to be much more efficient when PPgenIX is produced in the IMS close to PPgenIX transporters (Figure 29). Free PPgenIX and PPgenIX accumulation are toxic and cause cellular damage. Hence, localization of CPOX in the IMS instead of the cytosol is an evolutionary advantage to protect cellular fitness.

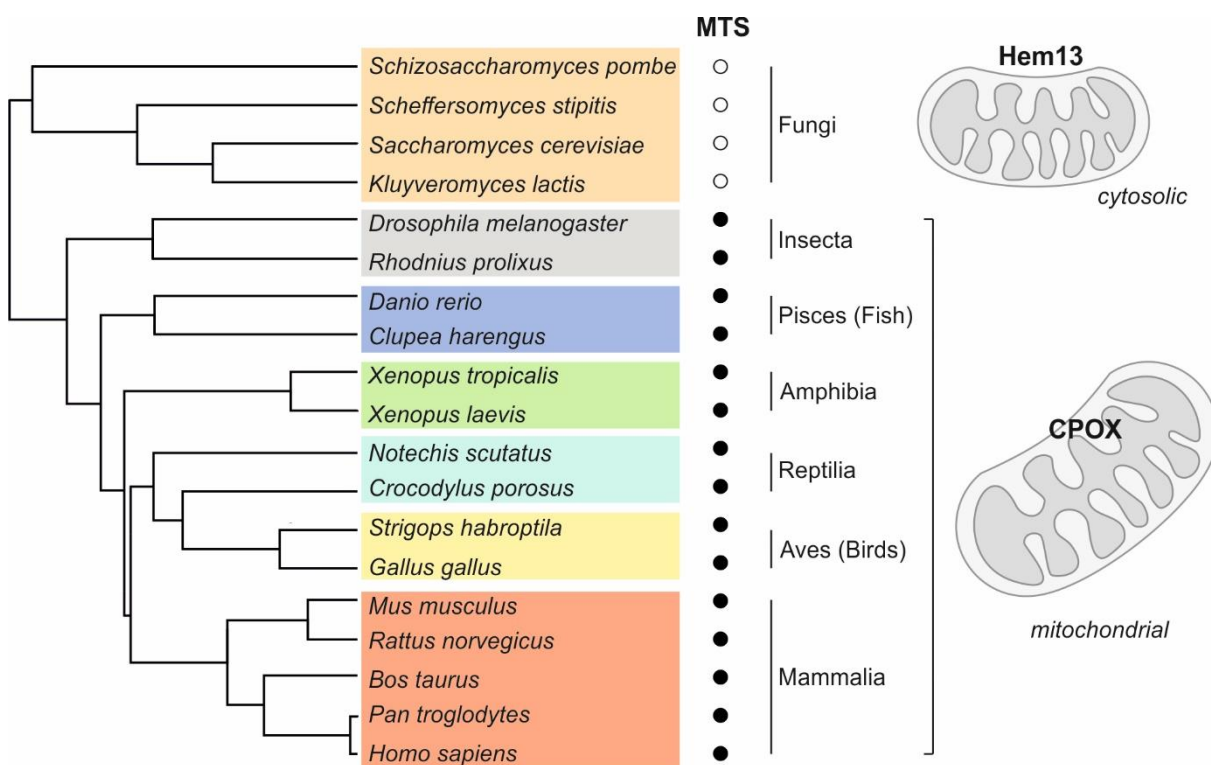


*Figure 28: CPOX is localized to the intermembrane space of mitochondria in higher eukaryotes*

In higher eukaryotes, CPOX contains an MTS and is localized to the mitochondrial intermembrane space. In contrast, the CPOX homologue Hem13, which is expressed in yeasts, does not contain an MTS and is localized to the cytosol.

#### *Aspects of protoporphyrinogen IX toxicity*

PPgenIX accumulation is toxic. When it cannot be converted to PPIX by PPOX, which directly hands it over to FECH, accumulated PPgenIX is able to autoxidize. The resulting PPIX leads to disease development in form of variegate porphyria that is characterized by neurological disorders and photosensitivity of the skin [216, 240, 271, 359, 360]. PPIX toxicity is associated with different characteristics of the molecule (Figure 29). One important aspect is the phototoxicity of porphyrin and porphyrin intermediates [361]. The other aspect affects PPIX hydrophobicity and accompanying cytotoxicity. As a highly hydrophobic molecule, PPIX will bind to any available hydrophobic surfaces in the cell. Hereby, it can intercalate into lipid bilayers disturbing various cellular processes [217, 249].

## Discussion

The phototoxicity of porphyrins is based on ROS production upon light exposure in a type I or type II photosensitized oxidation reaction [361, 362]. During these reactions, irradiation excites the porphyrin ring due to its electron rich structure. The excess energy is then transferred either directly onto oxygen or onto another present molecule, finally leading to the formation of ROS including hydroxyl radicals, super oxide anion radicals (type I) or singlet oxygen (type II) [361, 363-365]. Different porphyrins hereby exert different grades of phototoxicity. In *in vitro* experiments, PPIX acted as the most potent photosensitizer, followed by CPPIII and uroporphyrin III [366]. PPIX has an absorption maximum at 405 nm and strongly absorbs UVA (320-400 nm), but also shows absorption peaks at 410, 504, 538, 576 and 630 nm, a range that can penetrate skin and cause lesions [367, 368]. Porphyrin-mediated ROS production has been demonstrated to cause significant lipid peroxidation triggering ferroptosis. In a recent publication, peroxiredoxin 3 (Prx3) has been identified to bind to PPIX and counteract PPIX-mediated cell death [369]. PPIX-mediated cell death could be rescued by ferrostatin-1 and liproxstatin-1, efficient ferroptosis inhibitors. Similarly, ROS scavengers like N-acetylcysteine (NAC) could prevent PPIX-induced cell death [369, 370]. Besides ferroptosis, a few studies also reported PPIX-mediated cell death via apoptosis or necroptosis [371, 372]. Which kind of cell death is initiated seems to be dependent on the cell type, other stresses, and cellular environment. Ferroptosis is triggered upon excitation of PPIX by light, whereas apoptosis and necroptosis are observed independent of exposure to light. Importantly, PPIX has not only been detected in mitochondria, but also in the cytosol, ER, Golgi, and nucleus [369, 373]. Mitochondria can export PPIX via ATP-binding cassette super-family G member 2 (ABCG2) and are therefore able to reduce the burden of PPIX accumulation [374, 375]. However, it is not clear, how PPIX then reaches other cellular compartments. Apart from the non-specific damage caused by PPIX through light-induced ROS formation and ferroptosis, PPIX has also been shown to induce protein aggregation [373, 375]. It binds to target proteins and thereby induces local unfolding. Excitation of protein-bound PPIX produces singlet oxygen, which results in oxidation of methionines to methionine sulfone or sulfoxide, leading to aggregation of the respective protein-PPIX complex with other protein-PPIX complexes via non-covalent interactions [376, 377]. PPIX-mediated aggregation has been observed to affect the cytoskeleton, ER stress-related proteins, subunits of the proteasome and components of the autophagic machinery [377]. Further, PPIX-induced protein aggregation is not only limited to light exposed skin, but also found in inner organs, suggesting endogenous ROS originating for example from inflammation may also contribute [376].

## Mitochondrial CPOX localization prevents ROS formation and porphyrin toxicity

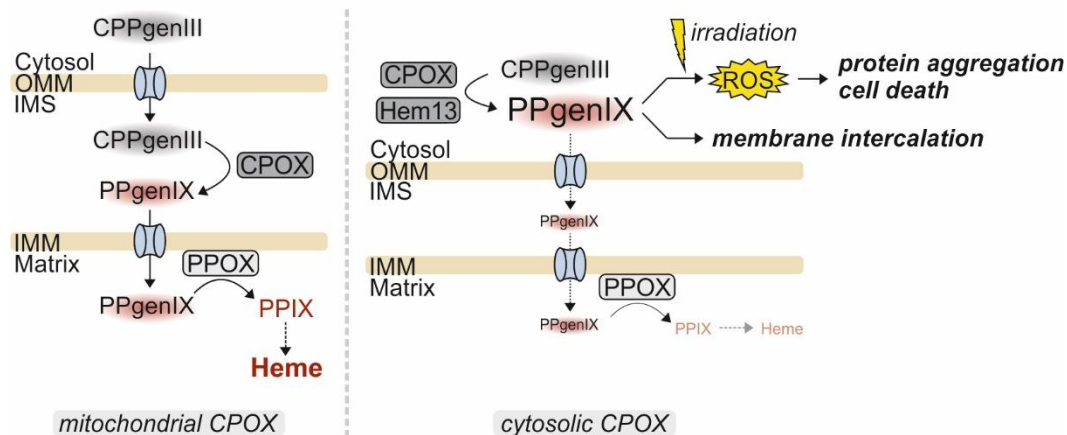


**Figure 29: Mitochondrial localization of CPOX prevents PPgenIX accumulation and its toxic effects**

When CPOX is in the IMS, its product PPgenIX can efficiently be overhanded to PPOX and converted to PPIX and finally to heme. When CPOX is in the cytosol, PPgenIX is still efficiently produced, but its transport over OMM and IMM is inefficient, leading to accumulation of PPgenIX in the cytosol. This has cyto- and phototoxic effects as it results in protein aggregation and cell death upon irradiation and in membrane intercalation of PPIX independent of environmental influences.

#### *Protoporphyrin(ogen)IX and cancer*

Tumor cells reprogram different metabolic pathways to meet their requirements for growth, energy production or nutrient acquisition. One aspect of the altered cancer cell metabolism is disbalanced heme biosynthesis. Cancer cells require high amounts of heme for different reasons, for example to meet their high energy demand by increased production of OXPHOS complexes [378, 379]. Therefore, they display a higher heme biosynthesis rate and increased uptake of heme in comparison to normal cells [380-382]. Especially the earlier enzymes of heme biosynthesis are upregulated in certain cancer types, for example ALAS1 in non-small-cell lung cancer (NSCLC) cells, PBGD in cervical, prostate and breast cancers or UROD in breast, head, and neck cancer [381, 382]. Remarkably, in some cancers, for example glioblastoma, there is a downregulation of the last heme biosynthesis enzyme FECH, which uses PPIX as substrate [383, 384]. A recent study further analyzed the genetic background of heme metabolism rewiring and named it “porphyrin overdrive” [385]. Comparing gene essentiality scores of available CRISPR/Cas9 screens for the heme biosynthesis enzymes in different cancers, it was revealed that UROD and CPOX seem to be strong oncogenes [297, 385-388]. In line with these findings, increased PPIX levels are a hallmark of many cancer types and used to diagnose and treat the respective cancers [360, 389]. In photodynamic and sonodynamic therapy (PDT, SDT), the ability of PPIX to be excited by light and ultra-sound is used to trigger death of tumor cells. To increase therapeutic efficiency, cells are given 5-ALA, the product of ALAS1, to circumvent the rate-limiting step of heme biosynthesis and promote PPIX accumulation [368, 390-393]. Due to the increased nutrient uptake and ROS production of cancer cells, they are more sensitive to PPIX-induced cell death and can be eliminated in a selective manner.

## Discussion

To sum everything up, the evolutionary shift in CPOX localization from cytosol to IMS is beneficial, because it presumably supports efficient handover of PPgenIX to PPOX and prevents PPIX accumulation, which is highly toxic by promoting ROS production, protein aggregation and cell death, mainly in form of ferroptosis.

## 4. Outlook

In this study, CPOX was identified as novel interactor of ALR. It could be shown that CPOX contains at least one structural disulfide, which is required for stabilization the IMS. This disulfide is suggested to be introduced by sulfhydryl oxidase ALR. ALR had previously exclusively been associated with the disulfide relay, hence the present work provides new insights into ALR's expanding relevance for mitochondrial homeostasis. Notably, it was not possible to show a direct impact of ALR on the CPOX redox status. Neither treatment of cells with ALR inhibitor MB-6 nor siRNA-mediated depletion of ALR changed the CPOX redox status in cells (data not included). The hypothesis of ALR introducing a disulfide bond in CPOX originates from the covalent interaction of both proteins, as demonstrated by denaturing affinity precipitation. Consequently, one future goal is to further analyze the ALR-CPOX interaction and identify the influence of ALR on CPOX. To investigate the nature of the interaction between CPOX and ALR and visualize it in a direct way, a radioactive IP-reIP experiment will be performed. In order to determine, if ALR directly impacts the CPOX redox status, the CPOX redox status under ALR inhibited condition will be dynamically assessed in oxidation kinetics *in vitro* and in the cellular context.

Besides the interaction with ALR, this thesis revealed a complex multi-step maturation for CPOX, in which the IMMP1/2 complex catalyzes a rate-limiting cleavage step. The CPOX disulfide plays an interesting role during the maturation process, as it does not only influence stability of the mature protein, but also seems to impact IMMP1/2 cleavage kinetics. Together, the processes involved in CPOX maturation might represent new ways of heme biosynthesis regulation and underline the individuality and tight orchestration of protein maturation. To identify all proteases involved in CPOX processing, future experiments will include working with KO cell lines or siRNA-mediated depletion of the candidate proteases, targeting for example of MIP or ATP23. Similar tools will also be used to find out, which proteases are involved in CPOX degradation in case of destabilization or aggregation of the protein. Another interesting feature of the CPOX protein is the conserved negative amino acid stretch at the N-terminus of the mature protein, whose function is yet unknown. To test the impact of this negative stretch on CPOX processing, stability and functionality, a pulse chase experiment of a CPOX variant without the negative stretch will be performed. In addition, the ability of a this CPOX variant to complement for CPOX depletion will be analyzed on Western blot, via HPLC and in terms of growth after galactose shift.

Moreover, many physiological questions affecting CPOX and its role in heme biosynthesis are still open. Although the CPOX enzyme has been focus of various investigation over the last decades, no reaction mechanism has been identified yet. Based on the CPOX crystal structure, an active center has been suggested, but not reliably determined. To define a CPOX active site and thereby gain deeper insight into the CPOX-mediated catalysis of CPPgenIII to PPgenIX, our lab is attempting to co-crystallize CPOX

## Outlook

with its substrate bound. Explaining the discrepancy between CPOX and Hem13 localization, we propose a theory, in which CPOX evolutionarily relocated from the cytosol to the mitochondrial intermembrane space for efficient handover of PPgenIX to PPOX to prevent toxic PPgenIX and PPIX accumulation. Investigating the potential disadvantages of cytosolic CPOX localization and the severity of loss of CPOX function for the cell, ferroptosis measurements will be performed in cells expressing CPOX variants with different localization and cysteine pattern. An important aspect in the context of porphyrin toxicity and porphyrin-mediated cell death is the trafficking of porphyrin and its precursors. To learn more about porphyrin trafficking, interactome studies of CPOX and PPOX are a powerful tool and can help to identify novel PPgenIX- or PPIX-binding proteins. For expanded research on heme biosynthesis regulation and porphyrin trafficking, the employment of a physiologically relevant system can be of use. An erythroid cell line like MEL or a liver cell line like HepG2 are fitting model systems, as these cell types display increased heme biosynthesis rates. To study the general effects of heme depletion on the cellular system and under different stress conditions such as glucose starvation or hypoxia, the HEK293 Flp-In™ T-Rex™ CPOX KO cell line generated in the course of this work is a powerful tool.

## 5. Methods

### 5.1 Molecular Biology

#### 5.1.1 Polymerase chain reaction (PCR)

To amplify DNA of interest, a polymerase chain reaction was performed. For this purpose, the 10x Phusion reaction buffer (500 mM Tris-HCl pH 9.2, 22.5 mM MgCl<sub>2</sub>, 160 mM (NH<sub>4</sub>)<sub>2</sub>SO<sub>4</sub>, 20% DMSO, 1% Triton X-100) was prepared and the PCR reaction mixture was prepared as indicated in Table 2. Oligonucleotide primers should display an overlap of at least 15 bases with the template DNA sequence and can contain additional bases at the end to add restriction sites or tags to the gene of interest. The melting temperature  $T_M$  of the individual primers should not differ more than 5°C to ensure efficient amplification.

*Table 2: PCR reaction mixture pipetting scheme*

Component	Amount
DNA template [100 ng/μl]	1 μl
10x Phusion buffer	5 μl
dNTPs [10 mM]	1 μl
Forward Primer [10 μM]	1 μl
Reverse Primer [10 μM]	1 μl
Phusion polymerase	0.2 μl
ddH <sub>2</sub> O	Ad 50 μl

The PCR was run under the conditions presented in Table 3. Here, T[X] is the annealing temperature for the used primers, which is usually around 5°C below their  $T_M$ . t[x] is the elongation time and varies depending on the polymerase that is used. Phusion polymerase amplifies DNA with a speed of 2 kb/min.

*Table 3: PCR program*

	Initial Denaturing	Denaturing	Annealing	Elongation	Final Elongation	Storage
<b>T [°C]</b>	95	95	T[X]	72	72	4
<b>t [min]</b>	05:00	00:30	01:00	t[x]	10:00	∞
<b>Cycles</b>	1x	30x			1x	Hold

#### 5.1.2 Site-directed mutagenesis

Site-directed mutagenesis enables alterations in single codons of a gene of interest on plasmid DNA. To achieve a single codon mutation, oligonucleotide primers complementary to the region of interest were designed with a length of around 30 bases. The desired mutation was included in the middle of the sequence of these primers, so they could still bind efficiently to the DNA. A PCR mixture was prepared with these oligonucleotides according to Table 4 and a PCR was run according to conditions shown in Table 5. The annealing temperature T[X] is dependent on the plasmids' melting temperature

## Methods

$T_M$ . The elongation time for site-directed mutagenesis is unusually long, as the whole plasmid needs to be amplified.

After PCR, 1  $\mu$ l of *DpnI* was added to the mixture and digested for 1 h at 37°C. *DpnI* specifically digests methylated DNA, thereby eliminating remaining template DNA from the sample. The newly synthesized plasmid was ready to be transformed into competent *E.coli* DH5 $\alpha$ .

Table 4: PCR reaction mixture pipetting scheme for site-directed mutagenesis

Component	Amount
DNA template [100 ng/ $\mu$ l]	1 $\mu$ l
10x Phusion buffer	2.5 $\mu$ l
dNTPs [10 mM]	0.5 $\mu$ l
Forward Primer [10 $\mu$ M]	1.25 $\mu$ l
Reverse Primer [10 $\mu$ M]	1.25 $\mu$ l
Phusion polymerase	2.5 $\mu$ l
ddH <sub>2</sub> O	Ad 25 $\mu$ l

Table 5: PCR program for site-directed mutagenesis

	Initial Denaturing	Denaturing	Annealing	Elongation	Final Elongation	Storage
<b>T [°C]</b>	95	95	T[X]	72	72	4
<b>t [min]</b>	00:30	00:30	01:00	05:00	10:00	$\infty$
<b>Cycles</b>	1x	30x			1x	Hold

### 5.1.3 Agarose gel electrophoresis

To separate plasmid DNA or PCR products according to size, agarose gel electrophoresis was performed. DNA carries negative charge and hence migrates through an agarose matrix from cathode to anode, when voltage is applied. For agarose gel electrophoresis, DNA sample is mixed with a 6x loading dye (18% glycerol, 0.12% Orange G dye) and loaded on 1-2% agarose gels in 1x TAE buffer (8 mM Tris, 10 mM EDTA pH 8, 1.14 % acetic acid) next to a molecular weight standard for size comparison. A constant voltage of 135 V was applied for 40 minutes. After the run, DNA fragments on the gel were stained with SYBR™ Orange. For further applications, the DNA bands were cut out from the gel matrix and extracted by using the Macherey-Nagel™ NucleoSpin™ Gel and PCR Clean-up kit according to manufacturer's guidelines.

### 5.1.4 Restriction digest and ligation of DNA

For cloning of DNA parts into the required plasmid or subcloning from one plasmid to another, restriction digest by endonucleases and subsequent ligation is necessary. The restriction digest was prepared as described in Table 6 and incubated for 1 h at 37°C. For clean-up, agarose gel electrophoresis was performed as described previously. Digested plasmid DNA and insert were ligated by a T4 ligase according to Table 7. The molar ratio of insert to plasmid should be between 3:1 and

7:1. The ligation reaction was incubated for 1 h at RT or overnight at 16°C, before being ready for transformation into competent *E.coli* DH5α for amplification of the new construct.

Table 6: Restriction digest reaction mixture

Component	PCR product (insert) digest	Vector digest
DNA	25 µl	2 µl
10x FastDigest buffer	4 µl	5 µl
Restriction enzyme 1	1 µl	1 µl
Restriction enzyme 2	1 µl	1 µl
ddH <sub>2</sub> O	Ad 40 µl	Ad 50 µl

Table 7: Ligation reaction mixture

Component	Amount
Digested PCR product (insert)	15 µl
Digested vector	1 µl
10x T4 Ligase Buffer	2 µl
T4 ligase	0.2 µl
ddH <sub>2</sub> O	Ad 20 µl

5.1.5 Transformation of plasmid DNA into chemically competent *E. coli* DH5α  
 Plasmid DNA was transformed into chemically competent *E.coli* DH5α cells for plasmid amplification. *E.coli* DH5α cells were made chemically competent by treatment with calcium chloride. For transformation, half of a ligation reaction or 0.1 µg of plasmid DNA were mixed with a suspension of competent cells and incubated on ice for 30 minutes. Cells were heat shocked at 42°C for 90 seconds and then rapidly cooled down on ice. 1 ml of LB medium (1% tryptone/peptone, 0.5% yeast extract, 0.5% NaCl) was added to the cells, followed by a recovery phase of 1 h at 37°C. Afterwards, cells were pelleted for 15 seconds at 11,000 xg and supernatant was removed down to 50 µl. The cell pellet was resuspended in the remaining supernatant and plated on LB-agar plates (1% bacto-tryptone, 0.5% yeast extract, 0.5% NaCl, 1.5% agar, pH-adjusted to 7.5 with NaOH) supplemented with the appropriate antibiotic for selection of successful transformation. Plates were incubated overnight at 37°C.

5.1.6 Plasmid isolation from *E.coli*  
 Plasmids were isolated from 5 ml liquid cultures of *E.coli* in LB-Medium with the respective antibiotic that were inoculated from single colonies and grown overnight at 37°C. For isolation, the Nucleospin™ Plasmid kit by Macherey-Nagel was used according to manufacturer's guidelines. Concentration of the extracted plasmid was determined by measuring absorption at 260 nm and the purity was controlled by measuring the absorbance ratio at 260/280 nm.

## Methods

### 5.2 Mammalian Tissue Culture

#### 5.2.1 Culturing human cells

In this work, HEK293 cells and HepG2 (hepatocellular carcinoma) cells were employed. Both are adherent cell lines. They were cultured on 10 cm dishes in 10 ml of Dulbecco's modified Eagle medium with glutamine and high glucose levels (DMEM; ThermoFisher) supplemented with 10% fetal bovine serum (FBS) and 1% penicillin/streptomycin (ThermoFisher) at 37°C and 5% CO<sub>2</sub>. All cells based on CPOX KO were grown in "Super Medium" – Dulbecco's modified Eagle medium with glutamine and high glucose levels supplemented with 10% fetal bovine serum (FBS), 1% penicillin/streptomycin (ThermoFisher), 1x MEM non-essential amino acids (Sigma), 1 mM sodium pyruvate (Sigma) and 50 µg/ml uridine. The cells were passaged regularly – every 3 to 4 days – at a confluency of ~80-90%. For passaging of the cells, growth medium was removed completely and cells were carefully washed with 4 ml of prewarmed 1x PBS. PBS was aspirated and 1 ml of 1 ml trypsin/EDTA (0.005 % trypsin, 0.02 % EDTA; Gibco) was added to the cells. HEK293 cells were incubated with trypsin for 1 minute at RT, HepG2 cells required a 5-minute incubation at 37°C to detach. Trypsinized cells were resuspended in 9 ml of growth medium and the respective amount of cell suspension was transferred to fresh 10 cm dishes and filled up to 10 ml with fresh growth medium.

#### 5.2.2 Seeding human cells

To be seeded for an experiment, cells were trypsinized and resuspended in fresh growth medium as described previously for passaging of cells. 10 µl of cell suspension were mixed with the same amount of a 0.5% trypan blue solution to stain for living cells. Stained cells were counted with the Logos Luna II™ cell counter. The required amount of cells was taken from the cell suspension, mixed with fresh growth medium and distributed to new plates. For experiments involving several washing steps or steps where cells are heavily stressed, plates were coated with poly-L-lysine prior to seeding.

#### 5.2.3 Freezing and thawing of human cells

All used cell lines were kept at -80°C for short term (up to 4 weeks) and at -190°C in liquid nitrogen for long term storage. To prepare cells for storage, they were trypsinized and resuspended in growth medium as described previously. Cells were then pelleted at 300 xg and 4°C for 5 minutes and supernatant was removed. The cell pellet was resuspended in 1 ml of freezing medium (90% FBS + 10% DMSO) per 10 cm dish of cells and transferred to cryotubes with 0.5 ml of cell suspension per tube. Tubes were placed on ice and quickly transferred to -80°C. To thaw cells for usage in the lab, they were shortly warmed up in a water bath at 37°C and then resuspended in 5 ml growth medium. The cells were pelleted by centrifugation at 300 xg for 5 minutes and resuspended in 10 ml fresh growth medium and transferred to a 10 cm dish.

#### 5.2.4 siRNA-mediated knockdown in human cells

To deplete proteins from cells using siRNA, a reverse transfection was done in 6-well or 48-well format according to manufacturer's guidelines. For this, siRNA solution was mixed gently with Opti-MEM® I medium (Thermo Fisher) directly in the well. Lipofectamine™ RNAiMAX (Thermo Fisher) was added to the well and mixed gently again. The mixture was incubated for 10 minutes at RT. In the meantime, cells were prepared for seeding according to section 5.2.2 and seeded on top of the transfection mixture with 100,000 cell per ml. Amounts need to be scaled up and down according to plate size and cell amount (Table 8).

*Table 8: Required amounts for siRNA-mediated reverse transfection of cells with Lipofectamine™ RNAiMAX*

Plate	Plating volume	Cell number	Opti-MEM	siRNA amount	Final siRNA concentration	Lipofectamine™ RNAiMAX
48-well	200 µl	20,000	40 µl	2.4 pmol	10 nM	0.4 µl
6-well	2.5 ml	250,000	500 µl	30 pmol	10 nM	5 µl

#### 5.2.5 Generation of CRISPR/Cas9-mediated knockout cell lines

The so-called CRISPR/Cas9 system was used to generate knockout cell lines. CRISPR/Cas stands for Clustered Regularly Interspaced Short Palindromic Repeats/CRISPR-associated systems and is derived from bacteria, which use this system to silence invading nucleic acids [394]. Guide RNAs (gRNAs) target the Cas9 endonuclease to certain sites on the DNA to introduce double-strand breaks, which then need to be repaired by the cell via homologous recombination (HR) or non-homologous end joining (NHEJ). These DNA repair mechanisms are error-prone and will likely lead to insertions or deletions (indels), resulting in a silencing of the affected gene.

For design of gRNA sequences, suitable target exons in the gene of interest were identified using information of the Ensembl.org genome browser and fitting PAMs (protospacer adjacent motifs), binding sites for Cas9 were predicted by the CHOPCHOP tool. Complementary oligonucleotide primers were chosen based on the CHOPCHOP suggestions. Per gene, two different sites were chosen as targets, to produce knockouts based on different gene alterations. The oligonucleotides were annealed by heating up to 95°C followed by a slow cool down to RT and cloned into the pSpCas9(bb)-2a-GFP plasmid, which also encodes for Cas9, in a simultaneous digest ligation reaction. The new constructs encoding for Cas9 and the respective gRNA were transformed into competent *E.coli* DH5α and amplified as described above. 300,000 HEK293 Flp-In™ T-Rex™ host cells were seeded onto 6-well plates. 3 µg DNA were incubated with 9 µl polyethylenimine (PEI) in 300 µl growth medium for 10 minutes and added to the cells for transfection. 24 h after transfection, successfully transfected cells were sorted by fluorescence assisted cell sorting (FACS) into tubes containing fresh medium. FACS sorting was done by Christoph Göttlinger in the FACS facility of the Centre of Molecular Biosciences at

## Methods

the University of Cologne. Cells recovered for 96 h. Afterwards, they were trypsinized as described before, diluted to 7 cells/ml and seeded onto 96-well plates to produce single cell colonies. At confluency, colonies were transferred onto 24-well plates followed by 6 well plates. Samples from all clones were prepared for SDS-PAGE and subjected to Western blot analysis to test for presence of the protein of interest.

### 5.2.6 Generation of stable inducible cell lines with the Flp-In™ T-Rex™ system

Stable inducible cell lines were generated using the Flp-In™ T-Rex™ system. This system uses the Flp recombinase from *Saccharomyces Cerevisiae* and site-specific recombination to integrate a gene of interest into a specific site of the genome. Flp-In™ T-Rex™ host cell lines contain a FRT site, the target for the Flp recombinase, which is regulated by a Tet-repressor and allow induction of expression via tetracycline addition. To produce new stable cell lines, the gene of interest (GOI) was cloned into the pcDNA5/FRT/TO vector, where it is flanked by FRT sites. The vector also contains a hygromycin resistance gene. Cells need to be co-transfected with the pcDNA5/FRT/TO vector carrying the GOI and pOG44 vector carrying the gene for the Flp recombinase flp-F70L so that the Flp recombinase can mediate the targeted insertion of the GOI at the FRT site existing in the host cells. For transfection, 500,000 Flp-In™ T-Rex™ host cells were seeded onto 6-well plates. The next day, medium was exchanged to fresh growth medium. The day after, 100 µl of pure DMEM without any supplements was mixed with 200 ng pcDNA5/FRT/TO vector and 800 ng pOG44 vector. After addition of 8 µl FuGENE HD transfection reagent (Promega) and a 10-incubation at RT, the transfection mix was added dropwise to the cells. One well was not transfected to serve as control. 24 h later, cells were trypsinized and transferred to 10 cm dishes. After another 24 h, selection was started by exchanging medium to growth medium supplemented with 100 µg/ml hygromycin and 10 µg/ml blasticidin. Selection medium was exchanged every 3 to 4 days until control cells died and colonies started to form on the transfected plates. Colonies were picked, transferred to 6-well plates and grown until confluency. Colonies were then transferred to 10 cm dishes and tested for expression of the GOI by addition of 1 µg/ml doxycycline and Western blot analysis.

### 5.2.7 Generation of stable inducible cell lines with the PiggyBac system

A quick way to generate stable inducible cell lines is the PiggyBac Transposon System (Systembio). The PiggyBac (PB) transposon is a genetic element that can be moved between vectors and chromosomes in a cut and paste mechanism via the PB transposase. It recognizes transposon-specific inverted terminal repeat sequences (ITRs) that are located on both ends of the PB transposon vector and moves content from one genetic site to another. Hence, GOIs can be integrated into TTAA sites of chromosomes efficiently. For PB transfection, the GOI was cloned into the PB-CuO-MCS-IRES-GFP-EF1-CymR-Puro vector. This vector expresses the GOI under a CMV promotor, the CymR cumate repressor that makes the system inducible and a puromycin resistance. For transfection, 500,000 cells were

seeded onto 6-well plates with one well as untransfected control. 800 ng of vector encoding for PB transposase and 2 µg PB-CuO-MCS-IRES-GFP-EF1-CymR-Puro vector with GOI were mixed with 100 µl pure DMEM. 8 µl FuGENE HD transfection reagent (Promega) were added, the mixture was vortexed for 10 seconds, spun down and incubated for 10 minutes at RT. Afterwards, the mixture was added dropwise to the cells. 48 h after transfection, medium was exchanged to growth medium containing 2µg/ml puromycin. Selection medium was exchanged every 3 to 4 days until control cells dies and transfected cells started to grow again. When cells reached confluency, expression of GOI was tested by induction with 30 µg/ml cumate and analysis by Western blot.

#### 5.2.8 Galactose shift

Cells were shifted from glucose to galactose medium so they need to rely on respiration instead of glycolysis as major ATP source. In order to shift cells to galactose, they were trypsinized at around 80% confluency as described above and resuspended and seeded in galactose medium (DMEM without glucose supplemented with 10% fetal bovine serum (FBS), 1% penicillin/streptomycin (ThermoFisher), 1x MEM non-essential amino acids (Sigma), 1 mM sodium pyruvate (Sigma), 50 µg/ml uridine and 4.5 g/l galactose).

#### 5.2.9 Proliferation assay

Expression of the gene of interest in stable cell lines was induced by addition of doxycycline 24 h before seeding. Doxycycline amounts were titrated previously to reach expression levels of the protein of interest similar to endogenous levels. A 48-well plate was coated with poly-L-lysine and 15,000 cells in 500 µl medium were seeded per well in replicates of four. In case of galactose shift experiments, a galactose shift was performed during seeding as described before. Medium was exchanged every day. For medium exchange, 250 µl old medium were aspirated from the well and 250 µl fresh medium were added carefully. For stable cell lines, medium always contained the respective amount of doxycycline to ensure constant protein expression.

#### 5.2.10 Immunofluorescence

15,000 cells were seeded onto poly-L-lysine coated coverslips in 12-well plates and protein expression was induced with 1 µg/ml doxycycline. After 48 h, cells were stained with MitoTracker™ Deep Red (Thermo Fisher) in a dilution of 1:100,000 for 1 h at 37°C. Afterwards, fixation was done with 4% paraformaldehyde for 15 minutes. Coverslips were washed 3x with PBS and incubated in fresh blocking buffer (10mM HEPES-KOH pH 7.4, 3% BSA, 0.3 % Triton X-100) for 1 h. Coverslips were incubated in blocking buffer containing primary antibody (1:400) for 1 h at RT, washed 3x with PBS and transferred to blocking buffer containing fluorescent secondary antibody (1:400) for 1h at RT in the dark. After three additional washing steps with PBS, nuclei of the samples were stained with DAPI. 0.5 ml DAPI (1 µg/ml) were added onto the samples for 15 min at RT in the dark. Samples were washed with PBS one

## Methods

last time and placed onto drops of prewarmed ProLong™ Gold antifade mounting medium (ThermoFisher) onto coverslips. Samples were dried over night at 4°C in the dark and sealed with nail polish the next day. Samples were imaged with a Leica LSM980 Airyscan 2 confocal laser scanning microscope and a plan-apochromat 63x/1,4 oil objective at the imaging facility at the Cologne Excellence Cluster for Aging and Aging-Associated Diseases (CECAD).

### 5.3 Protein Biochemistry

#### 5.3.1 SDS-PAGE

Sodium dodecyl sulphate (SDS) polyacrylamide gel electrophoresis (PAGE) allows separation of proteins by their size. The underlying principle is denaturation of proteins by the detergent SDS, which adds negative charge to proteins with an even charge to mass ratio. Hence, proteins can migrate through the polyacrylamide matrix from cathode to anode when voltage is applied. Larger proteins will migrate slower than small ones. Two systems were employed in this work to separate protein samples, the Tris-Glycine system [395] and the Tris-Tricine system[396]. Samples for both systems were prepared by lysis of cells in 1x Laemmli buffer (60 mM Tris pH 6.8, 2% SDS, 10% glycerol, 0.0025% bromophenol blue) or resuspension of protein pellets in 1x Lämmli buffer. For reducing SDS-PAGE, samples additionally contained 50 mM dithiothreitol (DTT). Before loading, samples were heated up to 95°C for 10 minutes.

The Tris-Glycine system is regularly used in this work for separation of protein samples from cell lysates, immuno- and affinity-precipitations and redox shift assays. Tris-Glycine gels were prepared according to Table 9. Gels were run in 1x running buffer (25 mM Tris, 190 mM glycine, 0.1% SDS) by applying a voltage of 150 V for 90-120 minutes. Redox shift samples were run at 50 V for 16 h.

*Table 9: Pipetting scheme for Tris-Glycine acrylamide gels*

Component	Running gel		Stacking gel
	12%	16%	
<b>ddH<sub>2</sub>O</b>	5.2 ml	3.3 ml	3.6 ml
<b>1.875 M Tris-HCl pH 8.8</b>	2.9 ml	2.9 ml	-
<b>0.6 M Tris-HCl pH 6.8</b>	-	-	0.5 ml
<b>30% acrylamide, 0.6% bisacrylamide</b>	4.7 ml	7.5 ml	0.8 ml
<b>10% SDS</b>	137.5 µl	137.5 µl	50 µl
<b>Trichlorethyhanol (TCE)</b>	70 µl	70 µl	-
<b>10% Ammonium persulfate</b>	100 µl	100 µl	50 µl
<b>Tetramethylethylenediamine</b>	10 µl	10 µl	10 µl

The Tris-Tricine system is used when small proteins below ~20 kDa should be resolved or when a sharp separation of protein bands is required. In this work, Tris-Tricine gels were used to resolve samples from radioactive pulse chase experiments and oxidation kinetics. Tris-Tricine gels were prepared as shown in Table 10. They were run in a system with two different buffers, cathode buffer (0.1 M Tris, 0.1 M Tricine, 0.1% SDS) and anode buffer (0.2 M Tris-HCl pH 8.9) at 180 V at 4°C for 24 h.

Table 10: Pipetting scheme for Tris-Tricine acrylamide gels

Component	Base gel	17% Running gel	Stacking gel
<b>30% acrylamide, 0.6% bisacrylamide</b>	13.4 ml	17 ml	1.66 ml
<b>Gel Buffer (3 M Tris-HCl pH 8.45 + 0.3% SDS)</b>	4.4 ml	10 ml	1.1 ml
<b>ddH<sub>2</sub>O</b>	2.2 ml	-	7.2 ml
<b>Glycerol</b>	-	3.17 ml	-
<b>10% Ammonium persulfate</b>	100 µl	200 µl	100 µl
<b>Tetramethylethylenediamine</b>	50 µl	20 µl	24 µl

The Precision Plus Protein™ Dual Color Standard (Biorad) was used as molecular weight marker in all cases.

### 5.3.2 Western Blot

For immunological detection of proteins of interest or detection of radioactively labelled proteins, proteins were transferred from SDS polyacrylamide gels onto nitrocellulose membranes with 0.2 µm pore size (VWR) via Western blot. For the semi-dry transfer method, gel and membrane were equilibrated in 1x blotting buffer (20 mM Tris, 150 mM glycine, 0.08% SDS, 20% methanol). Then, a transfer “sandwich” was built up by placing the gel onto the membrane between two Whatman paper stacks à two papers each soaked in 1x blotting buffer, so that the proteins can run from the top (cathode) to the membrane at the bottom side (anode) of the chamber. Transfer was performed for 90 minutes at 100 mA for one small gel and 200 mA for two small or one big gel.

### 5.3.3 Immunological detection of proteins

After Western blot, protein bands were visualized by staining with antibodies followed by detection via chemiluminescence. For this purpose, Western blot membranes were blocked in 5% MTBS (5% blocking grade milk powder, 150 mM NaCl, 50 mM Tris-HCl pH 7.6) for 30 minutes at RT to prevent unspecific binding of antibody. Afterwards, membranes were incubated in the respective antibody diluted in 5% MTBS over night at 4°C. The next day, membranes were washed 3x for 10 minutes with 1x TBS (150 mM NaCl, 50 mM Tris-HCl pH 7.6) and incubated in secondary antibody diluted in 5% MTBS for 1 h at RT. Secondary antibodies are raised against origin species of primary antibodies to bind them specifically and are coupled to horseradish peroxidase (HRP) for chemiluminescent detection. Blots were washed 3x for 10 minutes in 1x TBS again and imaged at the Biorad ChemiDoc™ Touch imaging device. Chemiluminescence was induced by adding a 1:1 mixture of enhanced chemiluminescence (ECL) I (100 mM Tris pH 8.5, 0.022% luminol, 0.0033% p-coumaric acid) and II (100 mM Tris pH 8.5, 0.2% H<sub>2</sub>O<sub>2</sub>) to the blots before inserting them into the machine.

### 5.3.4 Autoradiography

After Western blotting, membranes were dried and molecular weight marker bands were marked with ink containing small amounts of radioactive sulfur <sup>35</sup>S. Membranes were exposed to radioactivity-

## Methods

sensitive Storage Phosphor Screens BAS-IP (GE Healthcare) for 3 to 28 days. Signal was detected at the Typhoon FLA9500 Imaging System (GE Healthcare). Screens could be reused after being blanked with high intensity light for 1 h with the FLA Image Eraser (GE Healthcare).

### 5.3.5 Native and denaturing immunoprecipitation

To display protein-protein interactions in HEK293 cell lines, native immunoprecipitation (IP) or affinity purification (AP) experiments were performed. The experimental procedure of these two only differs in the matrix used for pulldown of proteins of interest. For IP experiments, an antibody-coupled agarose matrix is used, whereas a Strep-Tactin<sup>®</sup>-coupled agarose matrix is used of APs. HA-tagged proteins were pulled down via monoclonal anti-HA agarose from mouse (Sigma), endogenous CPOX was enriched via protein-A-agarose matrix (Expedeon) loaded with anti-CPOX antibody (St. John's laboratory) and Strep-tagged proteins were purified over Strep Tactin<sup>®</sup> TACS agarose (iba). Native lysis enables analysis of all kinds of protein-protein interactions, whereas denaturing lysis only conserves covalent bonds.

For the experiment, 3,000,000 cells were seeded onto 15 cm dishes, induced with doxycycline or cumate depending on the cell line and grown for 96 h until reaching around 80-90% confluency. Cells were placed on ice and incubated *in situ* with 20 mM N-ethyl-maleimide (NEM) for 10 minutes to prevent thiol-exchange reactions. Afterwards, cells were detached from plates using a rubber policeman and pelleted at 700 xg at 4°C for 3 minutes.

For native lysis, cell pellets were resuspended and lysed for 1h on ice in native IP buffer containing 1% Triton X-100 (100mM Na-Pi pH 8.1, 100 mM NaCl, 1% Triton X-100). For denaturing lysis, cells were resuspended in denaturing IP buffer without Triton x-100 (30 mM Tris-HCl pH 8.1, 150 mM NaCl, 1 mM EDTA) and SDS was added to a final concentration of 1.6%. Samples were incubated at RT for 10 minutes and then heated up to 95°C for 5 to 20 minutes depending on the sample volume. Afterwards, samples were sonified with two times 15 cycles at an amplitude of 80% to disrupt remaining DNA and improve lysis. Then, 2.5x the amount of denaturing IP buffer containing 2.5% Triton X-100 was added to the lysates to replace SDS, which would interfere with binding of proteins to antibody or Strep Tactin<sup>®</sup>-coupled beads. Lysates were incubated for 1 h on ice.

Totals were taken after the 1 h incubation and prepared for SDS-PAGE by adding 4x reducing Lämmli buffer to a final concentration of 1x (60 mM Tris pH 6.8, 2% SDS, 10% glycerol, 0.0025% bromophenol blue, 50 mM DTT) and sonifying them in 10 cycles at an amplitude of 80%. Simultaneously, remaining cell lysate was distributed to 1.5 ml tubes and cleared at 20,000 xg at 4°C for 1 h. Beads were equilibrated in native or denaturing IP buffer containing 1% Triton X-100 by washing them 3x for 1 minute at 2,000 xg at 4°C. Cleared lysate was pooled and incubated with beads tumbling over night at 4°C to allow for binding of prey protein to the beads. After that, beads were washed 5x for 1 minute at 2,000 xg at 4°C with native or denaturing IP buffer containing 1% Triton X-100. A last washing step was

performed with native or denaturing IP buffer without Triton X-100. Then, beads were eluted in 1x Lämmli buffer (with 50 mM DTT for reducing conditions) at 95°C for two times 10 minutes. Totals were heated up to 95°C for 10 minutes. Samples were analyzed via SDS-PAGE and Western blot.

#### 5.3.6 Alkaline extraction

Alkaline extraction enables differentiation between soluble and membrane-bound or aggregated proteins. In this work, alkaline extraction in a Na<sub>2</sub>CO<sub>3</sub> buffer was done on isolated mitochondria to assess submitochondrial localization of proteins of interest.

For mitochondrial isolation, cells from two confluent 15 cm dishes were rinsed with ice-cold PBS, detached using a rubber policeman and pelleted at 500 xg at 4°C for 5 minutes. Pellets were resuspended in isotonic buffer (225 mM mannitol, 75 mM sucrose, 10 mM HEPES-KOH pH 7.4, 1 mM EGTA) and transferred to a pre-cooled Potter S homogenizer cylinder. Cells were homogenized on ice at 1,000 rpm by moving the cylinder slowly up and down (1 stroke). After 15 strokes, lysate was cleared from nuclei and cell debris two times at 600 xg at 4°C for 5 minutes. Supernatant contained isolated crude mitochondria and was from now on always pipetted using a cut pipette tip to minimize shear forces. Supernatant was transferred to fresh tubes and centrifuged at 8,000 xg at 4°C for 5 minutes to pellet crude mitochondria. Supernatant was discarded and mitochondria were carefully resuspended in fresh isotonic buffer for washing. They were pelleted again at 6,000 xg at 4°C for 10 minutes resuspended in isotonic buffer and concentration of mitochondria was assessed using Bradford ROTI<sup>®</sup> Quant Assay (Roth) according to manufacturer's guidelines and measuring absorption at 600 nm.

200 µg freshly isolated mitochondria were centrifuged at 10,000 xg at 4°C for 5 minutes. Mitochondrial pellet was resuspended in ice-cold 0.1 M Na<sub>2</sub>CO<sub>3</sub> buffer pH 11.05 and incubated on ice for 1 h. Total was taken at this point and prepared for SDS-PAGE by addition of reducing Lämmli buffer. Mitochondrial suspension was filled up to 14 ml with Na<sub>2</sub>CO<sub>3</sub> buffer and ultracentrifuged at 90,000 xg for 30 minutes at 4°C. After centrifugation, the supernatant was collected and protein was precipitated by adding TCA to a final concentration of 10% and freezing samples at -80°C. Samples were thawed on ice again and precipitated protein was pelleted at 20,000 xg at 4°C for 30 minutes. Pellets were washed with acetone two times, dried and resuspended in 1x reducing Lämmli buffer. The pellet from ultracentrifugation was carefully washed with water, then resuspended in water and mixed with 4x reducing Lämmli buffer. All samples, including total, were boiled at 95°C for 5 minutes and analyzed via SDS-PAGE and Western blot.

#### 5.3.7 Inverse redox shift assay

The inverse shift assay helps assess the cysteine redox state of proteins. Thiol-active molecules, in this case mm(PEG)<sub>12</sub>, are used to modify free cysteines. These modifications alter the protein's running behavior on SDS-PAGE due to added molecular mass and different charge to mass ratio, allowing redox

## Methods

state determination. For the inverse shift assay, cells were seeded onto poly-L-lysine-coated 6-well plates and let grow until 40-50% confluency. Then, cells were put on ice and the sample for steady-state redox state determination was washed and incubated with PBS containing 20 mM NEM for 10 minutes. NEM modifies and therefore blocks free thiols to prevent further modification later during the experiment. Unmodified, minimal, and maximum shift controls did not require this pretreatment and were only washed with cold PBS. Then, PBS was aspirated and 8% TCA was added to rapidly acidify samples to reversibly protonate reactive thiols and trap the redox state while precipitating the protein [303, 304]. Samples were frozen at  $-80^{\circ}\text{C}$  for 1 h and thawed again at RT afterwards. Precipitated protein was pelleted at 13,000 xg at  $4^{\circ}\text{C}$  for 15 minutes and washed with 5% TCA at the same conditions. TCA solution was completely removed and protein pellets were dissolved in 1x Lämmli buffer containing 10 mM of the non-thiol reductant TCEP to reduce previously oxidized cysteines and incubated at  $95^{\circ}\text{C}$  for 15 minutes. Afterwards, these previously oxidized cysteines were modified with the larger mm(PEG)<sub>12</sub> and incubated at RT in the dark for 1 h. Then, samples could be analyzed via SDS-PAGE and Western blot.

### 5.3.8 Radioactive pulse chase

Protein stability and processing over time was dynamically assessed in a radioactive pulse chase experiment. For this experiment, 250,000 cells were seeded onto poly-L-lysine coated 35 mm dishes 48 h before the experiment. On the day of the experiment, stable cell lines were induced with 1  $\mu\text{g}/\text{ml}$  doxycycline for 1 h. Then, cells were starved of cysteine and methionine in starvation medium (DMEM without cysteine and methionine (Sigma), 100 mM HEPES-KOH pH 7.4, for stable cell lines 1  $\mu\text{g}/\text{ml}$  doxycycline) for 15 minutes at  $37^{\circ}\text{C}$ . Then, newly synthesized protein was labelled by incubating cells in pulse medium, starvation medium supplemented with Easytag™ Express <sup>35</sup>S Protein Labeling Mix (Perkin Elmer) at 100-200  $\mu\text{Ci}/\text{ml}$ , for 15 minutes at  $37^{\circ}\text{C}$ . Radioactive pulse medium was washed away and proteins were “chased” by keeping cells in chase medium (DMEM high glucose, 20 mM L-methionine, 100 mM HEPES-KOH pH 7.4) at  $37^{\circ}\text{C}$  for different times. After the respective time had passed, cells were put on ice, washed with PBS, and detached from the plate using a rubber policeman. Then cells were pelleted at 600 xg for 5 minutes and denaturing IP was performed as described in section 5.3.5. Samples were analyzed via Tris-Tricine SDS-PAGE, Western blot, and autoradiography.

### 5.3.9 Oxidation kinetic

The redox state of a protein can dynamically be assessed over time in an oxidation kinetic experiment. For this, 250,000 cells were seeded onto poly-L-lysine coated 35 mm dishes and induced with 1  $\mu\text{g}/\text{ml}$  doxycycline for 2 h two days after seeding. Then a radioactive pulse chase was performed as described in section 5.3.8, but the chase was stopped by putting cells on ice, washing with PBS and adding 8% TCA to the cells to precipitate protein. Samples were frozen over night at  $-20^{\circ}\text{C}$  and thawed at RT the next day. Protein was pelleted at 13,000 xg at  $4^{\circ}\text{C}$  for 15 minutes and washed with 5% TCA at the same

conditions. Afterwards, TCA was removed samples were resuspended in Buffer A (0.2 M Tris pH 7.5, 6 M urea, 10 mM EDTA, 2 % SDS). The unmodified control was dissolved in pure buffer A, whereas chase samples were dissolved in buffer A containing 16.6 mM mm(PEG)<sub>12</sub> and the fully reduced TCEP control was resuspended in buffer A with 20 mM TCEP and boiled at 95°C for 5 minutes before mm(PEG)<sub>12</sub> was added. All samples had now a volume of 60 µl and were incubated at RT for 1 h in the dark. After that, denaturing IP buffer without Triton X-100 was added up to 200 µl sample volume and denaturing IP was performed as described in section 5.3.5. Samples were analyzed via Tris-Tricine SDS-PAGE, Western blot, and autoradiography.

#### 5.3.10 Whole cell proteomics

To determine the proteome of a certain cell type and identify changes in the cellular proteome upon overexpression or knockout/knockdown of different proteins, a whole cell proteome dataset is generated. For this, 500,000 cells per sample are seeded in 6-well plates in four replicates per condition and induced with doxycycline if necessary. Two days later, cells reached confluency and were harvested in PBS and pelleted in low binding tubes at 300 xg for 7 minutes. Cell pellets were lysed in lysis buffer (1x PBS, 4% SDS) supplemented with 1x protease inhibitor cocktail (Sigma) and sonified 20 times at an amplitude of 30% to degrade chromatin. Afterwards samples were heated up to 95°C for 5 minutes. Then acetone precipitation was performed. 4x the volume of ice-cold acetone was added to each sample and frozen at -80°C over night. The next day, protein precipitate was pelleted at 16,000xg for 15 minutes at 4°C and washed two times with ice-cold acetone for 5 minutes at 16,000xg at 4°C. Pellets were let dry and resuspended in urea lysis buffer (8 M urea, 50 mM triethylammoniumbicarbonate (TEAB)) supplemented with 1x protease inhibitor cocktail. Protein concentration was determined for each sample using the Pierce™ Coomassie Plus protein determination assay (Thermo Fisher) according to manufacturer's guidelines and measuring absorption at 660 nm. 50 µg protein per sample were transferred to fresh low binding tubes reduced with 5 mM DTT for 1 h at 37°C and acetylated with 40 mM chloroacetamide (CAA) in the dark for 30 minutes. Afterwards, in solution digest was begun by digestion of samples with Lys-C protease at an enzyme:substrate ratio of 1:200 for 4 h at 25°C. Then, samples were diluted with 50 mM TEAB to achieve a final urea concentration in the samples below 2 M and digested with trypsin at an enzyme:substrate ratio of 1:75 at 25°C overnight. To stop digest, samples were acidified by addition of formic acid (FA) to a final concentration of 1% and cleared by centrifugation at 20,000 xg for 5 minutes. Simultaneously, stage tips containing a C18 matrix at the tip were equilibrated with methanol, buffer A (0.1% FA) and buffer B (0.1% FA in acetonitrile). After equilibration, samples were loaded onto stage tips, washed, dried, and measured at the proteomics facility of CECAD.

## Methods

### 5.3.11 Generation of an interactome

Interactome datasets give detailed information on interaction partners of proteins of interest with high sensitivity. To generate an interactome dataset, IP or AP experiments were performed as described in section 5.3.5 and eluted in 1x Lämmli buffer without bromophenol blue. Afterwards, in gel digest was performed. Therefore, samples were loaded and run on SDS-PAGE until they just entered the running gel completely. The gel was fixed for 1 h in fixing solution (10% acetic acid, 20% methanol). Bands were cut out and chopped into small pieces that were transferred to fresh low binding tubes. Pieces were covered in 50 mM ammoniumbicarbonate (ABC)/50% acetonitrile (ACN), vortexed and incubated for 20 minutes. Solution was discarded and the step repeated. Then samples were reduced by incubation in 10 mM DTT for 30 minutes at 55°C. DTT was removed, gel pieces were covered in ACN for 15 minutes, ACN was discarded and 55 mM CAA solution was added for acetylation. After 30 minutes, CAA was removed and ACN was added for 15 minutes and discarded again. New ACN was added to cover gel pieces completely for 10 minutes. Then ACN was removed from the gel pieces and they were dried in a speedvac for 5 minutes. Dried gel pieces were swollen in digest solution (50 mM ABC, 1 ng/μl Lys-C, 9 ng/μl trypsin) for 30 minutes at 4°C before excess digest solution was removed and gel pieces were covered with 50 mM ABC and incubated at 37°C over night. The next day, supernatant was transferred to fresh low binding tubes and extraction of digested peptides from the gel pieces was started by incubation in 30%ACN/3% Trifluoroacetic acid (TFA) for 20 minutes followed by incubation in ACN for another 20 minutes. All supernatants were pooled and dried down in a speedvac to 50 μl. Samples were acidified with 1% FA, loaded on stage tips as described at section 5.3.10 and sent to the proteomics facility for measurement.

### 5.3.12 HPLC-based measurement of heme biosynthesis intermediates

Heme biosynthesis intermediates from cell lysates were measured via HPLC/MS. For this, stable cell lines were induced with doxycycline 48 h before seeding. For each cell line, 500,000 cells per well were seeded onto 6-well plates in replicates of six. Directly after seeding, cells were induced again. 24 h after seeding, cells were put on ice, washed with 1 ml ice-cold PBS, and harvested. Two of the six replicates were harvested in 1 ml PBS each using a rubber policeman and protein concentration was determined using the Pierce BCA assay kit (Thermo Fisher) according to manufacturer's guidelines for later data normalization. The other four replicates were covered in 1 mL of extraction buffer (80% methanol, 5% FA; previously stored at -80°C) and incubated at -80°C for 30-60 minutes. Then lysed cells were transferred to 1.5 ml tubes using a rubber policeman. Cell debris was pelleted at 20,000 xg for 20 minutes at 4 °C. 700 μl of supernatant were transferred to a fresh tube and stored at -80 °C until further use. On the day of HPLC/MS analysis, extraction buffer was removed by drying samples in a speedvac and the remaining pellet was dissolved in measurement buffer (50% methanol, 50% ACN).

Chromatography was performed on a Nexera XR 40 series HPLC (Shimadzu) using a Nucleodur Sphinx RP, 3 $\mu$ m, 150x2 mm (Macherey Nagel). The column temperature was maintained at 40°C and the sample tray at 4°C. Samples (10  $\mu$ l) were injected at a flow rate of 0.4 ml/min using 0.1% formic acid and acetonitrile as mobile phases A and B, respectively. Metabolites were eluted using the 20min gradient profile 0 min, 2% B; 0-2 min, 2% B; 2-9 min, 100% B; 9-13 min 100% B; 13-13.1 min, 2% B. The LCMS-8060 triple quadrupole mass spectrometer with electro spray ionization (Shimadzu) was operated in positive mode. Scheduled multiple reaction monitoring (MRM) was used to monitor analyte parent ion to product ion formation. MRM conditions were optimized using authentic standard chemicals including: coproporphyrin III ([M+H] 655.10>596.20, 655.10>537.25, 655.10>523.20), coproporphyrin III tetramethyl ester ([M+H] 711.20>565.30, 711.20>551.25, 711.20>638.20), protoporphyrin IX ([M+H] 563.10>504.15, 563.10>445.15, 563.10>431.25). Both Q1 and Q3 quadrupoles were maintained in unit resolution. LabSolutions LCMS v5.118 software was used for data acquisition and LabSolutions Postrun for processing (both Shimadzu). Metabolites were quantified by scheduled MRM peak integration.

Sample preparation for HPLC/MS measurements were performed by Dylan Stobbe, Riemer Lab, University of Cologne. HPLC/MS measurements and data processing was done by Dr. Jan Jirschitzka, Neundorf Lab, University of Cologne.

## 5.4 Bioinformatics

### 5.4.1 Protein sequence conservation analysis

Protein sequence conservation was analyzed by alignment of protein sequences in Jalview 2.11.1.3 [309] and visualized by creation of logo plots with the tool WebLogo 3 [397], where the letter size of the amino acid abbreviation corresponds to its degree of conservation.

### 5.4.2 Protein structure visualization

Information on solved protein structures were acquired from the RCSB Protein Data Bank (PDB) and opened, analyzed, and visualized with PyMOL 3.0. Unsolved protein structures were predicted, visualized, and analyzed with the AlphaFold Protein Structure Database.

### 5.4.3 Analysis of proteomics data

Proteomics data was analyzed by the proteomics facility and provided as .xlsx file. The data was further analyzed with Microsoft Excel 2019 and visualized as volcano plot with Origin 2020 SR0 or as heatmap with Microsoft Excel 2019 and CoreIDRAW X7.

### 5.4.4 Quantification and statistical analysis

Signal intensities of immunoblots were quantified using Biorad ImageLab 5.2. Signal intensities of autoradiographies were quantified using the Fiji package of ImageJ 1.53 C. Error bars represent standard deviations as determined in Microsoft Excel 2019.

## Methods

### 5.4.5 Data availability

Data generated or used in the course of this work is stored on the SOFS server of the Riemer laboratory and can be accessed by all lab members.

## 6. Materials

### 6.1 Plasmids and cell lines

Table 11: Cell lines and plasmids used in this work

Cell line	Plasmid	Gene
HepG2	-	-
HEK293	-	-
HEK293 Flp-In <sup>TM</sup> T-Rex <sup>TM</sup> host	-	-
HEK293 Flp-In <sup>TM</sup> T-Rex <sup>TM</sup> + Mock	pcDNA5/FRT/TO	-
HEK293 Flp-In <sup>TM</sup> T-Rex <sup>TM</sup> + ALR-Strep	pcDNA5/FRT/TO	ORF ALR
HEK293 Flp-In <sup>TM</sup> T-Rex <sup>TM</sup> + ALR-HA	pcDNA5/FRT/TO	ORF ALR
HEK293 Flp-In <sup>TM</sup> T-Rex <sup>TM</sup> CPOX KO	-	-
HEK293 Flp-In <sup>TM</sup> T-Rex <sup>TM</sup> CPOX KO + CPOX-HA WT	pcDNA5/FRT/TO	ORF CPOX
HEK293 Flp-In <sup>TM</sup> T-Rex <sup>TM</sup> CPOX KO + CPOX-HA 10CA	pcDNA5/FRT/TO	ORF CPOX (C127, C164, C192, C198, C239, C281, C304, C319, C357, C373 → A)
HEK293 Flp-In <sup>TM</sup> T-Rex <sup>TM</sup> CPOX KO + CPOX-HA 4CA	pcDNA5/FRT/TO	ORF CPOX (C164, C192, C304, C357 → A)
HEK293 Flp-In <sup>TM</sup> T-Rex <sup>TM</sup> CPOX KO + CPOX-HA C164,192A	pcDNA5/FRT/TO	ORF CPOX (C164, C192 → A)
HEK293 Flp-In <sup>TM</sup> T-Rex <sup>TM</sup> CPOX KO + CPOX-HA C304,357A	pcDNA5/FRT/TO	ORF CPOX (C304, C357 → A)
HEK293 Flp-In <sup>TM</sup> T-Rex <sup>TM</sup> CPOX KO + CPOX-HA C164,357A	pcDNA5/FRT/TO	ORF CPOX (C164, C357 → A)
HEK293 Flp-In <sup>TM</sup> T-Rex <sup>TM</sup> CPOX KO + CPOX-HA C164A	pcDNA5/FRT/TO	ORF CPOX (C164 → A)
HEK293 Flp-In <sup>TM</sup> T-Rex <sup>TM</sup> CPOX KO + CPOX-HA C192A	pcDNA5/FRT/TO	ORF CPOX (C192 → A)
HEK293 Flp-In <sup>TM</sup> T-Rex <sup>TM</sup> CPOX KO + CPOX-HA C304A	pcDNA5/FRT/TO	ORF CPOX (C304 → A)
HEK293 Flp-In <sup>TM</sup> T-Rex <sup>TM</sup> CPOX KO + CPOX-HA C357A	pcDNA5/FRT/TO	ORF CPOX (C357 → A)
HEK293 Flp-In <sup>TM</sup> T-Rex <sup>TM</sup> CPOX KO + CPOX-HA $\Delta$ 1-88	pcDNA5/FRT/TO	ORF CPOX ( $\Delta$ 1-88)
HEK293 Flp-In <sup>TM</sup> T-Rex <sup>TM</sup> CPOX KO + CPOX-HA 10CA $\Delta$ 1-88	pcDNA5/FRT/TO	ORF CPOX ( $\Delta$ 1-88; C127, C164, C192, C198, C239, C281, C304, C319, C357, C373 → A)
HEK293 Flp-In <sup>TM</sup> T-Rex <sup>TM</sup> CPOX KO + CPOX-HA 4CA $\Delta$ 1-88	pcDNA5/FRT/TO	ORF CPOX ( $\Delta$ 1-88; C164, C192, C304, C357 → A)
HEK293 Flp-In <sup>TM</sup> T-Rex <sup>TM</sup> CPOX KO + Hem13-HA	pcDNA5/FRT/TO	ORF Hem13

## Materials

HEK293 Flp-In™ T-Rex™ CPOX KO + CPOX-HA WT + Mock	pcDNA5/FRT/TO PB-CuO-MCS-IHRES- GFP-EF1-CymR-Puro	ORF CPOX -
HEK293 Flp-In™ T-Rex™ CPOX KO + CPOX-HA WT + ALR-Strep	pcDNA5/FRT/TO PB-CuO-MCS-IHRES- GFP-EF1-CymR-Puro	ORF CPOX ORF ALR
HEK293 Flp-In™ T-Rex™ CPOX KO + CPOX-HA 10CA + Mock	pcDNA5/FRT/TO PB-CuO-MCS-IHRES- GFP-EF1-CymR-Puro	ORF CPOX (C127, C164, C192, C198, C239, C281, C304, C319, C357, C373 → A) -
HEK293 Flp-In™ T-Rex™ CPOX KO + CPOX-HA 10CA + ALR-Strep	pcDNA5/FRT/TO PB-CuO-MCS-IHRES- GFP-EF1-CymR-Puro	ORF CPOX (C127, C164, C192, C198, C239, C281, C304, C319, C357, C373 → A) ORF ALR
HEK293 Flp-In™ T-Rex™ CPOX KO + CPOX-HA 4CA + ALR-Strep	pcDNA5/FRT/TO PB-CuO-MCS-IHRES- GFP-EF1-CymR-Puro	ORF CPOX (C164, C192, C304, C357 → A) ORF ALR
HEK293 Flp-In™ T-Rex™ CPOX KO + CPOX-HA C164,192A + Mock	pcDNA5/FRT/TO PB-CuO-MCS-IHRES- GFP-EF1-CymR-Puro	ORF CPOX (C164, C192 → A) -
HEK293 Flp-In™ T-Rex™ CPOX KO + CPOX-HA C164,192A + ALR-Strep	pcDNA5/FRT/TO PB-CuO-MCS-IHRES- GFP-EF1-CymR-Puro	ORF CPOX (C164, C192 → A) ORF ALR
HEK293 Flp-In™ T-Rex™ CPOX KO + CPOX-HA C304,357A + Mock	pcDNA5/FRT/TO PB-CuO-MCS-IHRES- GFP-EF1-CymR-Puro	ORF CPOX (C304, C357 → A) -
HEK293 Flp-In™ T-Rex™ CPOX KO + CPOX-HA C304,357A + ALR-Strep	pcDNA5/FRT/TO PB-CuO-MCS-IHRES- GFP-EF1-CymR-Puro	ORF CPOX (C304, C357 → A) ORF ALR
HEK293 Flp-In™ T-Rex™ CPOX KO + CPOX-HA C164,304A + Mock	pcDNA5/FRT/TO PB-CuO-MCS-IHRES- GFP-EF1-CymR-Puro	ORF CPOX (C164, C304 → A) -
HEK293 Flp-In™ T-Rex™ CPOX KO + CPOX-HA C164,304A + ALR-Strep	pcDNA5/FRT/TO PB-CuO-MCS-IHRES- GFP-EF1-CymR-Puro	ORF CPOX (C164, C304 → A) ORF ALR
HEK293 Flp-In™ T-Rex™ CPOX KO + CPOX-HA C164A + Mock	pcDNA5/FRT/TO PB-CuO-MCS-IHRES- GFP-EF1-CymR-Puro	ORF CPOX (C164 → A) -
HEK293 Flp-In™ T-Rex™ CPOX KO + CPOX-HA C164A + ALR-Strep	pcDNA5/FRT/TO PB-CuO-MCS-IHRES- GFP-EF1-CymR-Puro	ORF CPOX (C164 → A) ORF ALR

HEK293 Flp-In <sup>TM</sup> T-Rex <sup>TM</sup> CPOX KO + CPOX-HA C192A + Mock	pcDNA5/FRT/TO PB-CuO-MCS-IHRES- GFP-EF1-CymR-Puro	ORF CPOX (C192 → A) -
HEK293 Flp-In <sup>TM</sup> T-Rex <sup>TM</sup> CPOX KO + CPOX-HA C192A + ALR-Strep	pcDNA5/FRT/TO PB-CuO-MCS-IHRES- GFP-EF1-CymR-Puro	ORF CPOX (C192 → A) ORF ALR
HEK293 Flp-In <sup>TM</sup> T-Rex <sup>TM</sup> CPOX KO + CPOX-HA C304A + Mock	pcDNA5/FRT/TO PB-CuO-MCS-IHRES- GFP-EF1-CymR-Puro	ORF CPOX (C304 → A) -
HEK293 Flp-In <sup>TM</sup> T-Rex <sup>TM</sup> CPOX KO + CPOX-HA C304A + ALR-Strep	pcDNA5/FRT/TO PB-CuO-MCS-IHRES- GFP-EF1-CymR-Puro	ORF CPOX (C304 → A) ORF ALR
HEK293 Flp-In <sup>TM</sup> T-Rex <sup>TM</sup> CPOX KO + CPOX-HA C357A + Mock	pcDNA5/FRT/TO PB-CuO-MCS-IHRES- GFP-EF1-CymR-Puro	ORF CPOX (C357 → A) -
HEK293 Flp-In <sup>TM</sup> T-Rex <sup>TM</sup> CPOX KO + CPOX-HA C357A + ALR-Strep	pcDNA5/FRT/TO PB-CuO-MCS-IHRES- GFP-EF1-CymR-Puro	ORF CPOX (C357 → A) ORF ALR
HEK293 Flp-In <sup>TM</sup> T-Rex <sup>TM</sup> IMMP1/2 double KO + CPOX-HA WT	pcDNA5/FRT/TO	ORF CPOX
HEK293 Flp-In <sup>TM</sup> T-Rex <sup>TM</sup> + CPOX-HA WT	pcDNA5/FRT/TO	ORF CPOX

## 6.2 Oligonucleotides

Table 12: Oligonucleotide primers used in this work

Oligo	5' → 3' Sequence	Purpose
CPOX guide 1 exon 1 fwd	CCACCGGTCCACAGAAAAGTTGG	CRISPR/Cas9 KO of CPOX
CPOX guide 1 exon 1 rev	CCAACCTTTTCTGTGGACCGGTGG	CRISPR/Cas9 KO of CPOX
CPOX guide 2 exon 1 fwd	AGCTCGCCCAGGTCGGTCACAGG	CRISPR/Cas9 KO of CPOX
CPOX guide 2 exon 1 rev	CCTGTGACCGACCTGGGCGAGCT	CRISPR/Cas9 KO of CPOX
CPOX KO sequencing primer fwd	GTGCAGCTCGCCGGCTCAATACTCCG	Sequencing of CRISPR/Cas9 KO of CPOX
CPOX KO sequencing primer rev	GTCCATACCTGCAAGCAGAGGGCTAGTG	Sequencing of CRISPR/Cas9 KO of CPOX
CPOX-HA WT in pcDNA5 fwd	GCGAAGCTTATGGCCTTGACAGCTGGGCAGGCTGAG CTCGGGCC	Subcloning of CPOX from pOTB7 to pcDNA5/FRT/TO with HindIII

## Materials

CPOX-HA WT in pcDNA5 rev	GCGCGGCCGCTCAAGCGTAATCTGGAACATCGTATG GGTAACGCACCCAGTCCCTTGGAT	Subcloning of CPOX from pOTB7 to pcDNA5/FRT/TO with NotI adding an HA tag
CPOX C164A fwd	CCAGGCCAGGTGGCCAGGCTCTGGC	Site-directed mutagenesis
CPOX C164A rev	GCCAGAGCCTGGGCCACCTGGGCTGG	Site-directed mutagenesis
CPOX C192A fwd	GGCGGCATCAGCGCTGTACTTCAAGATGG	Site-directed mutagenesis
CPOX C192A rev	CCATCTTGAAGTACAGCGCTGATGCCGCC	Site-directed mutagenesis
CPOX C304A fwd	CTGAAGGAGGCTGCTGACCAGCATGGTCC	Site-directed mutagenesis
CPOX C304A rev	GGACCATGCTGGTCAGCAGCCTCCTTCAG	Site-directed mutagenesis
CPOX C357A fwd	CTTTGTACAGAGCGCTGCCAGGGCTGTAG	Site-directed mutagenesis
CPOX C357A rev	CTACAGCCCTGGCAGCGCTCTGTACAAAG	Site-directed mutagenesis
CPOX Δ1-88 fwd	GCGAAGCTTATGGCCACCGCCGCTTCGG	Subcloning of CPOX without the first 88 amino acids with HindIII
CPOX Δ1-88 rev	GTTGCGGCCGCTCAAGCGTAATCTGGAACATCGTAT GGG	Subcloning of CPOX without the first 88 amino acids with NotI adding an HA tag
Hem13-HA fwd	GCGAAGCTTATGCCTGCCCTCAAGATCCAAGGAAT CTTCC	Cloning of Hem13 into pcDNA5/FRT/TO with HindIII
Hem13-HA rev	GTTGCGGCCGCTCAAGCGTAATCTGGAACATCGTAT GGGTATTTAACCCACTCTCTTG	Cloning of Hem13 into pcDNA5/FRT/TO with NotI adding an HA tag
ALR-Strep fwd	GGTGCTAGCGCCACCATGGCGGCGCCCGGCGAG	Subcloning of ALR into PB-CuO-MCS-IHRES-GFP-EF1-CymR-Puro with NheI
ALR-Strep rev	ACCATTTAAATCTATTTCTCAAATTGTGGATGACTCCA TGCACCTCCGTACAGGAGCCATCCTTCCAGCCGTC GCG	Subcloning of ALR into PB-CuO-MCS-IHRES-GFP-EF1-CymR-Puro with Swal adding a Strep tag

## 6.3 Antibodies

Table 13: Antibodies used in this work

Antibody	Source	Identifier
Rabbit polyclonal αHA	Sigma	SAB4300603
Mouse monoclonal αStrep	Qiagen	34850
Rabbit polyclonal αALR	[398]	-
Rabbit polyclonal αCPOX	St. John's Laboratory	STJ23214
Rabbit polyclonal αMIA40	[398]	-
Rabbit polyclonal αAK2	[312]	-
Rabbit polyclonal αMTCH2	Lena Pernas	-
Rabbit polyclonal αAIFM1	Merck	AB16501
Rabbit polyclonal αSMAC	Sigma	PRS2411
Rabbit polyclonal αHAX1	Invitrogen	PA-27592
Rabbit monoclonal αALAS1	abcam	ab154860
Mouse monoclonal αActin	Thermo Fisher	MA5-11869

Rabbit polyclonal $\alpha$ YME1L1	proteintech	11510-1-AP
Goat $\alpha$ rabbit Alexa488	Invitrogen	A11008
Goat $\alpha$ Rabbit HRP	ImmunoReagents	GtxRb-003-DHRPX
Goat $\alpha$ Mouse HRP	ImmunoReagents	GtxMu-003-DHRPX

#### 6.4 siRNA

*Table 14: siRNAs used in this work*

<b>SiRNA</b>	<b>Supplier</b>	<b>Identifier</b>	<b>Name in this work</b>
Hs_CHCHD4_5	Qiagen	SI04197354	MIA40 #1
Hs_CHCHD4_6	Qiagen	SI04292176	MIA40 #2
Hs_GFER_1	Qiagen	SI00426748	ALR #1
Hs_GFER_6	Qiagen	SI04250491	ALR #2
AllStars Neg. Control siRNA	Qiagen	1027281	Control

## 7. Abbreviations

Å	Angström
AAA	ATPases associated with diverse cellular activities
ABC	Ammoniumbicarbonate
ABCB	ATP-binding cassette sub-family B member
ABCG2	ATP-binding cassette super-family G member 2
ACN	Acetonitrile
ADP	Adenosine diphosphate
ADP	ALA dehydratase porphyria
AF	Acifluorfen
AFG3L2	ATPase family gene 3-like 2
AIFM1	Apoptosis-inducing factor mitochondria-associated 1
AIP	Acute intermittent porphyria
AK2	Adenylate kinase 2
5-ALA	5-aminolevulinic acid
ALAD	ALA dehydratase
ALAS	5-aminolevulinic acid synthase
ALR	Augmenter of liver regeneration
AMP	Adenosine monophosphate
ANT	Adenine nucleotide translocator
AP	Affinity purification/precipitation
ATP	Adenosine triphosphate
Atp6	ATPase 6
ATP23	ATPase 23
BCA	Bicinchoninic acid
BSA	Bovine serum albumin
°C	Degree Celsius
CAA	Chloroacetamide
Ccp1	Cytochrome c peroxidase
CCS1	Copper chaperone for SOD1
C/EBP	CCAAT/enhancer-binding protein
CECAD	Cologne Excellence Cluster for Aging and Aging-Associated Diseases
CEP	Congenital erythropoietic porphyria
CHL	Cytochrome c heme lyase
CJ	Cristae junction
CLPP	Caseinolytic peptidase proteolytic subunit
CLPX	Caseinolytic peptidase chaperone subunit
cm	Centimeter(s)
CMC1	CX <sub>9</sub> C motif containing 1
CO <sub>2</sub>	Carbondioxide
COA7	Cytochrome c oxidase assembly factor 7
COX	cytochrome c oxidase
CPOX	Coproporphyrinogen oxidase
CPPIII	Coproporphyrin III
CPPgenIII	Coproporphyrinogen III

CRISPR/Cas9	Clustered Regularly Interspaced Short Palindromic Repeats/CRISPR-associated systems 9
CS	Contact site
CYC1	Cytochrome c <sub>1</sub>
Cyt c	Cytochrome c
DAPI	4',6-diamidino-2-phenylindole
dd	Doubly distilled
DHODH	Dihydroorotate dehydrogenase
DKO	Double knockout
<i>D.m.</i>	<i>Drosophila melanogaster</i>
DMEM	Dulbecco's modified Eagle medium
DMSO	Dimethylsulfoxid
DNA	Deoxyribonucleic acid
dNTP	Deoxynucleosidtriphosphate
<i>D.r.</i>	<i>Danio rerio</i>
DTT	Dithiothreitol
ECL I/II	Enhanced chemiluminescence I/II
<i>E.coli</i>	<i>Escherichia coli</i>
EDTA	Ethylenediaminetetraacetic acid
EKLF	Erythroid Krüppel-like factor
EPP	Erythropoietic protoporphyria
ER	Endoplasmic reticulum
ERO1	ER oxidoreductin 1
Erv1	Essential for respiration and viability 1
FA	Formic acid
FABP	Fatty acid-binding protein
FACS	Fluorescence assisted cell sorting
FAD	Flavin adenine dinucleotide
FBS	Fetal bovine serum
f.c.	Fold change
FECH	Ferrochelatase
FLVCR1b	Feline leukaemia virus subgroup C receptor 1b
g	Gram(s)
GAPDH	Glyceraldehyde phosphate dehydrogenase
GATA-1	GATA binding factor 1
<i>G.g.</i>	<i>Gallus gallus</i>
GOI	Gene of interest
GPD2	Glycerol 3-phosphate dehydrogenase 2
GPDH	Glycerol-3-phosphate dehydrogenase
gRNA	Guide RNA
GSH	Reduced glutathione
GST	Glutathione-S-transferase
Gut2	Glycerol utilization 2
h	Hour(s)
HAX1	HCLS1 associated protein X-1

## Abbreviations

HBP	Heme-binding protein
HCP	Hereditary coproporphyria
HEBP2	Heme-binding protein 2
HEK293	Human embryonic kidney
Hem1/13	Heme biosynthesis/13
HGMD	Human Gene Mutation Database
HMB	Hydroxymethylbilane
HMBS	Hydroxymethylbilane synthase
HEPES	4-(2-hydroxyethyl)-1-piperazineethanesulfonic acid
HepG2	Hepatocellular carcinoma
HIF-1	Hypoxia inducible factor
HPLC	High performance liquid chromatography
HR	Homologous recombination
HRM	Heme regulatory motif
HRP	Horseradish peroxidase
<i>H.s.</i>	<i>Homo sapiens</i>
HSP	Heat shock protein
HTRA2	HtrA serine peptidase 2
IAP	Inhibitors of apoptosis
IMM	Inner mitochondrial membrane
IMMP	Inner mitochondrial membrane protease
Imp	Inner membrane protease
IMS	Intermembrane space
IP	Immunoprecipitation
IRE	Iron responsive element
IRP	Iron regulatory/responsive protein
ITR	Inverted terminal repeat sequence
ITS	IMS targeting signal sequence
kb	Kilobase(s)
KD	Knockdown
<i>K.l.</i>	<i>Kluyveromyces lactis</i>
KO	Knockout
l	Liter(s)
LONP	Lon protease
M	Molar
mA	Milliampere
MB-6	MitoBloCK-6
mCK	Mitochondrial creatine kinase
MCU	Mitochondrial calcium uniporter
MEL	Murine erythroleukemia
MFRN	Mitoferrin
Mgr2	Mitochondrial genome required 2
MIA40/Mia40	Mitochondrial import and assembly protein
MICOS	Mitochondrial contact site and cristae organizing system
MICU1/2	Mitochondrial calcium uptake 1/2

min	Minute(s)
MIP	Mitochondrial intermediate peptidase
MISS	Mitochondrial IMS sorting sequence
ml	Milliliter(s)
μl	Microliter(s)
<i>M.m.</i>	Mus musculus
mM	Millimolar
μM	Micromolar
μm	Micrometer(s)
Moco	Molybdenum cofactor
MPP	Matrix processing peptidase
MRM	Multiple reaction monitoring
MrpL32	Mitochondrial ribosomal protein, large subunit 32
MS	Mass spectrometry
MTBS	Milk dissolved in tris buffered saline
MTCH2	Mitochondrial carrier homolog 2
MTS	Mitochondrial targeting signal
NAC	N-acetylcysteine
NADH	Nicotinamide adenine dinucleotide
NADPH	Nicotinamide adenine dinucleotide phosphate
NDP	Nucleoside diphosphate
NDUF	NADH:ubiquinone oxidoreductase subunit
NEM	N-ethyl-maleimide
NF-E2	Nuclear factor erythroid 2
ng	Nanogram(s)
NHEJ	Non-homologous end joining
nm	Nanometer(s)
nM	Nanomolar
NME4/NDPK-D	Nucleoside–diphosphate kinase
NMPP	N-methylprotoporphyrin
NO	Nitric oxide
NOS	Nitric oxide synthase
NOX4	NADPH oxidase 4
NRF1	Nuclear respiratory factor 1
NSCLC	Non-small-cell lung cancer
NTP	Nucleoside triphosphate
O <sub>2</sub>	Molecular oxygen
Oct1	Octapeptidyl aminopeptidase 1
OMA1	Overlapping activity with <i>m</i> -AAA protease 1
OMM	Outer mitochondrial membrane
OPA1	Optic atrophy 1
Osm1	Osmotic sensitivity 1
Ox.	Oxidized
PAM	Protospacer adjacent motifs
PARL	Presenilin-associated rhomboid like

## Abbreviations

PB	PiggyBac
PBG	Porphobilinogen
PBGD	Porphobilinogen deaminase
PBGS	Porphobilinogen synthase
PBS	Phosphate buffered saline
Pcp1	Processing of cytochrome c peroxidase 1
PCR	Polymerase chain reaction
PCT	Porphyria cutanea tarda
PDB	Protein Data Bank
PDI	Protein disulfide isomerase
PDT	Photodynamic therapy
PEI	Polyethyleneimine
PEG	Polyethylene glycol
PGRMC1/2	Progesterone receptor membrane component 1/2
PINK1	PTEN induced kinase 1
PLP	Pyridoxal 5'-phosphate
pmol	Picomole
PNPase	Polynucleotide phosphorylase
PPIX	Protoporphyrin IX
PPgenIX	Protoporphyrinogen IX
PPOX	Protoporphyrinogen oxidase
PRX/Prx	Peroxiredoxin
Red.	Reduced
<i>R.n.</i>	<i>Rattus norvegicus</i>
RNA	Ribonucleic acid
ROMO1	Reactive oxygen species modulator 1
ROS	Reactive oxygen species
RT	Room temperature
SA	Succinylacetone
SAM	Sorting and assembly machinery
<i>S.c.</i>	<i>Saccharomyces cerevisiae</i>
SDS	Sodium dodecyl sulphate
SDS-PAGE	Sodium dodecyl sulphate polyacrylamide gel electrophoresis
SDT	Sonodynamic therapy
<i>S.h.</i>	<i>Strigops habroptila</i>
SILAC	Stable isotope labeling by amino acids in cell culture
SLC25	Solute carrier family 25
SLP2	Stomatin-like protein 2
SOD1	Superoxide dismutase 1
Som1	Sorting mitochondrial 1
<i>S.s.</i>	<i>Scheffersomyces stipitis</i>
STARD7	StAR-related lipid transfer domain protein 7
SUCLA2	Beta subunit of succinyl-CoA synthetase
SUOX	Sulfite oxidase
TBS	Tris buffered saline

TCA	Tricarboxylic acid
TCE	Trichlorethyhanol
TCEP	Tris(2-chlorethyl)phosphate
TEAB	Triethylammoniumbicarbonate
TFA	Trifluoroacetic acid
TFRC	Transferrin receptor protein 1
TIM/Tim	Translocase of the inner membrane
TM	Transmembrane
T <sub>M</sub>	Melting temperature
TMEM14C	Transmembrane protein 14C
TOM	Translocase of the outer membrane
TRX1	Thioredoxin-1
T[X]	Annealing temperature
t[x]	Elongation time
UCP	Uncoupling protein
UPPIII	Uroporphyrinogen III
UROD	Uroporphyrinogen decarboxylase
UROS	Uroporphyrinogen synthase
UTR	Untranslated region
V	Volt
VDAC	Voltage-dependent anion channel
VP	Variegate porphyria
WT	Wildtype
XLP	X-linked protoporphyria
YME1L1	Yeast mitochondrial escape like 1

## Abbreviations

### Amino Acids

<b>Amino Acid</b>	<b>3-letter code</b>	<b>1-letter code</b>
Alanine	Ala	A
Arginine	Arg	R
Asparagine	Asn	N
Aspartate	Asp	D
Cysteine	Cys	C
Glutamate	Glu	E
Glutamine	Gln	Q
Glycine	Gly	G
Histidine	His	H
Isoleucine	Ile	I
Leucine	Leu	L
Lysine	Lys	K
Methionine	Met	M
Phenylalanine	Phe	F
Proline	Pro	P
Serine	Ser	S
Threonine	Thr	T
Tryptophane	Trp	W
Tyrosine	Tyr	Y
Valine	Val	V

## 8. Appendix

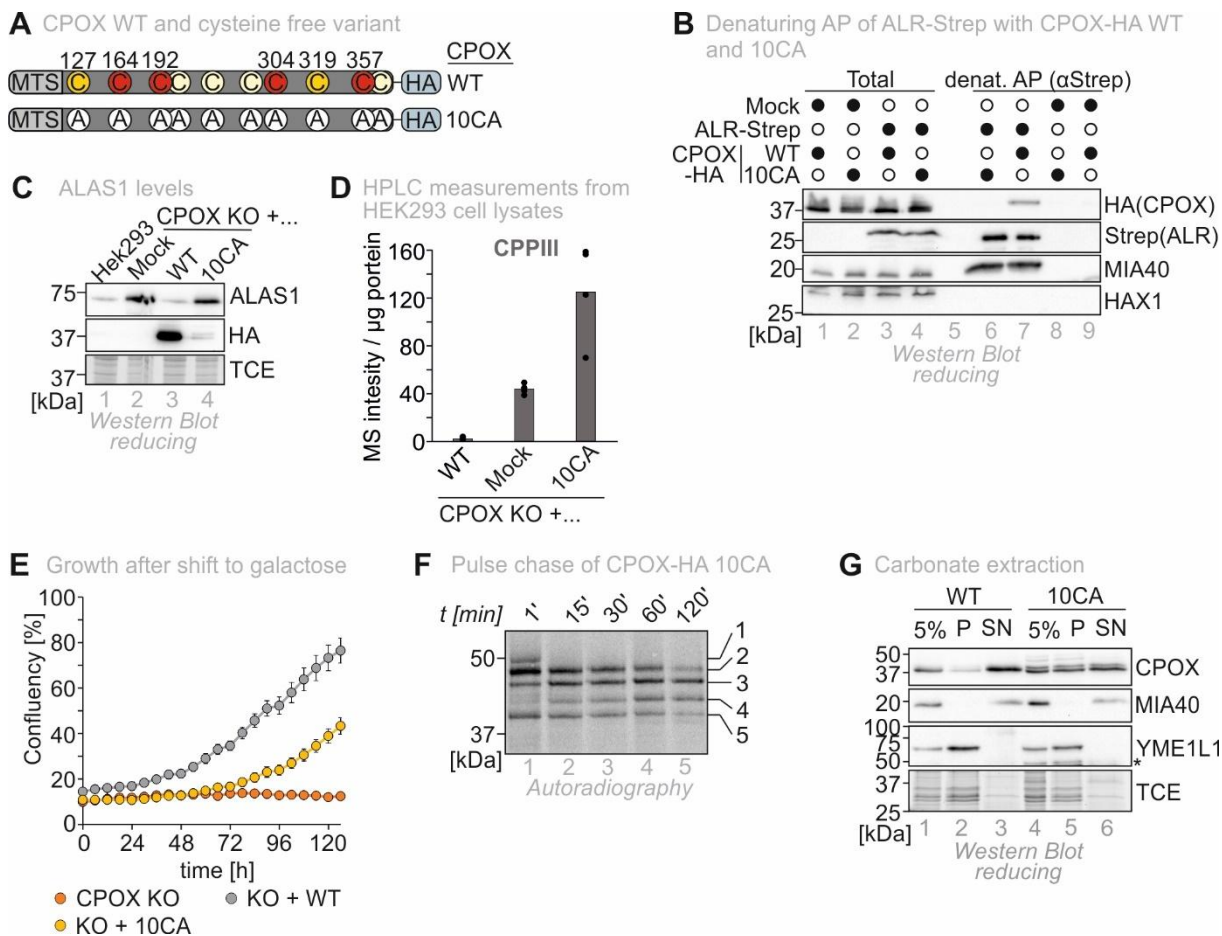


Figure S 1: Comparison of CPOX-HA WT and a cysteine-free CPOX variant

**A** CPOX-HA WT and a CPOX-HA variant lacking all 10 cysteines in the mature protein (10CA) were expressed on a CPOX KO background and compared in different experiments. **B** A denaturing AP of ALR-Strep was performed in CPOX KO cells co-expressing CPOX-HA WT or 10CA. **C** Western blot of cell lysates from HEK293 cells and CPOX KO cells complemented with a mock control, CPOX-HA WT or 10CA. TCE acts as loading control. **D** HPLC measurement of CPPIII from cell lysates of CPOX KO cells complemented with CPOX-HA WT, Mock or 10CA. **E** CPOX KO cells and CPOX KO cells complemented with CPOX-HA WT or 10CA were shifted from glucose to galactose at timepoint 0 and growth was measured over 120 h. **F** Pulse chase of CPOX-HA 10CA on CPOX KO background. **G** Carbonate extraction of CPOX-HA WT and 10CA. MIA40 is the soluble IMS control. YME1L1 is the IMM-bound control. TCE acts as loading control.

Appendix

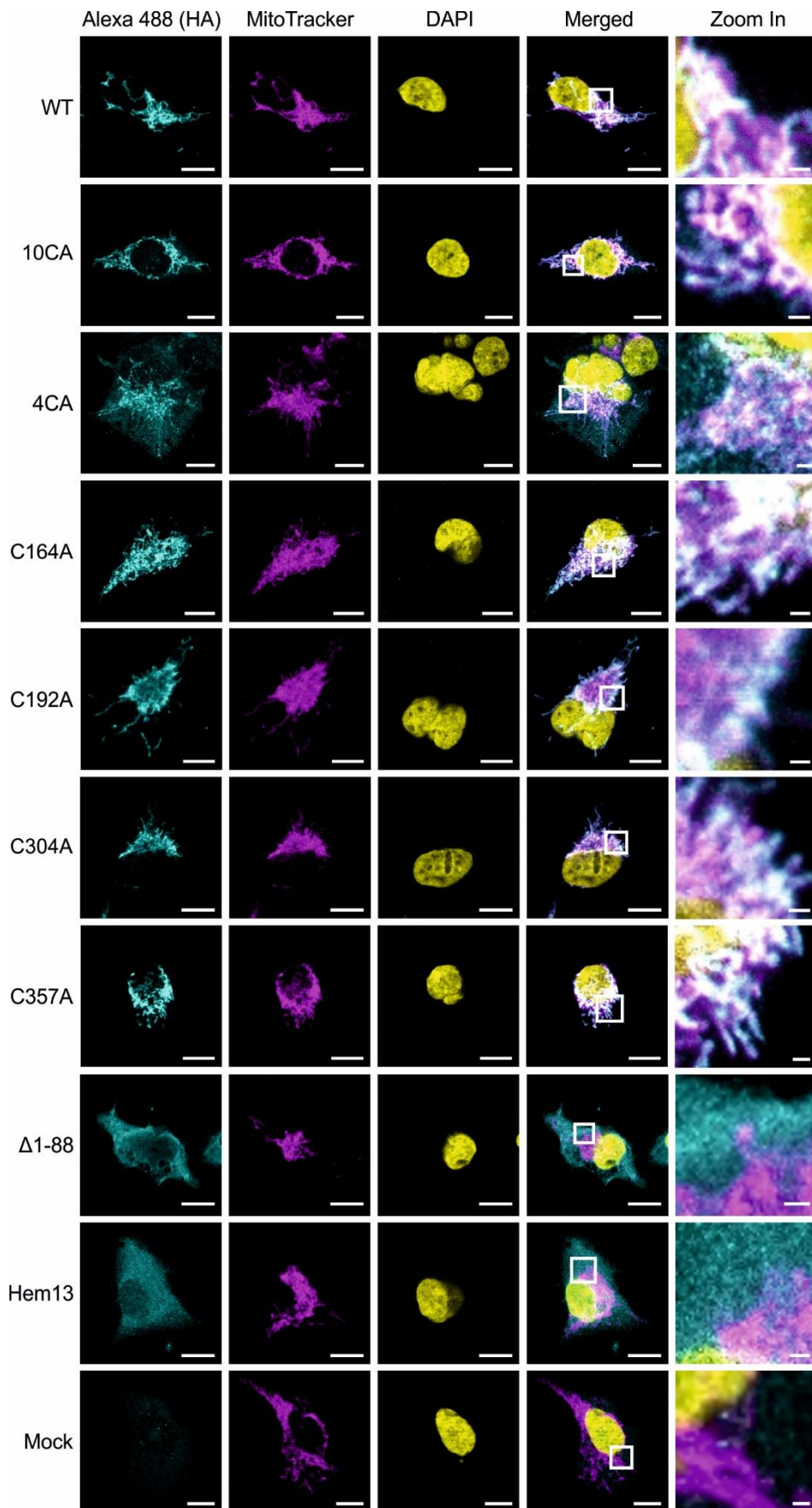


Figure S 2: Localization of CPOX-HA variants used in the course of this thesis

CPOX-HA constructs were stained with Alexa 488 (cyan, lane 1). Mitochondria were stained with MitoTracker™ Deep Red (magenta, lane 2). Nuclei were stained with DAPI (yellow, lane 3).

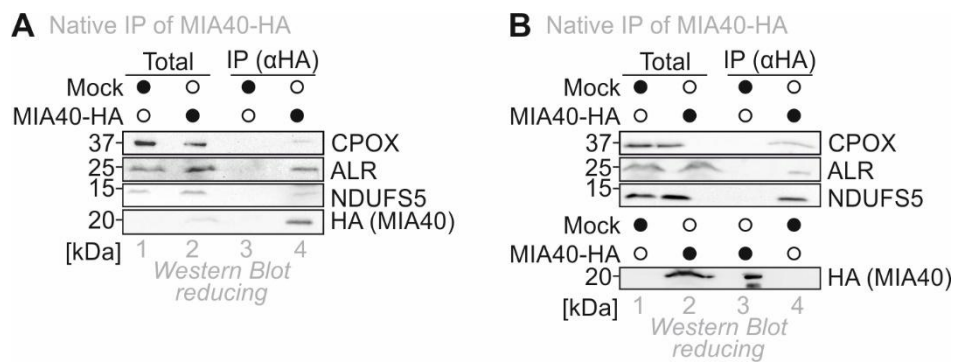
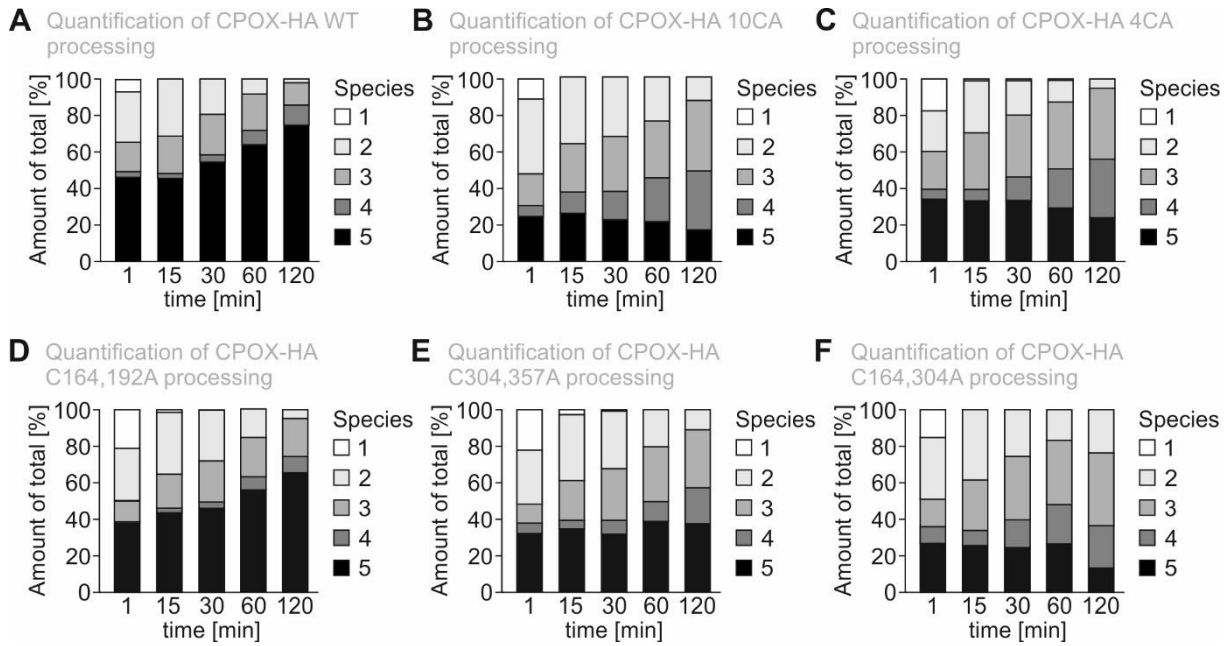


Figure S 3: MIA40 interacts with CPOX

**A, B** Native IPs of MIA40-HA showing its interaction with CPOX. ALR and NDUFS5 are positive controls.

## Appendix



*Figure S 4: CPOX variants lacking the C304-C357 cysteine pair are processed more slowly*

In pulse chase experiments, processing of CPOX-HA variants was followed over 1 to 120 minutes. Processing intermediates were quantified. **A** CPOX-HA WT (n=6). **B** CPOX-HA 10CA (n=2). **C** CPOX-HA 4CA (n=3). **D** CPOX-HA C164,192A (n=3). **E** CPOX-HA C304,357A (n=3). **F** CPOX-HA C164,304A (n=2).

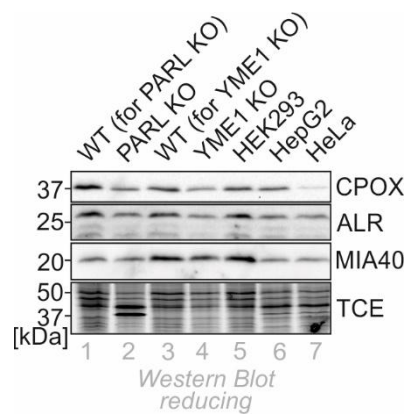


*Figure S 5: CPOX is unchanged in PARL and YME1 KO cells*

Lysates from different cell lines were subjected to Western blot analysis to check for CPOX running behavior and levels. ALR was detected as it interacts with CPOX. MIA40 acts as IMS localized loading control and should be unaffected by the KOs. TCE staining acts as another loading control.

## 9. References

1. Spinelli, J.B. and M.C. Haigis, *The multifaceted contributions of mitochondria to cellular metabolism*. Nat Cell Biol, 2018. **20**(7): p. 745-754.
2. van der Blik, A.M., M.M. Sedensky, and P.G. Morgan, *Cell Biology of the Mitochondrion*. Genetics, 2017. **207**(3): p. 843-871.
3. Lill, R., *Function and biogenesis of iron-sulphur proteins*. Nature, 2009. **460**(7257): p. 831-8.
4. Rhee, H.W., et al., *Proteomic mapping of mitochondria in living cells via spatially restricted enzymatic tagging*. Science, 2013. **339**(6125): p. 1328-1331.
5. Koreny, L., et al., *The convoluted history of haem biosynthesis*. Biol Rev Camb Philos Soc, 2022. **97**(1): p. 141-162.
6. Matuz-Mares, D., et al., *Mitochondrial Calcium: Effects of Its Imbalance in Disease*. Antioxidants (Basel), 2022. **11**(5).
7. Dietz, J.V., J.L. Fox, and O. Khalimonchuk, *Down the Iron Path: Mitochondrial Iron Homeostasis and Beyond*. Cells, 2021. **10**(9).
8. Garza, N.M., et al., *Mitochondrial copper in human genetic disorders*. Trends Endocrinol Metab, 2023. **34**(1): p. 21-33.
9. Wang, X., et al., *Mitochondrial Metal Ion Transport in Cell Metabolism and Disease*. Int J Mol Sci, 2021. **22**(14).
10. Chakrabarty, R.P. and N.S. Chandel, *Mitochondria as Signaling Organelles Control Mammalian Stem Cell Fate*. Cell Stem Cell, 2021. **28**(3): p. 394-408.
11. Pfanner, N., B. Warscheid, and N. Wiedemann, *Mitochondrial proteins: from biogenesis to functional networks*. Nat Rev Mol Cell Biol, 2019. **20**(5): p. 267-284.
12. Dadsena, S., L.E. King, and A.J. Garcia-Saez, *Apoptosis regulation at the mitochondria membrane level*. Biochim Biophys Acta Biomembr, 2021. **1863**(12): p. 183716.
13. Morgenstern, M., et al., *Quantitative high-confidence human mitochondrial proteome and its dynamics in cellular context*. Cell Metab, 2021. **33**(12): p. 2464-2483 e18.
14. Hoehne, M.N., et al., *Spatial and temporal control of mitochondrial H(2) O(2) release in intact human cells*. EMBO J, 2022. **41**(7): p. e109169.
15. Schulz, H., *Beta oxidation of fatty acids*. Biochim Biophys Acta, 1991. **1081**(2): p. 109-20.
16. Martinez-Reyes, I. and N.S. Chandel, *Mitochondrial TCA cycle metabolites control physiology and disease*. Nat Commun, 2020. **11**(1): p. 102.
17. McKay, R., et al., *Intramitochondrial localization of delta-aminolaevulate synthetase and ferrochelatase in rat liver*. Biochem J, 1969. **114**(3): p. 455-61.
18. Ferreira, G.C., *Ferrochelatase*. Int J Biochem Cell Biol, 1999. **31**(10): p. 995-1000.
19. Colombini, M., *Mitochondrial outer membrane channels*. Chem Rev, 2012. **112**(12): p. 6373-87.
20. Kruger, V., et al., *Identification of new channels by systematic analysis of the mitochondrial outer membrane*. J Cell Biol, 2017. **216**(11): p. 3485-3495.
21. Ferramosca, A. and V. Zara, *Mitochondrial Carriers and Substrates Transport Network: A Lesson from Saccharomyces cerevisiae*. Int J Mol Sci, 2021. **22**(16).
22. Palmieri, F., *The mitochondrial transporter family SLC25: identification, properties and physiopathology*. Mol Aspects Med, 2013. **34**(2-3): p. 465-84.
23. Huynen, M.A., et al., *Evolution and structural organization of the mitochondrial contact site (MICOS) complex and the mitochondrial intermembrane space bridging (MIB) complex*. Biochim Biophys Acta, 2016. **1863**(1): p. 91-101.
24. Stephan, T., et al., *MICOS assembly controls mitochondrial inner membrane remodeling and crista junction redistribution to mediate cristae formation*. EMBO J, 2020. **39**(14): p. e104105.
25. Fry, M.Y., et al., *In situ architecture of Opa1-dependent mitochondrial cristae remodeling*. EMBO J, 2024. **43**(3): p. 391-413.
26. Cogliati, S., et al., *Mitochondrial cristae shape determines respiratory chain supercomplexes assembly and respiratory efficiency*. Cell, 2013. **155**(1): p. 160-71.

27. Herrmann, J.M. and J. Riemer, *The intermembrane space of mitochondria*. Antioxid Redox Signal, 2010. **13**(9): p. 1341-58.
28. Zhang, Y., et al., *Uridine Metabolism and Its Role in Glucose, Lipid, and Amino Acid Homeostasis*. Biomed Res Int, 2020. **2020**: p. 7091718.
29. Jacobs, L. and J. Riemer, *Maintenance of small molecule redox homeostasis in mitochondria*. FEBS Lett, 2023. **597**(2): p. 205-223.
30. den Brave, F., et al., *Mitochondrial complexome and import network*. Trends Cell Biol, 2024. **34**(7): p. 578-594.
31. von Heijne, G., *Mitochondrial targeting sequences may form amphiphilic helices*. EMBO J, 1986. **5**(6): p. 1335-42.
32. Habib, S.J., W. Neupert, and D. Rapaport, *Analysis and prediction of mitochondrial targeting signals*. Methods Cell Biol, 2007. **80**: p. 761-81.
33. Hartl, F.U., et al., *Successive translocation into and out of the mitochondrial matrix: targeting of proteins to the intermembrane space by a bipartite signal peptide*. Cell, 1987. **51**(6): p. 1027-37.
34. Araiso, Y., et al., *Structure of the mitochondrial import gate reveals distinct preprotein paths*. Nature, 2019. **575**(7782): p. 395-401.
35. Lesnik, C., et al., *OM14 is a mitochondrial receptor for cytosolic ribosomes that supports co-translational import into mitochondria*. Nat Commun, 2014. **5**: p. 5711.
36. Gold, V.A., et al., *Visualization of cytosolic ribosomes on the surface of mitochondria by electron cryo-tomography*. EMBO Rep, 2017. **18**(10): p. 1786-1800.
37. Young, J.C., N.J. Hoogenraad, and F.U. Hartl, *Molecular chaperones Hsp90 and Hsp70 deliver preproteins to the mitochondrial import receptor Tom70*. Cell, 2003. **112**(1): p. 41-50.
38. Backes, S., et al., *The chaperone-binding activity of the mitochondrial surface receptor Tom70 protects the cytosol against mitoprotein-induced stress*. Cell Rep, 2021. **35**(1): p. 108936.
39. Meinecke, M., et al., *Tim50 maintains the permeability barrier of the mitochondrial inner membrane*. Science, 2006. **312**(5779): p. 1523-6.
40. Lytovchenko, O., et al., *Signal recognition initiates reorganization of the presequence translocase during protein import*. EMBO J, 2013. **32**(6): p. 886-98.
41. Sim, S.I., et al., *Structural basis of mitochondrial protein import by the TIM23 complex*. Nature, 2023. **621**(7979): p. 620-626.
42. Maruszczak, K.K., et al., *Structure prediction analysis of human core TIM23 complex reveals conservation of the protein translocation mechanism*. FEBS Open Bio, 2024.
43. Caumont-Sarcos, A., et al., *Transmembrane Coordination of Preprotein Recognition and Motor Coupling by the Mitochondrial Presequence Receptor Tim50*. Cell Rep, 2020. **30**(9): p. 3092-3104 e4.
44. Richter, F., et al., *ROMO1 is a constituent of the human presequence translocase required for YME1L protease import*. J Cell Biol, 2019. **218**(2): p. 598-614.
45. Zhou, X., et al., *Molecular pathway of mitochondrial preprotein import through the TOM-TIM23 supercomplex*. Nat Struct Mol Biol, 2023. **30**(12): p. 1996-2008.
46. Ieva, R., et al., *Mgr2 functions as lateral gatekeeper for preprotein sorting in the mitochondrial inner membrane*. Mol Cell, 2014. **56**(5): p. 641-52.
47. Matta, S.K., A. Kumar, and P. D'Silva, *Mgr2 regulates mitochondrial preprotein import by associating with channel-forming Tim23 subunit*. Mol Biol Cell, 2020. **31**(11): p. 1112-1123.
48. Dvorakova-Hola, K., et al., *Glycine-rich loop of mitochondrial processing peptidase alpha-subunit is responsible for substrate recognition by a mechanism analogous to mitochondrial receptor Tom20*. J Mol Biol, 2010. **396**(5): p. 1197-210.
49. Taylor, A.B., et al., *Crystal structures of mitochondrial processing peptidase reveal the mode for specific cleavage of import signal sequences*. Structure, 2001. **9**(7): p. 615-25.
50. Herrmann, J.M. and K. Hell, *Chopped, trapped or tacked--protein translocation into the IMS of mitochondria*. Trends Biochem Sci, 2005. **30**(4): p. 205-11.

## References

51. Jan, P.S., et al., *Som1, a third component of the yeast mitochondrial inner membrane peptidase complex that contains Imp1 and Imp2*. Mol Gen Genet, 2000. **263**(3): p. 483-91.
52. Burri, L., et al., *Mature DIABLO/Smac is produced by the IMP protease complex on the mitochondrial inner membrane*. Mol Biol Cell, 2005. **16**(6): p. 2926-33.
53. Gakh, O., P. Cavadini, and G. Isaya, *Mitochondrial processing peptidases*. Biochim Biophys Acta, 2002. **1592**(1): p. 63-77.
54. Esser, K., et al., *The mitochondrial IMP peptidase of yeast: functional analysis of domains and identification of Gut2 as a new natural substrate*. Mol Genet Genomics, 2004. **271**(5): p. 616-26.
55. Ieva, R., et al., *Mitochondrial inner membrane protease promotes assembly of presequence translocase by removing a carboxy-terminal targeting sequence*. Nat Commun, 2013. **4**: p. 2853.
56. Luo, W., H. Fang, and N. Green, *Substrate specificity of inner membrane peptidase in yeast mitochondria*. Mol Genet Genomics, 2006. **275**(5): p. 431-6.
57. Chen, X., et al., *Signal peptides having standard and nonstandard cleavage sites can be processed by Imp1p of the mitochondrial inner membrane protease*. J Biol Chem, 1999. **274**(53): p. 37750-4.
58. Gomes, F., et al., *Proteolytic cleavage by the inner membrane peptidase (IMP) complex or Oct1 peptidase controls the localization of the yeast peroxiredoxin Prx1 to distinct mitochondrial compartments*. J Biol Chem, 2017. **292**(41): p. 17011-17024.
59. Nunnari, J., T.D. Fox, and P. Walter, *A mitochondrial protease with two catalytic subunits of nonoverlapping specificities*. Science, 1993. **262**(5142): p. 1997-2004.
60. Lu, B., et al., *A mutation in the inner mitochondrial membrane peptidase 2-like gene (Impmp2l) affects mitochondrial function and impairs fertility in mice*. Biol Reprod, 2008. **78**(4): p. 601-10.
61. Bharadwaj, M.S., et al., *Examination of bioenergetic function in the inner mitochondrial membrane peptidase 2-like (Impmp2l) mutant mice*. Redox Biol, 2014. **2**: p. 1008-15.
62. McQuibban, G.A., S. Saurya, and M. Freeman, *Mitochondrial membrane remodelling regulated by a conserved rhomboid protease*. Nature, 2003. **423**(6939): p. 537-41.
63. Jeyaraju, D.V., et al., *Structural and mechanistic basis of Parl activity and regulation*. Cell Death Differ, 2011. **18**(9): p. 1531-9.
64. Meissner, C., et al., *The mitochondrial intramembrane protease PARL cleaves human Pink1 to regulate Pink1 trafficking*. J Neurochem, 2011. **117**(5): p. 856-67.
65. Saita, S., et al., *PARL mediates Smac proteolytic maturation in mitochondria to promote apoptosis*. Nat Cell Biol, 2017. **19**(4): p. 318-328.
66. Saita, S., et al., *PARL partitions the lipid transfer protein STARD7 between the cytosol and mitochondria*. EMBO J, 2018. **37**(4).
67. Chao, J.R., et al., *Hax1-mediated processing of HtrA2 by Parl allows survival of lymphocytes and neurons*. Nature, 2008. **452**(7183): p. 98-102.
68. Lysyk, L., et al., *Insights into the catalytic properties of the mitochondrial rhomboid protease PARL*. J Biol Chem, 2021. **296**: p. 100383.
69. Wai, T., et al., *The membrane scaffold SLP2 anchors a proteolytic hub in mitochondria containing PARL and the i-AAA protease YME1L*. EMBO Rep, 2016. **17**(12): p. 1844-1856.
70. Gerdes, F., T. Tatsuta, and T. Langer, *Mitochondrial AAA proteases--towards a molecular understanding of membrane-bound proteolytic machines*. Biochim Biophys Acta, 2012. **1823**(1): p. 49-55.
71. Atorino, L., et al., *Loss of m-AAA protease in mitochondria causes complex I deficiency and increased sensitivity to oxidative stress in hereditary spastic paraplegia*. J Cell Biol, 2003. **163**(4): p. 777-87.
72. Duvezin-Caubet, S., et al., *OPA1 processing reconstituted in yeast depends on the subunit composition of the m-AAA protease in mitochondria*. Mol Biol Cell, 2007. **18**(9): p. 3582-90.

73. Esser, K., et al., *A novel two-step mechanism for removal of a mitochondrial signal sequence involves the mAAA complex and the putative rhomboid protease Pcp1*. J Mol Biol, 2002. **323**(5): p. 835-43.
74. Ishihara, N., et al., *Regulation of mitochondrial morphology through proteolytic cleavage of OPA1*. EMBO J, 2006. **25**(13): p. 2966-77.
75. Tatsuta, T., et al., *m-AAA protease-driven membrane dislocation allows intramembrane cleavage by rhomboid in mitochondria*. EMBO J, 2007. **26**(2): p. 325-35.
76. Rainey, R.N., et al., *A new function in translocation for the mitochondrial i-AAA protease Yme1: import of polynucleotide phosphorylase into the intermembrane space*. Mol Cell Biol, 2006. **26**(22): p. 8488-97.
77. Finger, Y. and J. Riemer, *Protein import by the mitochondrial disulfide relay in higher eukaryotes*. Biol Chem, 2020. **401**(6-7): p. 749-763.
78. Arnesano, F., et al., *Folding studies of Cox17 reveal an important interplay of cysteine oxidation and copper binding*. Structure, 2005. **13**(5): p. 713-22.
79. Longen, S., et al., *Systematic analysis of the twin cx(9)c protein family*. J Mol Biol, 2009. **393**(2): p. 356-68.
80. Chang, H.C., et al., *Augmenter of liver regeneration regulates cellular iron homeostasis by modulating mitochondrial transport of ATP-binding cassette B8*. Elife, 2021. **10**.
81. Petrunaro, C., et al., *The Ca(2+)-Dependent Release of the Mia40-Induced MICU1-MICU2 Dimer from MCU Regulates Mitochondrial Ca(2+) Uptake*. Cell Metab, 2015. **22**(4): p. 721-33.
82. Weckbecker, D., et al., *Atp23 biogenesis reveals a chaperone-like folding activity of Mia40 in the IMS of mitochondria*. EMBO J, 2012. **31**(22): p. 4348-58.
83. Morgenstern, M., et al., *Definition of a High-Confidence Mitochondrial Proteome at Quantitative Scale*. Cell Rep, 2017. **19**(13): p. 2836-2852.
84. Hangen, E., et al., *Interaction between AIF and CHCHD4 Regulates Respiratory Chain Biogenesis*. Mol Cell, 2015. **58**(6): p. 1001-14.
85. Fass, D., *Disulfide bonding in protein biophysics*. Annu Rev Biophys, 2012. **41**: p. 63-79.
86. Daithankar, V.N., et al., *Structure of the human sulfhydryl oxidase augmenter of liver regeneration and characterization of a human mutation causing an autosomal recessive myopathy*. Biochemistry, 2010. **49**(31): p. 6737-45.
87. Weiss, K.R., J.; Riemer, J., *Chapter 15 - Compartmentalized disulfide bond formation pathways*, in *Redox Chemistry and Biology of Thiols*, M.A.C. Beatriz Alvarez, Gustavo Salinas, Madia Trujillo, Editor. 2022, Academic Press. p. 321 - 340.
88. Hoseini, H., et al., *The cytosolic cochaperone Sti1 is relevant for mitochondrial biogenesis and morphology*. FEBS J, 2016. **283**(18): p. 3338-52.
89. Jores, T., et al., *Cytosolic Hsp70 and Hsp40 chaperones enable the biogenesis of mitochondrial beta-barrel proteins*. J Cell Biol, 2018. **217**(9): p. 3091-3108.
90. Banci, L., et al., *Molecular chaperone function of Mia40 triggers consecutive induced folding steps of the substrate in mitochondrial protein import*. Proc Natl Acad Sci U S A, 2010. **107**(47): p. 20190-5.
91. Banci, L., et al., *MIA40 is an oxidoreductase that catalyzes oxidative protein folding in mitochondria*. Nat Struct Mol Biol, 2009. **16**(2): p. 198-206.
92. Naoe, M., et al., *Identification of Tim40 that mediates protein sorting to the mitochondrial intermembrane space*. J Biol Chem, 2004. **279**(46): p. 47815-21.
93. Reinhardt, C., et al., *AIF meets the CHCHD4/Mia40-dependent mitochondrial import pathway*. Biochim Biophys Acta Mol Basis Dis, 2020. **1866**(6): p. 165746.
94. Salscheider, S.L., et al., *AIFM1 is a component of the mitochondrial disulfide relay that drives complex I assembly through efficient import of NDUFS5*. EMBO J, 2022. **41**(17): p. e110784.
95. Sideris, D.P., et al., *A novel intermembrane space-targeting signal docks cysteines onto Mia40 during mitochondrial oxidative folding*. J Cell Biol, 2009. **187**(7): p. 1007-22.

## References

96. Peleh, V., E. Cordat, and J.M. Herrmann, *Mia40 is a trans-site receptor that drives protein import into the mitochondrial intermembrane space by hydrophobic substrate binding*. *Elife*, 2016. **5**.
97. Koch, J.R. and F.X. Schmid, *Mia40 targets cysteines in a hydrophobic environment to direct oxidative protein folding in the mitochondria*. *Nat Commun*, 2014. **5**: p. 3041.
98. Habich, M., et al., *Vectorial Import via a Metastable Disulfide-Linked Complex Allows for a Quality Control Step and Import by the Mitochondrial Disulfide Relay*. *Cell Rep*, 2019. **26**(3): p. 759-774 e5.
99. Herrmann, J.M. and R. Kohl, *Catch me if you can! Oxidative protein trapping in the intermembrane space of mitochondria*. *J Cell Biol*, 2007. **176**(5): p. 559-63.
100. Erdogan, A.J., et al., *The mitochondrial oxidoreductase CHCHD4 is present in a semi-oxidized state in vivo*. *Redox Biol*, 2018. **17**: p. 200-206.
101. Bien, M., et al., *Mitochondrial disulfide bond formation is driven by intersubunit electron transfer in Erv1 and proofread by glutathione*. *Mol Cell*, 2010. **37**(4): p. 516-28.
102. Schaefer-Ramadan, S., S.A. Gannon, and C. Thorpe, *Human augmenter of liver regeneration: probing the catalytic mechanism of a flavin-dependent sulfhydryl oxidase*. *Biochemistry*, 2013. **52**(46): p. 8323-32.
103. Peker, E., et al., *Erv1 and Cytochrome c Mediate Rapid Electron Transfer via A Collision-Type Interaction*. *J Mol Biol*, 2021. **433**(15): p. 167045.
104. Bihlmaier, K., et al., *The disulfide relay system of mitochondria is connected to the respiratory chain*. *J Cell Biol*, 2007. **179**(3): p. 389-95.
105. Farrell, S.R. and C. Thorpe, *Augmenter of liver regeneration: a flavin-dependent sulfhydryl oxidase with cytochrome c reductase activity*. *Biochemistry*, 2005. **44**(5): p. 1532-41.
106. Daithankar, V.N., S.R. Farrell, and C. Thorpe, *Augmenter of liver regeneration: substrate specificity of a flavin-dependent oxidoreductase from the mitochondrial intermembrane space*. *Biochemistry*, 2009. **48**(22): p. 4828-37.
107. Banci, L., et al., *Molecular recognition and substrate mimicry drive the electron-transfer process between MIA40 and ALR*. *Proc Natl Acad Sci U S A*, 2011. **108**(12): p. 4811-6.
108. Banci, L., et al., *An electron-transfer path through an extended disulfide relay system: the case of the redox protein ALR*. *J Am Chem Soc*, 2012. **134**(3): p. 1442-5.
109. Neal, S.E., et al., *Osm1 facilitates the transfer of electrons from Erv1 to fumarate in the redox-regulated import pathway in the mitochondrial intermembrane space*. *Mol Biol Cell*, 2017. **28**(21): p. 2773-2785.
110. Murschall, L.M., et al., *The C-terminal region of the oxidoreductase MIA40 stabilizes its cytosolic precursor during mitochondrial import*. *BMC Biol*, 2020. **18**(1): p. 96.
111. Dumont, M.E., J.F. Ernst, and F. Sherman, *Coupling of heme attachment to import of cytochrome c into yeast mitochondria. Studies with heme lyase-deficient mitochondria and altered apocytochromes c*. *J Biol Chem*, 1988. **263**(31): p. 15928-37.
112. Lill, R., et al., *Import of cytochrome c heme lyase into mitochondria: a novel pathway into the intermembrane space*. *EMBO J*, 1992. **11**(2): p. 449-56.
113. Allen, J.W., M.L. Ginger, and S.J. Ferguson, *Complexity and diversity in c-type cytochrome biogenesis systems*. *Biochem Soc Trans*, 2005. **33**(Pt 1): p. 145-6.
114. Diekert, K., et al., *Apocytochrome c requires the TOM complex for translocation across the mitochondrial outer membrane*. *EMBO J*, 2001. **20**(20): p. 5626-35.
115. Kawamata, H. and G. Manfredi, *Different regulation of wild-type and mutant Cu,Zn superoxide dismutase localization in mammalian mitochondria*. *Hum Mol Genet*, 2008. **17**(21): p. 3303-17.
116. Kawamata, H. and G. Manfredi, *Import, maturation, and function of SOD1 and its copper chaperone CCS in the mitochondrial intermembrane space*. *Antioxid Redox Signal*, 2010. **13**(9): p. 1375-84.
117. Suzuki, Y., et al., *Human copper chaperone for superoxide dismutase 1 mediates its own oxidation-dependent import into mitochondria*. *Nat Commun*, 2013. **4**: p. 2430.

118. Takeda, H., et al., *A multipoint guidance mechanism for beta-barrel folding on the SAM complex*. Nat Struct Mol Biol, 2023. **30**(2): p. 176-187.
119. Hohr, A.I., et al., *Assembly of beta-barrel proteins in the mitochondrial outer membrane*. Biochim Biophys Acta, 2015. **1853**(1): p. 74-88.
120. Kovermann, P., et al., *Tim22, the essential core of the mitochondrial protein insertion complex, forms a voltage-activated and signal-gated channel*. Mol Cell, 2002. **9**(2): p. 363-73.
121. Kizmaz, B., et al., *Protein insertion into the inner membrane of mitochondria: routes and mechanisms*. FEBS Open Bio, 2024. **14**(10): p. 1627-1639.
122. Curran, S.P., et al., *The role of the Tim8p-Tim13p complex in a conserved import pathway for mitochondrial polytopic inner membrane proteins*. J Cell Biol, 2002. **158**(6): p. 1017-27.
123. Vial, S., et al., *Assembly of Tim9 and Tim10 into a functional chaperone*. J Biol Chem, 2002. **277**(39): p. 36100-8.
124. Weinhaupl, K., et al., *Structural Basis of Membrane Protein Chaperoning through the Mitochondrial Intermembrane Space*. Cell, 2018. **175**(5): p. 1365-1379 e25.
125. Leonhard, K., et al., *Chaperone-like activity of the AAA domain of the yeast Yme1 AAA protease*. Nature, 1999. **398**(6725): p. 348-51.
126. Schreiner, B., et al., *Role of the AAA protease Yme1 in folding of proteins in the intermembrane space of mitochondria*. Mol Biol Cell, 2012. **23**(22): p. 4335-46.
127. Baker, M.J., et al., *Impaired folding of the mitochondrial small TIM chaperones induces clearance by the i-AAA protease*. J Mol Biol, 2012. **424**(5): p. 227-39.
128. Osman, C., et al., *Prohibitins interact genetically with Atp23, a novel processing peptidase and chaperone for the F1Fo-ATP synthase*. Mol Biol Cell, 2007. **18**(2): p. 627-35.
129. Plun-Favreau, H., et al., *Htra2 deficiency causes mitochondrial uncoupling through the F(1)F(0)-ATP synthase and consequent ATP depletion*. Cell Death Dis, 2012. **3**(6): p. e335.
130. Clausen, T., et al., *HTRA proteases: regulated proteolysis in protein quality control*. Nat Rev Mol Cell Biol, 2011. **12**(3): p. 152-62.
131. Vercellino, I. and L.A. Sazanov, *The assembly, regulation and function of the mitochondrial respiratory chain*. Nat Rev Mol Cell Biol, 2022. **23**(2): p. 141-161.
132. Guerrero-Castillo, S., et al., *The Assembly Pathway of Mitochondrial Respiratory Chain Complex I*. Cell Metab, 2017. **25**(1): p. 128-139.
133. Mukherjee, S. and A. Ghosh, *Molecular mechanism of mitochondrial respiratory chain assembly and its relation to mitochondrial diseases*. Mitochondrion, 2020. **53**: p. 1-20.
134. Kozjak-Pavlovic, V., *The MICOS complex of human mitochondria*. Cell Tissue Res, 2017. **367**(1): p. 83-93.
135. Rostovtseva, T. and M. Colombini, *ATP flux is controlled by a voltage-gated channel from the mitochondrial outer membrane*. J Biol Chem, 1996. **271**(45): p. 28006-8.
136. Rostovtseva, T. and M. Colombini, *VDAC channels mediate and gate the flow of ATP: implications for the regulation of mitochondrial function*. Biophys J, 1997. **72**(5): p. 1954-62.
137. Krishnamurthy, P.C., et al., *Identification of a mammalian mitochondrial porphyrin transporter*. Nature, 2006. **443**(7111): p. 586-9.
138. Chiabrando, D., et al., *The mitochondrial heme exporter FLVCR1b mediates erythroid differentiation*. J Clin Invest, 2012. **122**(12): p. 4569-79.
139. Pasquadibisceglie, A., et al., *Membrane Transporters Involved in Iron Trafficking: Physiological and Pathological Aspects*. Biomolecules, 2023. **13**(8).
140. Ruprecht, J.J. and E.R.S. Kunji, *The SLC25 Mitochondrial Carrier Family: Structure and Mechanism*. Trends Biochem Sci, 2020. **45**(3): p. 244-258.
141. Hewton, K.G., A.S. Johal, and S.J. Parker, *Transporters at the Interface between Cytosolic and Mitochondrial Amino Acid Metabolism*. Metabolites, 2021. **11**(2).
142. Borst, P., *The malate-aspartate shuttle (Borst cycle): How it started and developed into a major metabolic pathway*. IUBMB Life, 2020. **72**(11): p. 2241-2259.
143. Cobine, P.A., F. Pierrel, and D.R. Winge, *Copper trafficking to the mitochondrion and assembly of copper metalloenzymes*. Biochim Biophys Acta, 2006. **1763**(7): p. 759-72.

## References

144. Shaw, G.C., et al., *Mitoferrin is essential for erythroid iron assimilation*. *Nature*, 2006. **440**(7080): p. 96-100.
145. Paradkar, P.N., et al., *Regulation of mitochondrial iron import through differential turnover of mitoferrin 1 and mitoferrin 2*. *Mol Cell Biol*, 2009. **29**(4): p. 1007-16.
146. Li, P., et al., *Structures of Atm1 provide insight into [2Fe-2S] cluster export from mitochondria*. *Nat Commun*, 2022. **13**(1): p. 4339.
147. Pandey, A.K., et al., *Mitochondria export iron-sulfur and sulfur intermediates to the cytoplasm for iron-sulfur cluster assembly and tRNA thiolation in yeast*. *J Biol Chem*, 2019. **294**(24): p. 9489-9502.
148. Swenson, S.A., et al., *From Synthesis to Utilization: The Ins and Outs of Mitochondrial Heme*. *Cells*, 2020. **9**(3).
149. Tatsuta, T. and T. Langer, *Intramitochondrial phospholipid trafficking*. *Biochim Biophys Acta Mol Cell Biol Lipids*, 2017. **1862**(1): p. 81-89.
150. Tatsuta, T., M. Scharwey, and T. Langer, *Mitochondrial lipid trafficking*. *Trends Cell Biol*, 2014. **24**(1): p. 44-52.
151. Del Arco, A., et al., *Calcium regulation of mitochondrial carriers*. *Biochim Biophys Acta*, 2016. **1863**(10): p. 2413-21.
152. Garbincius, J.F. and J.W. Elrod, *Mitochondrial calcium exchange in physiology and disease*. *Physiol Rev*, 2022. **102**(2): p. 893-992.
153. Green, D.R. and F. Llambi, *Cell Death Signaling*. *Cold Spring Harb Perspect Biol*, 2015. **7**(12).
154. Scorrano, L., et al., *A distinct pathway remodels mitochondrial cristae and mobilizes cytochrome c during apoptosis*. *Dev Cell*, 2002. **2**(1): p. 55-67.
155. Burke, P.J., *Mitochondria, Bioenergetics and Apoptosis in Cancer*. *Trends Cancer*, 2017. **3**(12): p. 857-870.
156. Case, A.J., et al., *Mitochondrial-localized NADPH oxidase 4 is a source of superoxide in angiotensin II-stimulated neurons*. *Am J Physiol Heart Circ Physiol*, 2013. **305**(1): p. H19-28.
157. Shanmugasundaram, K., et al., *NOX4 functions as a mitochondrial energetic sensor coupling cancer metabolic reprogramming to drug resistance*. *Nat Commun*, 2017. **8**(1): p. 997.
158. Kaludercic, N., et al., *Monoamine oxidases as sources of oxidants in the heart*. *J Mol Cell Cardiol*, 2014. **73**: p. 34-42.
159. Giorgio, M., et al., *Electron transfer between cytochrome c and p66Shc generates reactive oxygen species that trigger mitochondrial apoptosis*. *Cell*, 2005. **122**(2): p. 221-33.
160. Dailey, H.A., *Terminal steps of haem biosynthesis*. *Biochem Soc Trans*, 2002. **30**(4): p. 590-5.
161. Shadel, G.S. and T.L. Horvath, *Mitochondrial ROS signaling in organismal homeostasis*. *Cell*, 2015. **163**(3): p. 560-9.
162. Godon, C., et al., *The H<sub>2</sub>O<sub>2</sub> stimulon in *Saccharomyces cerevisiae**. *J Biol Chem*, 1998. **273**(35): p. 22480-9.
163. Zhang, L., et al., *Mass spectrometry profiles superoxide-induced intramolecular disulfide in the FMN-binding subunit of mitochondrial Complex I*. *J Am Soc Mass Spectrom*, 2008. **19**(12): p. 1875-86.
164. Habich, M., S.L. Salscheider, and J. Riemer, *Cysteine residues in mitochondrial intermembrane space proteins: more than just import*. *Br J Pharmacol*, 2019. **176**(4): p. 514-531.
165. Mracek, T., Z. Drahotka, and J. Houstek, *The function and the role of the mitochondrial glycerol-3-phosphate dehydrogenase in mammalian tissues*. *Biochim Biophys Acta*, 2013. **1827**(3): p. 401-10.
166. Velayutham, M., et al., *Sulfite Oxidase Activity of Cytochrome c: Role of Hydrogen Peroxide*. *Biochem Biophys Rep*, 2016. **5**: p. 96-104.
167. Kappler, U. and J.H. Enemark, *Sulfite-oxidizing enzymes*. *J Biol Inorg Chem*, 2015. **20**(2): p. 253-64.
168. Dzeja, P. and A. Terzic, *Adenylate kinase and AMP signaling networks: metabolic monitoring, signal communication and body energy sensing*. *Int J Mol Sci*, 2009. **10**(4): p. 1729-1772.

169. Fujisawa, K., *Regulation of Adenine Nucleotide Metabolism by Adenylate Kinase Isozymes: Physiological Roles and Diseases*. Int J Mol Sci, 2023. **24**(6).
170. Wyss, M., et al., *Mitochondrial creatine kinase: a key enzyme of aerobic energy metabolism*. Biochim Biophys Acta, 1992. **1102**(2): p. 119-66.
171. Schlattner, U., M. Tokarska-Schlattner, and T. Wallimann, *Mitochondrial creatine kinase in human health and disease*. Biochim Biophys Acta, 2006. **1762**(2): p. 164-80.
172. Lacombe, M.L., et al., *The mitochondrial nucleoside diphosphate kinase (NDPK-D/NME4), a moonlighting protein for cell homeostasis*. Lab Invest, 2018. **98**(5): p. 582-588.
173. Wyse, A.T.S., et al., *The Role of Oxidative Stress and Bioenergetic Dysfunction in Sulfite Oxidase Deficiency: Insights from Animal Models*. Neurotox Res, 2019. **35**(2): p. 484-494.
174. Zhou, Y., et al., *DHODH and cancer: promising prospects to be explored*. Cancer Metab, 2021. **9**(1): p. 22.
175. Turilli-Ghisolfi, E.S., M. Lualdi, and M. Fasano, *Ligand-Based Regulation of Dynamics and Reactivity of Hemoproteins*. Biomolecules, 2023. **13**(4).
176. Baker, A., et al., *Catalase: A critical node in the regulation of cell fate*. Free Radic Biol Med, 2023. **199**: p. 56-66.
177. Battistuzzi, G., et al., *Redox properties of heme peroxidases*. Arch Biochem Biophys, 2010. **500**(1): p. 21-36.
178. Krol, M. and M. Kepinska, *Human Nitric Oxide Synthase-Its Functions, Polymorphisms, and Inhibitors in the Context of Inflammation, Diabetes and Cardiovascular Diseases*. Int J Mol Sci, 2020. **22**(1).
179. Forstermann, U. and W.C. Sessa, *Nitric oxide synthases: regulation and function*. Eur Heart J, 2012. **33**(7): p. 829-37, 837a-837d.
180. Sun, F., et al., *Crystal structure of mitochondrial respiratory membrane protein complex II*. Cell, 2005. **121**(7): p. 1043-57.
181. Kim, H.J., et al., *Structure, function, and assembly of heme centers in mitochondrial respiratory complexes*. Biochim Biophys Acta, 2012. **1823**(9): p. 1604-16.
182. Formosa, L.E., et al., *Mitochondrial COA7 is a heme-binding protein with disulfide reductase activity, which acts in the early stages of complex IV assembly*. Proc Natl Acad Sci U S A, 2022. **119**(9).
183. Tsiftoglou, A.S., A.I. Tsamadou, and L.C. Papadopoulou, *Heme as key regulator of major mammalian cellular functions: molecular, cellular, and pharmacological aspects*. Pharmacol Ther, 2006. **111**(2): p. 327-45.
184. Mense, S.M. and L. Zhang, *Heme: a versatile signaling molecule controlling the activities of diverse regulators ranging from transcription factors to MAP kinases*. Cell Res, 2006. **16**(8): p. 681-92.
185. Lunetti, P., et al., *Characterization of Human and Yeast Mitochondrial Glycine Carriers with Implications for Heme Biosynthesis and Anemia*. J Biol Chem, 2016. **291**(38): p. 19746-59.
186. Burch, J.S., et al., *Glutamine via alpha-ketoglutarate dehydrogenase provides succinyl-CoA for heme synthesis during erythropoiesis*. Blood, 2018. **132**(10): p. 987-998.
187. Labbe, R.F., T. Kurumada, and J. Onisawa, *The role of succinyl-CoA synthetase in the control of heme biosynthesis*. Biochim Biophys Acta, 1965. **111**(2): p. 403-15.
188. Tchaikovskii, V., R.J. Desnick, and D.F. Bishop, *Molecular expression, characterization and mechanism of ALAS2 gain-of-function mutants*. Mol Med, 2019. **25**(1): p. 4.
189. Braidotti, G., I.A. Borthwick, and B.K. May, *Identification of regulatory sequences in the gene for 5-aminolevulinic acid synthase from rat*. J Biol Chem, 1993. **268**(2): p. 1109-17.
190. Giono, L.E., C.L. Varone, and E.T. Canepa, *5-Aminolevulinic acid synthase gene promoter contains two cAMP-response element (CRE)-like sites that confer positive and negative responsiveness to CRE-binding protein (CREB)*. Biochem J, 2001. **353**(Pt 2): p. 307-16.
191. Li, B., J.O. Holloszy, and C.F. Semenkovich, *Respiratory uncoupling induces delta-aminolevulinic acid synthase expression through a nuclear respiratory factor-1-dependent mechanism in HeLa cells*. J Biol Chem, 1999. **274**(25): p. 17534-40.

## References

192. Scassa, M.E., et al., *Hepatic nuclear factor 3 and nuclear factor 1 regulate 5-aminolevulinic acid synthase gene expression and are involved in insulin repression*. J Biol Chem, 2004. **279**(27): p. 28082-92.
193. Biswas, M. and J.Y. Chan, *Role of Nrf1 in antioxidant response element-mediated gene expression and beyond*. Toxicol Appl Pharmacol, 2010. **244**(1): p. 16-20.
194. Kramer, M.F., P. Gunaratne, and G.C. Ferreira, *Transcriptional regulation of the murine erythroid-specific 5-aminolevulinic acid synthase gene*. Gene, 2000. **247**(1-2): p. 153-66.
195. Cox, T.C., et al., *Human erythroid 5-aminolevulinic acid synthase: promoter analysis and identification of an iron-responsive element in the mRNA*. EMBO J, 1991. **10**(7): p. 1891-902.
196. Bhasker, C.R., et al., *The putative iron-responsive element in the human erythroid 5-aminolevulinic acid synthase mRNA mediates translational control*. J Biol Chem, 1993. **268**(17): p. 12699-705.
197. Melefors, O., et al., *Translational control of 5-aminolevulinic acid synthase mRNA by iron-responsive elements in erythroid cells*. J Biol Chem, 1993. **268**(8): p. 5974-8.
198. May, B.K., et al., *Molecular regulation of heme biosynthesis in higher vertebrates*. Prog Nucleic Acid Res Mol Biol, 1995. **51**: p. 1-51.
199. Yamamoto, M., N. Hayashi, and G. Kikuchi, *Evidence for the transcriptional inhibition by heme of the synthesis of delta-aminolevulinic acid synthase in rat liver*. Biochem Biophys Res Commun, 1982. **105**(3): p. 985-90.
200. Yamamoto, M., N. Hayashi, and G. Kikuchi, *Translational inhibition by heme of the synthesis of hepatic delta-aminolevulinic acid synthase in a cell-free system*. Biochem Biophys Res Commun, 1983. **115**(1): p. 225-31.
201. Peoc'h, K., et al., *Regulation and tissue-specific expression of delta-aminolevulinic acid synthases in non-syndromic sideroblastic anemias and porphyrias*. Mol Genet Metab, 2019. **128**(3): p. 190-197.
202. Dailey, T.A., J.H. Woodruff, and H.A. Dailey, *Examination of mitochondrial protein targeting of haem synthetic enzymes: in vivo identification of three functional haem-responsive motifs in 5-aminolevulinic acid synthase*. Biochem J, 2005. **386**(Pt 2): p. 381-6.
203. Kubota, Y., et al., *Novel Mechanisms for Heme-dependent Degradation of ALAS1 Protein as a Component of Negative Feedback Regulation of Heme Biosynthesis*. J Biol Chem, 2016. **291**(39): p. 20516-29.
204. Tian, Q., et al., *Lon peptidase 1 (LONP1)-dependent breakdown of mitochondrial 5-aminolevulinic acid synthase protein by heme in human liver cells*. J Biol Chem, 2011. **286**(30): p. 26424-30.
205. Rondelli, C.M., et al., *The ubiquitous mitochondrial protein unfoldase CLPX regulates erythroid heme synthesis by control of iron utilization and heme synthesis enzyme activation and turnover*. J Biol Chem, 2021. **297**(2): p. 100972.
206. Yoshino, K., et al., *Haeme-regulated degradation of delta-aminolevulinic acid synthase 1 in rat liver mitochondria*. J Biochem, 2007. **142**(4): p. 453-8.
207. Hayashi, N., M. Terasawa, and G. Kikuchi, *Immunochemical studies of the turnover of delta-aminolevulinic acid synthase in rat liver mitochondria and the effect of hemin on it*. J Biochem, 1980. **88**(4): p. 921-6.
208. Yien, Y.Y. and M. Perfetto, *Regulation of Heme Synthesis by Mitochondrial Homeostasis Proteins*. Front Cell Dev Biol, 2022. **10**: p. 895521.
209. Kardon, J.R., et al., *Mitochondrial ClpX Activates a Key Enzyme for Heme Biosynthesis and Erythropoiesis*. Cell, 2015. **161**(4): p. 858-67.
210. Whittaker, M.M., A. Penmatsa, and J.W. Whittaker, *The Mtm1p carrier and pyridoxal 5'-phosphate cofactor trafficking in yeast mitochondria*. Arch Biochem Biophys, 2015. **568**: p. 64-70.
211. Bayeva, M., et al., *ATP-binding cassette B10 regulates early steps of heme synthesis*. Circ Res, 2013. **113**(3): p. 279-87.

212. Martinez, M., et al., *Stimulation of the human mitochondrial transporter ABCB10 by zinc-mesoporphrin*. PLoS One, 2020. **15**(11): p. e0238754.
213. Nilsson, R., et al., *Discovery of genes essential for heme biosynthesis through large-scale gene expression analysis*. Cell Metab, 2009. **10**(2): p. 119-30.
214. Jaffe, E.K., *The Remarkable Character of Porphobilinogen Synthase*. Acc Chem Res, 2016. **49**(11): p. 2509-2517.
215. Liu, G., et al., *Heme biosynthesis depends on previously unrecognized acquisition of iron-sulfur cofactors in human amino-levulinic acid dehydratase*. Nat Commun, 2020. **11**(1): p. 6310.
216. Phillips, J.D., *Heme biosynthesis and the porphyrias*. Mol Genet Metab, 2019. **128**(3): p. 164-177.
217. Hamza, I. and H.A. Dailey, *One ring to rule them all: trafficking of heme and heme synthesis intermediates in the metazoans*. Biochim Biophys Acta, 2012. **1823**(9): p. 1617-32.
218. Susa, S., et al., *The long, but not the short, presequence of human coproporphyrinogen oxidase is essential for its import and sorting to mitochondria*. Tohoku J Exp Med, 2003. **200**(1): p. 39-45.
219. Delfau-Larue, M.H., P. Martasek, and B. Grandchamp, *Coproporphyrinogen oxidase: gene organization and description of a mutation leading to exon 6 skipping*. Hum Mol Genet, 1994. **3**(8): p. 1325-30.
220. Elder, G.H. and J.O. Evans, *Evidence that the coproporphyrinogen oxidase activity of rat liver is situated in the intermembrane space of mitochondria*. Biochem J, 1978. **172**(2): p. 345-7.
221. Grandchamp, B., N. Phung, and Y. Nordmann, *The mitochondrial localization of coproporphyrinogen III oxidase*. Biochem J, 1978. **176**(1): p. 97-102.
222. Fukuda, Y., et al., *The severity of hereditary porphyria is modulated by the porphyrin exporter and Lan antigen ABCB6*. Nat Commun, 2016. **7**: p. 12353.
223. Ulrich, D.L., et al., *ATP-dependent mitochondrial porphyrin importer ABCB6 protects against phenylhydrazine toxicity*. J Biol Chem, 2012. **287**(16): p. 12679-90.
224. Lash, T.D., et al., *Normal and Abnormal Heme Biosynthesis. 1. Synthesis and Metabolism of Di- and Monocarboxylic Porphyrinogens Related to Coproporphyrinogen-III and Harderoporphyrinogen: A Model for the Active Site of Coproporphyrinogen Oxidase*. The Journal of Organic Chemistry, 1999. **64**(2): p. 464-477.
225. Elder, G.H. and J.O. Evans, *A radiochemical method for the measurement of coproporphyrinogen oxidase and the utilization of substrates other than coproporphyrinogen III by the enzyme from rat liver*. Biochem J, 1978. **169**(1): p. 205-14.
226. Lash, T.D., *The enigma of coproporphyrinogen oxidase: how does this unusual enzyme carry out oxidative decarboxylations to afford vinyl groups?* Bioorg Med Chem Lett, 2005. **15**(20): p. 4506-9.
227. Phillips, J.D., et al., *Crystal structure of the oxygen-dependant coproporphyrinogen oxidase (Hem13p) of Saccharomyces cerevisiae*. J Biol Chem, 2004. **279**(37): p. 38960-8.
228. Lee, D.S., et al., *Structural basis of hereditary coproporphyria*. Proc Natl Acad Sci U S A, 2005. **102**(40): p. 14232-7.
229. Schmitt, C., et al., *Mutations in human CPO gene predict clinical expression of either hepatic hereditary coproporphyria or erythropoietic harderoporphyria*. Hum Mol Genet, 2005. **14**(20): p. 3089-98.
230. Kim, D.H., et al., *The enzyme engineering of mutant homodimer and heterodimer of coproporphyrinogen oxidase contributes to new insight into hereditary coproporphyria and harderoporphyria*. J Biochem, 2013. **154**(6): p. 551-9.
231. Elder, G.H., et al., *Factors determining the sequence of oxidative decarboxylation of the 2- and 4-propionate substituents of coproporphyrinogen III by coproporphyrinogen oxidase in rat liver*. Biochem J, 1978. **169**(1): p. 215-23.
232. Daniel J. Nurco, C.J.M., Timothy P. Forsyth, Marilyn M. Olmstead, and Kevin M. Smith, *Conformational Flexibility in Dodecasubstituted Porphyrins*. Journal of the American Chemical Society 1996. **118** (44): p. 10918-10919.

## References

233. Anand, S., T. Hasan, and E.V. Maytin, *Mechanism of differentiation-enhanced photodynamic therapy for cancer: upregulation of coproporphyrinogen oxidase by C/EBP transcription factors*. *Mol Cancer Ther*, 2013. **12**(8): p. 1638-50.
234. Takahashi, S., et al., *Differential regulation of coproporphyrinogen oxidase gene between erythroid and nonerythroid cells*. *Blood*, 1998. **92**(9): p. 3436-44.
235. Conder, L.H., S.I. Woodard, and H.A. Dailey, *Multiple mechanisms for the regulation of haem synthesis during erythroid cell differentiation. Possible role for coproporphyrinogen oxidase*. *Biochem J*, 1991. **275 ( Pt 2)**(Pt 2): p. 321-6.
236. Amillet, J.M., N. Buisson, and R. Labbe-Bois, *Positive and negative elements involved in the differential regulation by heme and oxygen of the HEM13 gene (coproporphyrinogen oxidase) in Saccharomyces cerevisiae*. *Curr Genet*, 1995. **28**(6): p. 503-11.
237. Zagorec, M. and R. Labbe-Bois, *Negative control of yeast coproporphyrinogen oxidase synthesis by heme and oxygen*. *J Biol Chem*, 1986. **261**(6): p. 2506-9.
238. Susa, S., et al., *Heme inhibits the mitochondrial import of coproporphyrinogen oxidase*. *Blood*, 2002. **100**(13): p. 4678-9.
239. Koch, M., et al., *Crystal structure of protoporphyrinogen IX oxidase: a key enzyme in haem and chlorophyll biosynthesis*. *EMBO J*, 2004. **23**(8): p. 1720-8.
240. Qin, X., et al., *Structural insight into human variegate porphyria disease*. *FASEB J*, 2011. **25**(2): p. 653-64.
241. von und zu Fraunberg, M., T. Nyroen, and R. Kauppinen, *Mitochondrial targeting of normal and mutant protoporphyrinogen oxidase*. *J Biol Chem*, 2003. **278**(15): p. 13376-81.
242. Azuma, M., et al., *Adenine nucleotide translocator transports haem precursors into mitochondria*. *PLoS One*, 2008. **3**(8): p. e3070.
243. Yien, Y.Y., et al., *TMEM14C is required for erythroid mitochondrial heme metabolism*. *J Clin Invest*, 2014. **124**(10): p. 4294-304.
244. Dailey, H.A., et al., *Ferrochelatase at the millennium: structures, mechanisms and [2Fe-2S] clusters*. *Cell Mol Life Sci*, 2000. **57**(13-14): p. 1909-26.
245. Medlock, A., et al., *Substrate interactions with human ferrochelatase*. *Proc Natl Acad Sci U S A*, 2007. **104**(6): p. 1789-93.
246. Hoggins, M., et al., *Direct measurement of metal ion chelation in the active site of human ferrochelatase*. *Biochemistry*, 2007. **46**(27): p. 8121-7.
247. Taketani, S., Y. Adachi, and Y. Nakahashi, *Regulation of the expression of human ferrochelatase by intracellular iron levels*. *Eur J Biochem*, 2000. **267**(15): p. 4685-92.
248. Crooks, D.R., et al., *Posttranslational stability of the heme biosynthetic enzyme ferrochelatase is dependent on iron availability and intact iron-sulfur cluster assembly machinery*. *Blood*, 2010. **115**(4): p. 860-9.
249. Krishnamurthy, P., T. Xie, and J.D. Schuetz, *The role of transporters in cellular heme and porphyrin homeostasis*. *Pharmacol Ther*, 2007. **114**(3): p. 345-58.
250. Taketani, S., et al., *Molecular characterization of a newly identified heme-binding protein induced during differentiation of urine erythroleukemia cells*. *J Biol Chem*, 1998. **273**(47): p. 31388-94.
251. Zylka, M.J. and S.M. Reppert, *Discovery of a putative heme-binding protein family (SOUL/HBP) by two-tissue suppression subtractive hybridization and database searches*. *Brain Res Mol Brain Res*, 1999. **74**(1-2): p. 175-81.
252. Vincent, S.H. and U. Muller-Eberhard, *A protein of the Z class of liver cytosolic proteins in the rat that preferentially binds heme*. *J Biol Chem*, 1985. **260**(27): p. 14521-8.
253. Iwahara, S., et al., *Purification, characterization, and cloning of a heme-binding protein (23 kDa) in rat liver cytosol*. *Biochemistry*, 1995. **34**(41): p. 13398-406.
254. Watanabe, Y., K. Ishimori, and T. Uchida, *Dual role of the active-center cysteine in human peroxiredoxin 1: Peroxidase activity and heme binding*. *Biochem Biophys Res Commun*, 2017. **483**(3): p. 930-935.

255. Chakravarti, R., et al., *GAPDH regulates cellular heme insertion into inducible nitric oxide synthase*. Proc Natl Acad Sci U S A, 2010. **107**(42): p. 18004-9.
256. Sweeny, E.A., et al., *Glyceraldehyde-3-phosphate dehydrogenase is a chaperone that allocates labile heme in cells*. J Biol Chem, 2018. **293**(37): p. 14557-14568.
257. Donegan, R.K., et al., *Handling heme: The mechanisms underlying the movement of heme within and between cells*. Free Radic Biol Med, 2019. **133**: p. 88-100.
258. Gell, D.A., et al., *A novel haem-binding interface in the 22 kDa haem-binding protein p22HBP*. J Mol Biol, 2006. **362**(2): p. 287-97.
259. D'Anneo, A., et al., *Lipid chaperones and associated diseases: a group of chaperonopathies defining a new nosological entity with implications for medical research and practice*. Cell Stress Chaperones, 2020. **25**(6): p. 805-820.
260. Ghosh, K., et al., *Spectroscopic and biochemical characterization of heme binding to yeast Dap1p and mouse PGRMC1p*. Biochemistry, 2005. **44**(50): p. 16729-36.
261. Kaluka, D., et al., *Spectroscopic and mutagenesis studies of human PGRMC1*. Biochemistry, 2015. **54**(8): p. 1638-47.
262. Galmozzi, A., et al., *PGRMC2 is an intracellular haem chaperone critical for adipocyte function*. Nature, 2019. **576**(7785): p. 138-142.
263. Piel, R.B., 3rd, et al., *A Novel Role for Progesterone Receptor Membrane Component 1 (PGRMC1): A Partner and Regulator of Ferrochelatase*. Biochemistry, 2016. **55**(37): p. 5204-17.
264. Medlock, A.E., et al., *Identification of the Mitochondrial Heme Metabolism Complex*. PLoS One, 2015. **10**(8): p. e0135896.
265. Taketani, S., et al., *Involvement of ABC7 in the biosynthesis of heme in erythroid cells: interaction of ABC7 with ferrochelatase*. Blood, 2003. **101**(8): p. 3274-80.
266. Chen, W., H.A. Dailey, and B.H. Paw, *Ferrochelatase forms an oligomeric complex with mitoferrin-1 and Abcb10 for erythroid heme biosynthesis*. Blood, 2010. **116**(4): p. 628-30.
267. Maio, N., et al., *Dimeric ferrochelatase bridges ABCB7 and ABCB10 homodimers in an architecturally defined molecular complex required for heme biosynthesis*. Haematologica, 2019. **104**(9): p. 1756-1767.
268. Piel, R.B., 3rd, H.A. Dailey, Jr., and A.E. Medlock, *The mitochondrial heme metabolon: Insights into the complex(ity) of heme synthesis and distribution*. Mol Genet Metab, 2019. **128**(3): p. 198-203.
269. Dietz, J.V., et al., *Mitochondrial contact site and cristae organizing system (MICOS) machinery supports heme biosynthesis by enabling optimal performance of ferrochelatase*. Redox Biol, 2021. **46**: p. 102125.
270. Karim, Z., et al., *Porphyrias: A 2015 update*. Clin Res Hepatol Gastroenterol, 2015. **39**(4): p. 412-25.
271. Dickey, A.K., R.K. Leaf, and M. Balwani, *Update on the Porphyrias*. Annu Rev Med, 2024. **75**: p. 321-335.
272. Bissell, D.M. and B. Wang, *Acute Hepatic Porphyria*. J Clin Transl Hepatol, 2015. **3**(1): p. 17-26.
273. Stenson, P.D., et al., *Human Gene Mutation Database (HGMD): 2003 update*. Hum Mutat, 2003. **21**(6): p. 577-81.
274. Nordmann, Y., et al., *Harderoporphyria: a variant hereditary coproporphyria*. J Clin Invest, 1983. **72**(3): p. 1139-49.
275. Lamoril, J., et al., *Neonatal hemolytic anemia due to inherited harderoporphyria: clinical characteristics and molecular basis*. Blood, 1998. **91**(4): p. 1453-7.
276. Lamoril, J., et al., *A molecular defect in coproporphyrinogen oxidase gene causing harderoporphyria, a variant form of hereditary coproporphyria*. Hum Mol Genet, 1995. **4**(2): p. 275-8.
277. Grandchamp, B., J. Lamoril, and H. Puy, *Molecular abnormalities of coproporphyrinogen oxidase in patients with hereditary coproporphyria*. J Bioenerg Biomembr, 1995. **27**(2): p. 215-9.

## References

278. Moghe, A., et al., *Harderoporphyria: Case of lifelong photosensitivity associated with compound heterozygous coproporphyrinogen oxidase (CPOX) mutations*. *Mol Genet Metab Rep*, 2019. **19**: p. 100457.
279. Lamoril, J., et al., *Characterization of mutations in the CPO gene in British patients demonstrates absence of genotype-phenotype correlation and identifies relationship between hereditary coproporphyria and harderoporphyria*. *Am J Hum Genet*, 2001. **68**(5): p. 1130-8.
280. Hasanoglu, A., et al., *Harderoporphyria due to homozygosity for coproporphyrinogen oxidase missense mutation H327R*. *J Inher Metab Dis*, 2011. **34**(1): p. 225-31.
281. Rosipal, R., et al., *Systematic analysis of coproporphyrinogen oxidase gene defects in hereditary coproporphyria and mutation update*. *Hum Mutat*, 1999. **13**(1): p. 44-53.
282. Wiman, A., Y. Floderus, and P. Harper, *Two novel mutations and coexistence of the 991C>T and the 1339C>T mutation on a single allele in the coproporphyrinogen oxidase gene in Swedish patients with hereditary coproporphyria*. *J Hum Genet*, 2002. **47**(8): p. 407-12.
283. Conway, A.J., et al., *A mouse model of hereditary coproporphyria identified in an ENU mutagenesis screen*. *Dis Model Mech*, 2017. **10**(8): p. 1005-1013.
284. Mori, M., et al., *Hereditary cataract of the Nakano mouse: Involvement of a hypomorphic mutation in the coproporphyrinogen oxidase gene*. *Exp Eye Res*, 2013. **112**: p. 45-50.
285. Miyasaka, Y., et al., *A novel ENU-induced CpoX mutation causes microcytic hypochromic anemia in mice*. *Exp Anim*, 2022. **71**(4): p. 433-441.
286. Marcerro, J.R., et al., *The immunometabolite itaconate inhibits heme synthesis and remodels cellular metabolism in erythroid precursors*. *Blood Adv*, 2021. **5**(23): p. 4831-4841.
287. Ebert, P.S., et al., *Succinylacetone, a potent inhibitor of heme biosynthesis: effect on cell growth, heme content and delta-aminolevulinic acid dehydratase activity of malignant murine erythroleukemia cells*. *Biochem Biophys Res Commun*, 1979. **88**(4): p. 1382-90.
288. Richardson, D.R., P. Ponka, and D. Vyoral, *Distribution of iron in reticulocytes after inhibition of heme synthesis with succinylacetone: examination of the intermediates involved in iron metabolism*. *Blood*, 1996. **87**(8): p. 3477-88.
289. Corrigall, A.V., et al., *Inhibition of mammalian protoporphyrinogen oxidase by acifluorfen*. *Biochem Mol Biol Int*, 1994. **34**(6): p. 1283-9.
290. Corradi, H.R., et al., *Crystal structure of protoporphyrinogen oxidase from *Myxococcus xanthus* and its complex with the inhibitor acifluorfen*. *J Biol Chem*, 2006. **281**(50): p. 38625-33.
291. Shi, Z. and G.C. Ferreira, *Modulation of inhibition of ferrochelatase by N-methylprotoporphyrin*. *Biochem J*, 2006. **399**(1): p. 21-8.
292. Shetty, T., et al., *Heme Synthesis Inhibition Blocks Angiogenesis via Mitochondrial Dysfunction*. *iScience*, 2020. **23**(8): p. 101391.
293. Kabiri, Y., et al., *Mitochondrial Impairment by MitoBloCK-6 Inhibits Liver Cancer Cell Proliferation*. *Front Cell Dev Biol*, 2021. **9**: p. 725474.
294. Dabir, D.V., et al., *A small molecule inhibitor of redox-regulated protein translocation into mitochondria*. *Dev Cell*, 2013. **25**(1): p. 81-92.
295. Muzzioli, R. and A. Gallo, *The Interaction and Effect of a Small MitoBlock Library as Inhibitor of ALR Protein-Protein Interaction Pathway*. *Int J Mol Sci*, 2024. **25**(2).
296. Riemer, J., N. Bulleid, and J.M. Herrmann, *Disulfide formation in the ER and mitochondria: two solutions to a common process*. *Science*, 2009. **324**(5932): p. 1284-7.
297. Tsherniak, A., et al., *Defining a Cancer Dependency Map*. *Cell*, 2017. **170**(3): p. 564-576 e16.
298. DepMap, B., *DepMap 24Q2 Public*. 2024: Figshare+.
299. Panayiotou, C., N. Solaroli, and A. Karlsson, *The many isoforms of human adenylate kinases*. *Int J Biochem Cell Biol*, 2014. **49**: p. 75-83.
300. Becker, T. and R. Wagner, *Mitochondrial Outer Membrane Channels: Emerging Diversity in Transport Processes*. *Bioessays*, 2018. **40**(7): p. e1800013.
301. Guna, A., et al., *MTCH2 is a mitochondrial outer membrane protein insertase*. *Science*, 2022. **378**(6617): p. 317-322.

302. Gandhi, C.R., et al., *Liver-specific deletion of augmenter of liver regeneration accelerates development of steatohepatitis and hepatocellular carcinoma in mice*. *Gastroenterology*, 2015. **148**(2): p. 379-391 e4.
303. Ahmad, A., K.P. Madhusudanan, and V. Bhakuni, *Trichloroacetic acid and trifluoroacetic acid-induced unfolding of cytochrome c: stabilization of a native-like folded intermediate(1)*. *Biochim Biophys Acta*, 2000. **1480**(1-2): p. 201-10.
304. Rajalingam, D., et al., *Trichloroacetic acid-induced protein precipitation involves the reversible association of a stable partially structured intermediate*. *Protein Sci*, 2009. **18**(5): p. 980-93.
305. Calvo, S.E., et al., *Comparative Analysis of Mitochondrial N-Termini from Mouse, Human, and Yeast*. *Mol Cell Proteomics*, 2017. **16**(4): p. 512-523.
306. Mahrus, S., et al., *Global sequencing of proteolytic cleavage sites in apoptosis by specific labeling of protein N termini*. *Cell*, 2008. **134**(5): p. 866-76.
307. Crawford, E.D., et al., *The DegraBase: a database of proteolysis in healthy and apoptotic human cells*. *Mol Cell Proteomics*, 2013. **12**(3): p. 813-24.
308. Yeom, J., et al., *Comprehensive analysis of human protein N-termini enables assessment of various protein forms*. *Sci Rep*, 2017. **7**(1): p. 6599.
309. Waterhouse, A.M., et al., *Jalview Version 2--a multiple sequence alignment editor and analysis workbench*. *Bioinformatics*, 2009. **25**(9): p. 1189-91.
310. Peleh, V., et al., *Erv1 of Arabidopsis thaliana can directly oxidize mitochondrial intermembrane space proteins in the absence of redox-active Mia40*. *BMC Biol*, 2017. **15**(1): p. 106.
311. Cavallaro, G., *Genome-wide analysis of eukaryotic twin CX9C proteins*. *Mol Biosyst*, 2010. **6**(12): p. 2459-70.
312. Finger, Y., et al., *Proteasomal degradation induced by DPP9-mediated processing competes with mitochondrial protein import*. *EMBO J*, 2020. **39**(19): p. e103889.
313. Wischhof, L., et al., *AIFM1 beyond cell death: An overview of this OXPHOS-inducing factor in mitochondrial diseases*. *EBioMedicine*, 2022. **83**: p. 104231.
314. Herrmann, J.M. and J. Riemer, *Apoptosis inducing factor and mitochondrial NADH dehydrogenases: redox-controlled gear boxes to switch between mitochondrial biogenesis and cell death*. *Biol Chem*, 2021. **402**(3): p. 289-297.
315. Rothemann, R.A., et al., *Interaction with AK2A links AIFM1 to cellular energy metabolism*. *bioRxiv*, 2024: p. 2024.09.09.611957.
316. Sevrioukova, I.F., *Redox-linked conformational dynamics in apoptosis-inducing factor*. *J Mol Biol*, 2009. **390**(5): p. 924-38.
317. Shelar, S.B., et al., *Thioredoxin-dependent regulation of AIF-mediated DNA damage*. *Free Radic Biol Med*, 2015. **87**: p. 125-36.
318. Richardson, J.S., et al., *Broad Analysis of Vicinal Disulfides: Occurrences, Conformations with Cis or with Trans Peptides, and Functional Roles Including Sugar Binding*. *J Mol Biol*, 2017. **429**(9): p. 1321-1335.
319. Li, J. and B. Sha, *The structure of Tim50(164-361) suggests the mechanism by which Tim50 receives mitochondrial presequences*. *Acta Crystallogr F Struct Biol Commun*, 2015. **71**(Pt 9): p. 1146-51.
320. Lane, N., *Hot mitochondria?* *PLoS Biol*, 2018. **16**(1): p. e2005113.
321. Moreno-Loshuertos, R., et al., *How hot can mitochondria be? Incubation at temperatures above 43 degrees C induces the degradation of respiratory complexes and supercomplexes in intact cells and isolated mitochondria*. *Mitochondrion*, 2023. **69**: p. 83-94.
322. Clarke, A. and H.O. Portner, *Temperature, metabolic power and the evolution of endothermy*. *Biol Rev Camb Philos Soc*, 2010. **85**(4): p. 703-27.
323. Beignon, F., et al., *The multiple facets of mitochondrial regulations controlling cellular thermogenesis*. *Cell Mol Life Sci*, 2022. **79**(10): p. 525.
324. Arai, S., et al., *Mitochondria-targeted fluorescent thermometer monitors intracellular temperature gradient*. *Chem Commun (Camb)*, 2015. **51**(38): p. 8044-7.

## References

325. Sakaguchi, R., S. Kiyonaka, and Y. Mori, *Fluorescent sensors reveal subcellular thermal changes*. *Curr Opin Biotechnol*, 2015. **31**: p. 57-64.
326. Baffou, G., et al., *A critique of methods for temperature imaging in single cells*. *Nat Methods*, 2014. **11**(9): p. 899-901.
327. Macherel, D., et al., *The conundrum of hot mitochondria*. *Biochim Biophys Acta Bioenerg*, 2021. **1862**(2): p. 148348.
328. Savchuk, O.A., et al., *GFP fluorescence peak fraction analysis based nanothermometer for the assessment of exothermal mitochondria activity in live cells*. *Sci Rep*, 2019. **9**(1): p. 7535.
329. Chretien, D., et al., *Mitochondria are physiologically maintained at close to 50 degrees C*. *PLoS Biol*, 2018. **16**(1): p. e2003992.
330. Kruglov, A.G., et al., *Warm Cells, Hot Mitochondria: Achievements and Problems of Ultralocal Thermometry*. *Int J Mol Sci*, 2023. **24**(23).
331. Nicholls, D.G., *Mitochondrial proton leaks and uncoupling proteins*. *Biochim Biophys Acta Bioenerg*, 2021. **1862**(7): p. 148428.
332. Rossato, M., et al., *Human white adipocytes express the cold receptor TRPM8 which activation induces UCP1 expression, mitochondrial activation and heat production*. *Mol Cell Endocrinol*, 2014. **383**(1-2): p. 137-46.
333. Henry, B.A., et al., *Central leptin activates mitochondrial function and increases heat production in skeletal muscle*. *Endocrinology*, 2011. **152**(7): p. 2609-18.
334. Bouillaud, F., M.C. Alves-Guerra, and D. Ricquier, *UCPs, at the interface between bioenergetics and metabolism*. *Biochim Biophys Acta*, 2016. **1863**(10): p. 2443-56.
335. Vogtle, F.N., et al., *Mitochondrial protein turnover: role of the precursor intermediate peptidase Oct1 in protein stabilization*. *Mol Biol Cell*, 2011. **22**(13): p. 2135-43.
336. Gonda, D.K., et al., *Universality and structure of the N-end rule*. *J Biol Chem*, 1989. **264**(28): p. 16700-12.
337. Chew, A., et al., *Mutations in a putative zinc-binding domain inactivate the mitochondrial intermediate peptidase*. *Biochem Biophys Res Commun*, 1996. **226**(3): p. 822-9.
338. Isaya, G., F. Kalousek, and L.E. Rosenberg, *Amino-terminal octapeptides function as recognition signals for the mitochondrial intermediate peptidase*. *J Biol Chem*, 1992. **267**(11): p. 7904-10.
339. Hendrick, J.P., P.E. Hodges, and L.E. Rosenberg, *Survey of amino-terminal proteolytic cleavage sites in mitochondrial precursor proteins: leader peptides cleaved by two matrix proteases share a three-amino acid motif*. *Proc Natl Acad Sci U S A*, 1989. **86**(11): p. 4056-60.
340. Mossmann, D., C. Meisinger, and F.N. Vogtle, *Processing of mitochondrial presequences*. *Biochim Biophys Acta*, 2012. **1819**(9-10): p. 1098-106.
341. Schneider, K., et al., *iMLP, a predictor for internal matrix targeting-like sequences in mitochondrial proteins*. *Biol Chem*, 2021. **402**(8): p. 937-943.
342. Moller, S., M.D. Croning, and R. Apweiler, *Evaluation of methods for the prediction of membrane spanning regions*. *Bioinformatics*, 2001. **17**(7): p. 646-53.
343. Krogh, A., et al., *Predicting transmembrane protein topology with a hidden Markov model: application to complete genomes*. *J Mol Biol*, 2001. **305**(3): p. 567-80.
344. De Sancho, D., U. Doshi, and V. Munoz, *Protein folding rates and stability: how much is there beyond size?* *J Am Chem Soc*, 2009. **131**(6): p. 2074-5.
345. Bonn, F., et al., *Presequence-dependent folding ensures MrpL32 processing by the m-AAA protease in mitochondria*. *EMBO J*, 2011. **30**(13): p. 2545-56.
346. Yang, G., et al., *Atp23p and Atp10p coordinate to regulate the assembly of yeast mitochondrial ATP synthase*. *FASEB J*, 2021. **35**(6): p. e21538.
347. Zeng, X., W. Neupert, and A. Tzagoloff, *The metalloprotease encoded by ATP23 has a dual function in processing and assembly of subunit 6 of mitochondrial ATPase*. *Mol Biol Cell*, 2007. **18**(2): p. 617-26.
348. Vande Walle, L., et al., *Proteome-wide Identification of HtrA2/Omi Substrates*. *J Proteome Res*, 2007. **6**(3): p. 1006-15.

349. Radke, S., et al., *Mitochondrial protein quality control by the proteasome involves ubiquitination and the protease Omi*. J Biol Chem, 2008. **283**(19): p. 12681-5.
350. Li, W., et al., *Structural insights into the pro-apoptotic function of mitochondrial serine protease HtrA2/Omi*. Nat Struct Biol, 2002. **9**(6): p. 436-41.
351. Srinivasula, S.M., et al., *Inhibitor of apoptosis proteins are substrates for the mitochondrial serine protease Omi/HtrA2*. J Biol Chem, 2003. **278**(34): p. 31469-72.
352. Baker, M.J., et al., *Stress-induced OMA1 activation and autocatalytic turnover regulate OPA1-dependent mitochondrial dynamics*. EMBO J, 2014. **33**(6): p. 578-93.
353. Alavi, M.V., *OMA1-An integral membrane protease?* Biochim Biophys Acta Proteins Proteom, 2021. **1869**(2): p. 140558.
354. Hamon, M.P., A.L. Bulteau, and B. Friguet, *Mitochondrial proteases and protein quality control in ageing and longevity*. Ageing Res Rev, 2015. **23**(Pt A): p. 56-66.
355. Kan, K.T., J. Wilcock, and H. Lu, *Role of Yme1 in mitochondrial protein homeostasis: from regulation of protein import, OXPHOS function to lipid synthesis and mitochondrial dynamics*. Biochem Soc Trans, 2024. **52**(3): p. 1539-1548.
356. Schafer, A., et al., *Intramembrane proteolysis of Mgm1 by the mitochondrial rhomboid protease is highly promiscuous regarding the sequence of the cleaved hydrophobic segment*. J Mol Biol, 2010. **401**(2): p. 182-93.
357. Ehses, S., et al., *Regulation of OPA1 processing and mitochondrial fusion by m-AAA protease isoenzymes and OMA1*. J Cell Biol, 2009. **187**(7): p. 1023-36.
358. Klein, J.M. and G. Schwarz, *Cofactor-dependent maturation of mammalian sulfite oxidase links two mitochondrial import pathways*. J Cell Sci, 2012. **125**(Pt 20): p. 4876-85.
359. Singal, A.K. and K.E. Anderson, *Variagate Porphyria*, in *GeneReviews((R))*, M.P. Adam, et al., Editors. 1993: Seattle (WA).
360. Sachar, M., K.E. Anderson, and X. Ma, *Protoporphyrin IX: the Good, the Bad, and the Ugly*. J Pharmacol Exp Ther, 2016. **356**(2): p. 267-75.
361. Hussain, Z., et al., *Protoporphyrin IX-induced phototoxicity: Mechanisms and therapeutics*. Pharmacol Ther, 2023. **248**: p. 108487.
362. Brun, A. and S. Sandberg, *Mechanisms of photosensitivity in porphyric patients with special emphasis on erythropoietic protoporphyria*. J Photochem Photobiol B, 1991. **10**(4): p. 285-302.
363. Girotti, A.W., *Mechanisms of photosensitization*. Photochem Photobiol, 1983. **38**(6): p. 745-51.
364. Takeshita, K., et al., *In vivo oxygen radical generation in the skin of the protoporphyria model mouse with visible light exposure: an L-band ESR study*. J Invest Dermatol, 2004. **122**(6): p. 1463-70.
365. Baptista, M.S., et al., *Type I and Type II Photosensitized Oxidation Reactions: Guidelines and Mechanistic Pathways*. Photochem Photobiol, 2017. **93**(4): p. 912-919.
366. Aravind Menon, I., S.D. Persad, and H.B. Haberman, *A comparison of the phototoxicity of protoporphyrin, coproporphyrin and uroporphyrin using a cellular system in vitro*. Clin Biochem, 1989. **22**(3): p. 197-200.
367. Mahmoud, B.H., et al., *Effects of visible light on the skin*. Photochem Photobiol, 2008. **84**(2): p. 450-62.
368. Iinuma, S., et al., *A mechanistic study of cellular photodestruction with 5-aminolaevulinic acid-induced porphyrin*. Br J Cancer, 1994. **70**(1): p. 21-8.
369. Lynch, J., et al., *A PPIX-binding probe facilitates discovery of PPIX-induced cell death modulation by peroxiredoxin*. Commun Biol, 2023. **6**(1): p. 673.
370. Girotti, A.W., *Photosensitized oxidation of membrane lipids: reaction pathways, cytotoxic effects, and cytoprotective mechanisms*. J Photochem Photobiol B, 2001. **63**(1-3): p. 103-13.
371. Jiang, L., et al., *Protoporphyrin IX is a dual inhibitor of p53/MDM2 and p53/MDM4 interactions and induces apoptosis in B-cell chronic lymphocytic leukemia cells*. Cell Death Discov, 2019. **5**: p. 77.

## References

372. Xu, H., et al., *Protoporphyrin IX induces a necrotic cell death in human THP-1 macrophages through activation of reactive oxygen species/c-Jun N-terminal protein kinase pathway and opening of mitochondrial permeability transition pore*. *Cell Physiol Biochem*, 2014. **34**(6): p. 1835-48.
373. Maitra, D., et al., *Porphyryn-Induced Protein Oxidation and Aggregation as a Mechanism of Porphyria-Associated Cell Injury*. *Cell Mol Gastroenterol Hepatol*, 2019. **8**(4): p. 535-548.
374. Kobuchi, H., et al., *Mitochondrial localization of ABC transporter ABCG2 and its function in 5-aminolevulinic acid-mediated protoporphyrin IX accumulation*. *PLoS One*, 2012. **7**(11): p. e50082.
375. Elenbaas, J.S., et al., *A precursor-inducible zebrafish model of acute protoporphyria with hepatic protein aggregation and multiorganelle stress*. *FASEB J*, 2016. **30**(5): p. 1798-810.
376. Maitra, D., et al., *Protein-aggregating ability of different protoporphyrin-IX nanostructures is dependent on their oxidation and protein-binding capacity*. *J Biol Chem*, 2021. **297**(1): p. 100778.
377. Maitra, D., et al., *Oxygen and Conformation Dependent Protein Oxidation and Aggregation by Porphyrins in Hepatocytes and Light-Exposed Cells*. *Cell Mol Gastroenterol Hepatol*, 2019. **8**(4): p. 659-682 e1.
378. Kaur, P., et al., *Activated heme synthesis regulates glycolysis and oxidative metabolism in breast and ovarian cancer cells*. *PLoS One*, 2021. **16**(11): p. e0260400.
379. Wang, T., et al., *An Analysis of the Multifaceted Roles of Heme in the Pathogenesis of Cancer and Related Diseases*. *Cancers (Basel)*, 2021. **13**(16).
380. Sohoni, S., et al., *Elevated Heme Synthesis and Uptake Underpin Intensified Oxidative Metabolism and Tumorigenic Functions in Non-Small Cell Lung Cancer Cells*. *Cancer Res*, 2019. **79**(10): p. 2511-2525.
381. Hooda, J., et al., *Enhanced heme function and mitochondrial respiration promote the progression of lung cancer cells*. *PLoS One*, 2013. **8**(5): p. e63402.
382. Yang, X., et al., *Aminolevulinic Acid-Based Tumor Detection and Therapy: Molecular Mechanisms and Strategies for Enhancement*. *Int J Mol Sci*, 2015. **16**(10): p. 25865-80.
383. Teng, L., et al., *Silencing of ferrochelatase enhances 5-aminolevulinic acid-based fluorescence and photodynamic therapy efficacy*. *Br J Cancer*, 2011. **104**(5): p. 798-807.
384. Landes, R., et al., *A study of concentration changes of Protoporphyrin IX and Coproporphyrin III in mixed samples mimicking conditions inside cancer cells for Photodynamic Therapy*. *PLoS One*, 2018. **13**(8): p. e0202349.
385. Adapa, S.R., et al., *Porphyryn overdrive rewires cancer cell metabolism*. *Life Sci Alliance*, 2024. **7**(7).
386. Meyers, R.M., et al., *Computational correction of copy number effect improves specificity of CRISPR-Cas9 essentiality screens in cancer cells*. *Nat Genet*, 2017. **49**(12): p. 1779-1784.
387. Pacini, C., et al., *Integrated cross-study datasets of genetic dependencies in cancer*. *Nat Commun*, 2021. **12**(1): p. 1661.
388. Dempster, J.M., et al., *Agreement between two large pan-cancer CRISPR-Cas9 gene dependency data sets*. *Nat Commun*, 2019. **10**(1): p. 5817.
389. Nakayama, T., et al., *Dormant cancer cells accumulate high protoporphyrin IX levels and are sensitive to 5-aminolevulinic acid-based photodynamic therapy*. *Sci Rep*, 2016. **6**: p. 36478.
390. Gaullier, J.M., et al., *Subcellular localization of and photosensitization by protoporphyrin IX human keratinocytes and fibroblasts cultivated with 5-aminolevulinic acid*. *Photochem Photobiol*, 1995. **62**(1): p. 114-22.
391. Chung, C.W., et al., *Effect of surfactant on 5-aminolevulinic acid uptake and PpIX generation in human cholangiocarcinoma cell*. *Eur J Pharm Biopharm*, 2012. **80**(2): p. 453-8.
392. Hatakeyama, T., et al., *Efficacy of 5-aminolevulinic acid-mediated photodynamic therapy using light-emitting diodes in human colon cancer cells*. *Oncol Rep*, 2013. **29**(3): p. 911-6.
393. Li, Y., et al., *Cytotoxic effect of protoporphyrin IX to human Leukemia U937 cells under ultrasonic irradiation*. *Cell Physiol Biochem*, 2014. **33**(4): p. 1186-96.

394. Jinek, M., et al., *A programmable dual-RNA-guided DNA endonuclease in adaptive bacterial immunity*. *Science*, 2012. **337**(6096): p. 816-21.
395. Laemmli, U.K., *Cleavage of structural proteins during the assembly of the head of bacteriophage T4*. *Nature*, 1970. **227**(5259): p. 680-5.
396. Schagger, H., *Tricine-SDS-PAGE*. *Nat Protoc*, 2006. **1**(1): p. 16-22.
397. Crooks, G.E., et al., *WebLogo: a sequence logo generator*. *Genome Res*, 2004. **14**(6): p. 1188-90.
398. Fischer, M., et al., *Protein import and oxidative folding in the mitochondrial intermembrane space of intact mammalian cells*. *Mol Biol Cell*, 2013. **24**(14): p. 2160-70.